ANALYTICAL INVESTIGATION OF THE AERODYNAMIC STABILITY OF HELICAL VORTICES SHED FROM A HOVERING ROTOR

Bharat P. Gupta, et al

Rochester University

Prepared for:

U. S. Army Air Mobility Research and Development Laboratory

October 1973

Unclassified
Security Classification

AD 773026

DOCUMENT CONTROL DATA - R & D

(Security classification of title, body of abstract and indexing annotation must be entered when the overall report is classified)

1. ORIGINATING ACTIVITY (Corporate author)	2a. REPORT SECURITY CLASSIFICATION
University of Rochester, Rochester, New York	Unclassified
	2b. GROUP

3. REPORT TITLE

ANALYTICAL INVESTIGATION OF THE AERODYNAMIC STABILITY OF HELICAL VORTICES SHED FROM A HOVERING ROTOR

4. DESCRIPTIVE NOTES (Type of report and inclusive dates)
Final Report

5. AUTHOR(S) (First name, middle initial, last name)

Bharat P. Gupta
Robert G. Loewy

6. REPORT DATE	7a. TOTAL NO. OF PAGES	7b. NO. OF REFS
October 1973	146 / 150	30

8a. CONTRACT OR GRANT NO	9a. ORIGINATOR'S REPORT NUMBER(S)
DAAJ02-72-C-0042	USAAMRDL Technical Report 73-84
b. PROJECT NO Task 1F162204AA4201	
c.	9b. OTHER REPORT NO(S) (Any other numbers that may be assigned this report)
d.	

10. DISTRIBUTION STATEMENT

Approved for public release; distribution unlimited.

11. SUPPLEMENTARY NOTES	12. SPONSORING MILITARY ACTIVITY
	Eustis Directorate U.S. Army Air Mobility R&D Laboratory Fort Eustis, Virginia

13. ABSTRACT

A small-perturbation stability analysis of a doubly infinite array of interdigitated, right circular helical vortices has been formulated. This array corresponds to the vortices trailed from the tips of the blades of a helicopter rotor or propeller in static thrust or axial flight condition and at great distance from the plane of rotation of the blades. The analysis makes use of the Biot-Savart law of induction and the Vorticity Transport Theorem. The singularities in the Biot-Savart integration for self-induction have been eliminated by substituting appropriate approximate functions. Near-singular behavior in other integrals has been minimized by adding and subtracting functions with similar near-singular behavior and which have exact, closed-form integrals. The calculations of induced perturbation velocities and those required for the stability analysis have been programmed for digital computer.

Numerical results have been obtained for two-, three-, four-, five-, six-helix arrays representing the vortices trailing from the same number of blades. The special case of a single helix has been run and the results compared with those presently available from studies by Levy and Forsdyke and by Widnall. A continuum of instability modes has been found associated with all values of wave numbers; only modes with wave number 0 and 1 are so much as neutrally stable, and only for the case of a single helix. The most unstable modes involve the most axial motion of adjacent vortex segments relative to each other. By "adjacent segments" is meant vortex segments above and below each other (i.e., at the same azimuthal location) on adjacent coils of the same or neighboring helices. Furthermore, the larger the percentage of the helical arc length involved in such motion, the more rapidly the distortion will diverge. Maximum divergence rates in the unstable modes increase as the helix pitch decreases, increase as the number of helices increase, and decrease as the number of cycles of deformations in one turn of the helix (i.e., wave number) increases. The larger the helix filament core diameter, the more sensitive the analysis is to the means by which the singularities in the self-induction integrals are eliminated. Increasing core diameters, however, reduces the maximum divergence rates.

DD FORM 1 NOV 68 1473 REPLACES DD FORM 1473, 1 JAN 64 WHICH IS OBSOLETE FOR ARMY USE.

Unclassified
Security Classification

14. KEY WORDS	LINK A		LINK B		LINK C	
	ROLE	WT	ROLE	WT	ROLE	WT
Helicopter Rotors Helicopter Rotor Wake Wake Geometry Far Wake Stability Aerodynamic Stability Interdigitated Helical Vortices						

DISCLAIMERS

The findings in this report are not to be construed as an official Department of the Army position unless so designated by other authorized documents.

When Government drawings, specifications, or other data are used for any purpose other than in connection with a definitely related Government procurement operation, the United States Government thereby incurs no responsibility nor any obligation whatsoever; and the fact that the Government may have formulated, furnished, or in any way supplied the said drawings, specifications, or other data is not to be regarded by implication or otherwise as in any manner licensing the holder or any other person or corporation, or conveying any rights or permission, to manufacture, use, or sell any patented invention that may in any way be related thereto.

Trade names cited in this report do not constitute an official endorsement or approval of the use of such commercial hardware or software.

DISPOSITION INSTRUCTIONS

Destroy this report when no longer needed. Do not return it to the originator.

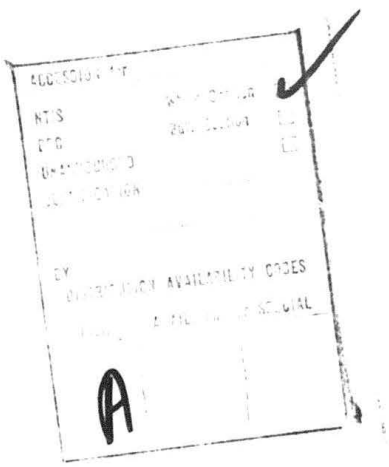

DEPARTMENT OF THE ARMY
U. S. ARMY AIR MOBILITY RESEARCH & DEVELOPMENT LABORATORY
EUSTIS DIRECTORATE
FORT EUSTIS, VIRGINIA 23604

This report has been reviewed by the Eustis Directorate, U. S. Army Air Mobility Research and Development Laboratory and is considered to be technically sound. The purpose of this program was to analytically investigate the aerodynamic stability of helical vortex arrays as shed from a hovering rotor of two, three, four, five, and six blades.

The program was conducted under the technical management of Donald J. Merkley of the Technology Applications Division of this Directorate.

Task 1F162204AA4201
Contract DAAJ02-72-C-0042
USAAMRDL Technical Report 73-84
October 1973

ANALYTICAL INVESTIGATION OF THE AERODYNAMIC STABILITY OF HELICAL VORTICES SHED FROM A HOVERING ROTOR

By

B. Gupta
R. Loewy

Prepared by

University of Rochester
Rochester, New York

for

EUSTIS DIRECTORATE
U. S. ARMY
AIR MOBILITY RESEARCH AND DEVELOPMENT LABORATORY
FORT EUSTIS, VIRGINIA

ABSTRACT

A small-perturbation stability analysis of a doubly infinite array of interdigitated, right circular helical vortices has been formulated. This array corresponds to the vortices trailed from the tips of the blades of a helicopter rotor or propeller in static thrust or axial flight condition and at great distance from the plane of rotation of the blades. The analysis makes use of the Biot-Savart law of induction and the Vorticity Transport Theorem. The singularities in the Biot-Savart integration for self-induction have been eliminated by substituting appropriate approximate functions. Near-singular behavior in other integrals has been minimized by adding and subtracting functions with similar near-singular behavior and which have exact, closed-form integrals. The calculations of induced perturbation velocities and those required for the stability analysis have been programmed for digital computer.

Numerical results have been obtained for two-, three-, four-, five-, six-helix arrays representing the vortices trailing from the same number of blades. The special case of a single helix has been run and the results compared with those presently available from studies by Levy and Forsdyke and by Widnall. A continuum of instability modes has been found associated with all values of wave numbers; only modes with wave number 0 and 1 are so much as neutrally stable, and only for the case of a single helix. The most unstable modes involve the most axial motion of adjacent vortex segments relative to each other. By "adjacent segments" is meant vortex segments above and below each other (i.e., at the same azimuthal location) on adjacent coils of the same or neighboring helices. Furthermore, the larger the percentage of the helical arc length involved in such motion, the more rapidly the distortion will diverge. Maximum divergence rates in the unstable modes increase as the helix pitch decreases, increase as the number of helices increase, and decrease as the number of cycles of deformations in one turn of the helix (i.e., wave number) increases. The larger the helix filament core diameter, the more sensitive the analysis is to the means by which the singularities in the self-induction integrals are eliminated. Increasing core diameters, however, reduces the maximum divergence rates.

TABLE OF CONTENTS

	Page
ABSTRACT	iii
LIST OF ILLUSTRATIONS	vii
LIST OF TABLES	ix
LIST OF SYMBOLS	x
CHAPTER 1 INTRODUCTION	1
1.1 Importance of an Accurate Knowledge of Wake Geometry.	1
1.2 Classical Methods of Wake-Induced Fields.	1
1.3 Vortex Tube Representations of Helical Wake and Distorted Wake Geometries.	2
1.4 Motivation for the Present Work and Description of the General Approach Adopted.	3
CHAPTER 2 THEORETICAL ANALYSIS.	6
2.1 Background.	6
2.2 Capsule Statement of the Work Done.	6
2.3 Development	7
2.3.1 Mathematical Definition of Infinite Helical Vortices.	7
2.3.2 Calculations of Induced Velocities.	8
2.4 Vorticity Transport Theorem	12
2.5 Perturbation Equations.	12
2.6 Type of Perturbations and Eigenvalue Equations	22
2.7 Stability Analysis	26
2.8 Symmetry Considerations for $n = 2$	27
CHAPTER 3 COMPUTER PROGRAM	29
3.1 General Description.	29
3.2 Treatment of Singularities in the Self-Induction Integrals.	29
3.3 Formulation of Eigenvalue Equations	33
3.4 Eigenvalue Analysis.	36
CHAPTER 4 RESULTS	39

Page

4.1 General. 39
4.2 Selection of Cases To Be Run. 39
4.3 Physical Description of Modal Deflections . 41
4.4 Levy and Forsdyke Case. 45
4.5 Widnall Case of Single Helix. 46
4.6 S.C. Crow's Case (Trailing Vortices From Fixed-Wing Aircraft Wings) 49
4.7 Discussion of Results 50
4.8 Comments on Absolute Maximum Wake Divergence Rates for Multibladed Rotors With Odd and Even Numbers of Blades. 61

CHAPTER 5 CONCLUSIONS 68

CHAPTER 6 RECOMMENDATIONS 69

LITERATURE CITED. 94

APPENDIXES

I. Limits for S. C. Crow's Case. 97
II. FORTRAN IV Source Listing. 100

DISTRIBUTION 133

LIST OF ILLUSTRATIONS

Figure		Page
1	Undistorted p^{th} and m^{th} Vortex Helices of Radius r, Pitch k, and Vortex Core Diameter 2ε.	70
2	Plot of Divergence Rate Against Phase Difference for a Two-Bladed Rotor	71
3	Major Steps in the Computer Program.	72
4	Perturbation Integrand $I = [kJ^{-3/2} \sin x \cos(\omega x)]$ . .	73
5	Perturbation Integrand $I = [kJ^{-3/2} x \sin x \sin(\omega x)]$ . .	74
6	Plot I: $I = [kJ^{-3/2} \sin x \cos x]$ Against x ; Plot II: $II = [\{kJ^{-3/2} \sin x \cos x\} - kx\{(1+k^3)x^2+\varepsilon^2\}^{3/2}]$ Against x.	75
7	Radial Perturbations in Wave Number = 0 Mode (Dilatational).	76
8	Radial Perturbations in Wave Number = 1 Mode. .	77
9	Axial Perturbations in Wave Number = 1 Mode . .	78
10	Radial Perturbations in Wave Number = 2 Mode . .	79
11	Axial Perturbations in Wave Number = 2 Mode . .	80
12	Radial Perturbations in Wave Number = 1/2 Mode .	81
13	Comparison of Various Perturbation Modes for Single Helix in Axial Direction	82
14	Plot of Maximum Divergence Rate vs Wave Number for Single Helix.	83
15	Plot of Maximum Divergence Rate vs Wave Number for Two-Bladed Rotor	84
16	Plot of Maximum Divergence Rate vs Wave Number for Three-Bladed Rotor.	85
17	Plot of Maximum Divergence Rate vs Wave Number for Four-Bladed Rotor	86

Figure		Page
18	Plot of Maximum Divergence Rate vs Wave Number for Five-Bladed Rotor	87
19	Plot of Maximum Divergence Rate vs Wave Number for Six-Bladed Rotor.	88
20	Real Component of Axial Perturbations for a Two-Bladed Rotor at Wave Number 0.0	89
21	Real Component of Axial Perturbations for a Two-Bladed Rotor at Wave Number 1.0	90
22	Absolute Maximum Divergence Rates for Multi-bladed Rotors of Varying Pitch.	91
23	Real Component of Axial Perturbations for a Three-Bladed Rotor at Wave Number 0.0 . . .	92
24	Real Component of Axial Perturbations for a Three-Bladed Rotor at Wave Number 1.5 . . .	93

LIST OF TABLES

Table		Page
I	Values of $\psi_{mp} = \psi_m - \psi_p$, the Phase Difference Constant for n-Bladed Rotor. . .	35
II	Number of Matrix Elements Resulting From Calculation K	36
III	Levy and Forsdyke Case, Comparison With the Present Study	47
IV	Case of Single-Blade, Divergence Rates Obtained in the Present Study Compared With the Values Obtained by Widnall	48
V	Results of This Analysis for S. C. Crow's Case	51
VI	Maximum Divergence Rates for Two-Bladed Rotor.	54
VII	Maximum Divergence Rates for Three-Bladed Rotor	55
VIII	Maximum Divergence Rates for Four-Bladed Rotor	56
IX	Maximum Divergence Rates for Five-Bladed Rotor	57
X	Maximum Divergence Rates for Six-Bladed Rotor.	58
XI	Absolute Maximum Divergence Rates for Multi-bladed Rotors of Varying Pitch.	60
XII	Eigenfunctions for the Most Unstable Eigenvalues of a Three-Bladed Rotor at Wave Numbers 0.0 and 1.5, Pitch = 0.1 and Core Size = 0.1 . .	63
XIII	Eigenfunctions for the Most Unstable Eigenvalues of a Two-Bladed Rotor at Wave Numbers 0.0 and 1.0, Pitch = 0.1 and Core Size = 0.1 . .	66
XIV	Comparison of Maximum Instability for Two- and Three-Bladed Rotors	67

LIST OF SYMBOLS

a	constant defined as $\sqrt{\frac{\varepsilon^2}{(1+k^2)}}$
a_o	lower limit in Gaussian Quadrature Formula
$A_k^{(n)}$	coefficients in the series expansion of the integral in the Gaussian Quadrature Formula
$\underline{\underline{A}}_{mm}$	3x3 matrix of complex elements representing self-induction for the m^{th} vortex
$\underline{\underline{A}}_{mn}$	3x3 matrix of complex elements representing mutual-inductance of m^{th} vortex on n^{th} vortex
b	distance between two trailing vortices from the aircraft
b_o	upper limit in the Gaussian Quadrature Formula
d	axial distance between two parallel elements which are closest to each other on two neighboring coils at the same circumferential position, nondimensionalized by r
d_c	cutoff arc length used in Crow's work
dx_m, dy_m, dz_m	differentials in x, y, z Cartesian coordinate directions along m^{th} vortex
$\vec{dL}_m$	elemental length vector on m^{th} vortex, feet
$\vec{dL}_m(\vec{r}_m+\delta\vec{r}_m)$	elemental length vector at the point $\vec{r}_m+\delta\vec{r}_m$ on m^{th} vortex due to the modified system of vortex helices, feet
D/L	disc loading, lb/ft^2
$\vec{e}_x, \vec{e}_y, \vec{e}_z$	unit vectors in Cartesian coordinate system
$\vec{e}_r, \vec{e}_\phi, \vec{e}_z$	unit vectors in cylindrical polar coordinate system
i	index describing i^{th} eigenvector
I	perturbation integrand
I_1 to I_8	analytically defined integrals for removal of numerical singularities from self-induction integrals

J_{mp}	square of the scalar distance between points on m^{th} and p^{th} vortex, modified to $\lvert\vec{R}_{mp}\rvert^2 + \epsilon_o^2$ for self-induction
k	pitch of the helix; axial displacement in one turn of helix is $2\pi k r$, dimensionless
k_s	wave number for S. C. Crow's case of the stability of aircraft trailing vortices
K	parameter used in computer program to identify the set of calculations corresponding to possible combinations of p and m as in the table on page 36
K_{mp}	first order quantity defined as $(x_m - x_p)(\delta x_m - \delta x_p) + (y_m - y_p)(\delta y_m - \delta y_p) + (z_m - z_p)(\delta z_m - \delta z_p)$
$L1$	parameter in the main computer program used for preselecting the two separate sets of integration subroutines
$LL1$	parameter in the main computer program which stops modifying the singular integrals beyond an upper limit of $xU = 2\pi$
m	index describing m^{th} vortex
M	parameter in the main computer program used for selecting the overall integration limits on perturbation integrals
n	number of blades in the rotor
p	index describing p^{th} vortex
q_{kp}	set of scalars which could be used for transformation from $\underline{x}_k$ to $\underline{y}_p$
$\underline{\underline{Q}}$	unitary matrix in decomposition of $\underline{\underline{A}}$ into the product $\underline{\underline{Q}}\underline{\underline{U}}$
r	radius of circular helix, feet
$\vec{r}_m$	position vector of point (x_m , y_m , z_m), non-dimensionalized by r
$\dot{r}_p, (r\dot{\phi}_p), \dot{z}_p$	steady induced velocities at a point on p^{th} helix in (r , ϕ , z) cylindrical polar directions; where $\dot{r}_p = \frac{d}{dt}(r_p)$, etc.

r_m, ϕ_m, z_m	cylindrical polar coordinate description of points on m^{th} vortex as functions of parameter θ_m and constants ψ_m and k
$\vec{R}_{mp}$	relative position vector of point on p^{th} vortex relative to point on m^{th} vortex, feet
t	time variable, seconds
$t_k^{(n)}$	nodes, roots of Legendre polynomials of degree n
T	period for one complete rotor revolution, seconds
$\vec{U}_p$	induced velocity on p^{th} vortex, ft/sec
$\vec{U}_p(\vec{r}_p + \delta\vec{r}_p)$	velocity at the point $\vec{r}_p + \delta\vec{r}_p$ on p^{th} vortex due to the modified system of vortex helices, ft/sec
$\underline{\underline{U}}$	upper triangular matrix in decomposition of $\underline{\underline{A}}$ into the product $\underline{\underline{Q}}\,\underline{\underline{U}}$
U_{xp}, U_{yp}, U_{zp}	x, y and z components of zeroth order induced velocities respectively, ft/sec
v_i	induced velocity or increase in velocity at the actuator disc, ft/sec
V_c	climb velocity in vertical flight, ft/sec
V_s	downward axial velocity in the fully developed slipstream, ft/sec
$\underline{x}$	eigenvector of the system of interdigitated vortex helices, nondimensionalized by r
x_s	axial coordinate in case of aircraft trailing vortices
$\underline{x}_k$	perturbation vector for k^{th} vortex; $\underline{x}_k = \underline{x}_k$
$\underline{x}_m$	eigenvector for m^{th} vortex having $\epsilon\hat{r}_m$, $r\epsilon\hat{\phi}_m$ and $\epsilon\hat{z}_m$ as its components
χ_{mp}	nondimensional quantity defined as the difference $(\theta_m - \theta_p)$ for all m and p
χ	special case of χ_{mp} where m = p; ie $(\theta_p' - \theta_p)$. See Figures 4, 5 and 6.

x_m, y_m, z_m	Cartesian coordinate description of points on m^{th} vortex as functions of parameter θ_m and constants ψ_m and k
XU	upper limit on analytically defined integrals for removal of numerical singularities from self-induction integrals
$\underset{\sim}{y}_j$	j^{th} left eigenvector
$\underset{\sim}{y}_p$	new perturbation vector as a result of an attempt toward simplifying the eigenmatrix equation
y_{mp}	defined as the difference ($x_{mp} - \psi_{mp}$)
z	constant defined as $\sinh^{-1}(\frac{XU}{a})$
α	exponential growth rate factor, complex, sec^{-1}
β_s	nondimensional wave number
$\delta\theta_m$	first-order perturbation of the helical coordinate θ_m along the m^{th} vortex
$\delta\vec{r}_m$	displacement perturbation vector of the point (x_m, y_m, z_m)
$\delta x_m, \delta y_m, \delta z_m$	first-order displacement perturbations of the point (x_m, y_m, z_m) in Cartesian coordinate directions
$\delta r_m, \delta\phi_m, \delta z_m$	first-order displacement perturbations of the point on m^{th} vortex in cylindrical polar coordinate directions
$\delta\dot{r}_m, \delta\dot{\phi}_m, \delta\dot{z}_m$	total time derivatives of quantities δr_m, $\delta\phi_m$, δz_m respectively
$\delta\hat{r}_m, \delta\hat{\phi}_m, \delta\hat{z}_m$	amplitude of displacement perturbations in r, ϕ and z directions respectively
$\delta\hat{r}_{i\lambda}, \delta\hat{\phi}_{i\lambda}, \delta\hat{z}_{i\lambda}$	i^{th} eigenvector components in r, ϕ and z directions corresponding to an eigenvalue λ
$\delta U_{xp}, \delta U_{yp}, \delta U_{zp}$	x, y and z components of first-order induced velocities respectively

ϵ	perturbation in d in radial or axial directions, nondimensionalized by r
ϵ_o	radius of finite core vortex, feet
ε	nondimensionalized 'core size' defined as ϵ_o/r
Γ_m	circulation strength of m^{th} vortex
θ	helical coordinate parameter used for describing a circular helix, dimensionless
θ_m	helical coordinate describing the circumferential position of m^{th} vortex
λ	set of complex eigenvalues for the perturbations of the system of interdigitated helices
ρ	mass density of air, slugs/ft^3
$\Phi(\tau)$	function to be integrated as a function of the variable τ
$\bar{\Phi}$	phase difference between eigenvectors $\underline{x}_1$ and $\underline{x}_2$ for system of two interdigitated helices
ψ_m	phase difference angle for m^{th} vortex
ψ_{mp}	nondimensional quantity defined as the difference ($\psi_m - \psi_p$) for all m and p
τ	normalized variable of integration used on page 32
ω	wave number of the perturbations, assigned real, dimensionless
$\dot{\xi}_p, \dot{\eta}_p, \dot{\zeta}_p$	induced velocity component at a point on p^{th} vortex in r, ϕ and z directions respectively due to perturbed system of vortex helices, ft/sec
$( )'$	prime on a variable corresponds to the position of the general point involved in the space integration as contrasted to the specific point at which induced velocity is being evaluated in self-induction integration
$( )_o$	zero-order quantities
$( )_1$	first-order quantities

CHAPTER 1

INTRODUCTION

1.1 IMPORTANCE OF AN ACCURATE KNOWLEDGE OF WAKE GEOMETRY

The geometry of the wake beneath a helicopter rotor is important to the accurate prediction of the airloads acting on the blades. Determination of such airloads is prerequisite to nearly every area of rotary-wing design including performance, vibrations, acoustics and structural integrity. An accurate knowledge of the wake-induced velocity field is also important for determining (1) interference effects between rotors, (2) positioning and effectiveness of auxiliary surfaces, (3) interference with the fuselage and other non-lifting bodies, etc.

The impact of wake geometry is felt directly in attempts to predict wake-induced velocity fields. Inability to do so with acceptable accuracy has limited the state of the art of helicopter rotor designs for perhaps a decade. This is a problem on which considerable emphasis has been and is still being placed. Some of the reasons for this emphasis include the following: (1) The desirability of attaining peak lift system performance is greater with helicopters than with conventional aircraft because of generally less favorable payload and power to gross weight ratios. (2) The distinctive acoustic signature of a lifting rotor can be troublesome, and this imposes requirements on the induced velocity field that have no counterparts in fixed-wing aircraft design. (3) Not only is the geometry of the rotor's vortex system considerably more complicated than that of a fixed-wing aircraft, but it is of greater influence, since rotation causes the wake vorticity to remain longer in the vicinity of the blades. (4) Unsteady effects must almost always be considered since velocity at the blade element varies with time even when the helicopter is in steady flight. (5) Aeroelastic effects are always a factor since rotor blades are relatively more flexible than conventional fixed wings.

1.2 CLASSICAL METHODS OF COMPUTING WAKE-INDUCED FIELDS

The simplest hovering theory is the so-called actuator disc analysis, where the induced velocities are calculated in terms of momentum and energy changes as the flow crosses an "actuator

disc". See, for example, Glauert [Reference 1], Shapiro [Reference 2] and Gessow and Meyers [Reference 3]. Refinements of this approach accounting for nonuniformities around the azimuth have been made by Mangler [Reference 4] and Loewy and Joglekar [Reference 5]. The next step taken in developing an analytical model of the hovering rotor was to consider the individual blade elements. The rotor disc was divided into elemental annuli through each of which the momentum change was equated to the blade element lift for a given blade pitch. This method was first introduced by S. Goldstein [Reference 6]. It has most recently been developed to account for experimental airfoil characteristics and labeled "nonlinear strip theory" by Jenny, Olson and Landgrebe [Reference 7].

1.3 VORTEX TUBE REPRESENTATION OF HELICAL WAKE AND DISTORTED WAKE GEOMETRIES

Considerable research has been and is being done to develop a rotary-wing equivalent to the classical lifting-line type of inflow analysis employed with success for fixed-wing aircraft. Among advances made in the last decade are methods of wake analysis which deal with the three-dimensional array of vorticity in the wake "shed and trailed"* from the finite number of blades in a lifting rotor. Such analyses [Miller, Reference 8; DuWaldt, Reference 9, etc.] have the following classical bases: (1) Making use of Prandtl's theory of airfoils, the wing is represented by a "lifting line" with a circulating flow around it. This circulating flow in turn gives rise to circulation, Γ, which is related to both the aerodynamic forces and the strength of a vortex called the "bound vortex" which is, essentially, the lifting line. (2) The aerodynamic forces are also related to the induced velocities at the lifting line through the angle of attack, on which dimensional analysis shows lift to be dependent. (3) A fundamental law of the mechanics of perfect fluids (Kelvin's theorem or the Helmholtz theorem) is involved; namely, that a vortex can not end in the middle of a fluid, so the bound vortex continues in the fluid beyond the extent of the blade, as a "free" vortex trailing from the wing tips. (4) Experience has shown that when a sheet of free vortices trails in a distributed manner from some significant spanwise length of a blade's trailing edge, it then rolls up into a pair of vortex tubes of equal strength and opposite directions and is "transported" away from the blade which trailed it by the rotational velocity and the downward

* "Shed" vorticity arises from time-wise variations in lift, "trailed" vorticity from spanwise variations. Only the latter kind is considered in this report.

axial induced velocity generated by the rotor. (5) The velocity induced at the airfoil by both bound and trailing vorticity is given by the Biot-Savart law of induction.

The classical wake is generally considered in two distinct parts: near wake and far wake. The near wake is defined as a set of circular helices of finite length trailing from the blade tips and near the blade roots, together with the "lifting line" or bound vortex representation of the rotor blades. The length of this set of trailing vortices is usually in terms of some number of rotations below the "lifting lines". The far wake, on the other hand, can be treated as consisting of an array of infinitely long, interdigitated circular helices as generated by the blade tip only.

The wake-induced field of a hovering rotor, therefore, can be inferred from proper consideration of trailing vorticity, i.e., a set of interdigitated circular vortex helices generated by the tip of each blade in the rotor. The question is, "How can this vortex helix representation be used to deal more fundamentally with rotor-induced flows?"

Although most of the recent methods of blade airload analysis represent a considerable improvement in the state of the art, they still do not permit accurate calculation of blade airloads and associated bending moments. The fact that wake geometry is prescribed in advance imposes a fundamental limit to such methods. Optimum rotor design is not likely to be achieved until a distorted wake geometry can be accounted for rather than prescribing a rigid helical geometry. Tarrarine [Reference 10], Landgrebe [Reference 11] and others have shown, using flow visualization techniques, that the actual rotor wake geometry differs significantly from the pure helix. Relatively recent efforts, therefore, have concentrated on the development of analytical methods for predicting the distorted helical geometry of the actual rotor wake. In one approach [Reference 5], the nonuniform velocity fields predicted by momentum theory have been used to calculate the distortion of a canted, but otherwise pure, helix. In others [References 12, 13], the self-induced distortions of a rotor wake represented by numerous discrete vortex elements are computed by application of the classical Biot-Savart law involving both numerical integration and iteration techniques.

1.4 MOTIVATION FOR THE PRESENT WORK AND DESCRIPTION OF THE GENERAL APPROACH ADOPTED

The determination and use of a distorted wake geometry, free

from the constraint of conforming with a pure helix, would be expected to provide a more accurate means for computing the instantaneous rotor flow field and the associated blade airloads. It seems significant to this objective that, in tests and wake geometry analyses, evidence of apparent instabilities in the tip vortex patterns was discerned; in experiments, rapid deviations from the helical geometry were observed [Reference 10], and during numerical integrations, the numbers seemed to diverge in successive iterations [Reference 11]. In either case, distorted rotor wakes were obtained. In Reference 11 it was noted that the portion of the wake in the immediate vicinity of the rotor plane (extremely near wake) did converge in the calculations, with the degree of convergence improving with increasing proximity to the rotor. This, presumably, is due to the fact that one end of the wake is tied to a blade whose position is prescribed. Close examination of the computed results, however, indicated that the wake did become unstable at moderate distances from the rotor. It therefore appears that to gain insight as to the completeness needed for acceptable theoretical rotor blade analysis methods, stability of the wake should be studied. Further, it seems prudent to examine the far wake first, both because of its greater simplicity and because of its apparently greater tendencies toward instability.

Two-dimensional flow fields behind a circular cylinder were found by Kármán [Reference 14] to be stable only when vortices were in the staggered formation, which has come to be known as the "Kármán Vortex Street". A "Kármán Vortex Street" might be thought of as the cross section of a right circular helical vortex on a plane through its axis. Such an analogy suggested that the interdigitated vortex helix system associated with two or more blades would, by extension of Karman's analysis, be more unstable than a single helical vortex. A literature survey revealed no analyses of the stability of an interdigitated vortex helix array such as might represent the wake of a multibladed rotor. An early stability analysis of a single helical vortex, however, was carried out by Levy and Forsdyke [Reference 15]. This work was prompted by flow visualization experiments in the wind tunnel with a stationary, circular disc with its polar axis parallel to the flow. At high values of Reynolds numbers, it was found that its wake consisted of a rotating helical vortex filament.

The Levy and Forsdyke analysis, while basically like that of Kármán, involved numerical techniques which, without modern computing, led to some erroneous results. Nevertheless, the approach adopted here for the stability analysis of interdigitated helical vortex systems follows the same general line. A system of helical vortices is postulated. Perturbation displacements are assumed, and the self-induced and mutual-induced

perturbation velocities at the perturbed vortices are calculated. Subsequently their growth rate is determined using the vorticity transport theorem. As was found in an independent study of the stability of a single helical vortex, published after the initiation of the research reported here [Widnall, Reference 16], the vortex system is unstable under most situations. The results of the analysis reported here, however, show that stability and growth rate of perturbations depend very strongly on the number of blades in the multi-bladed case.

CHAPTER 2

THEORETICAL ANALYSIS

2.1 BACKGROUND

Where instabilities exist, iterative techniques will not converge, and direct numerical integrations with respect to time will be greatly enhanced by a prior knowledge of the unstable modes and their rates of divergence. As noted in the preceding chapter, Levy and Forsdyke [Reference 15] considered a single, doubly infinite, constant-diameter, helical vortex. They found it to be unstable for disturbance modes with no distortion for vortex helix pitch angles less than 0.3 radian. Their analysis, however, suffered from several shortcomings. The numerical integration was performed using a planimeter, which is understandable, considering the early date of their work (1928), but nevertheless the loss in accuracy contributed to errors in their results, and the approximations used in evaluating the singular integrals were quite crude.

Widnall [Reference 16] recently investigated the stability of a single helical vortex filament with a finite core, using the method of matched asymptotic expansions. The results of that work, except for certain differences in evaluating the singular integrals encountered in the analysis, were obtained as a special case in the present investigation. In another relatively recent study, S. C. Crow [Reference 17] dealt with the stability of a pair of linear, parallel infinite vortices of constant strength, as trailed from the tips of the wings of fixed-wing aircraft. In theory, such a pair of trailing vortices could be given as a special case of the family of interdigitated, helical vortices considered here; specifically, a set of two interdigitated helical vortices as trailed from the tips of a two-bladed rotor, but with infinite pitch. In practice, the approximations used in performing the numerical integrations over space precluded such a quantitative comparison. However, Crow's study did provide insight into ways of looking into the mutual inductance effects of the two vortices in the present investigation.

2.2 CAPSULE STATEMENT OF THE WORK DONE

The present work deals with the stability of interdigitated

helical vortices, representing the part of the far wake trailed from the tips of multibladed helicopter rotors in hovering or vertical flight. A review of the literature revealed that only References 15 and 16, which are limited to single helices contained pertinent work. The analysis in this report involves the following steps: (1) An n-bladed, hovering rotor is represented by interdigitated, doubly infinite, right circular helical vortices of constant diameter. (2) The system of n vortices is perturbed from its normal helical configuration and position in radial, circumferential, and axial directions. (3) Application of the Biot-Savart law and the requirement that the time rate of perturbation displacements be compatible with the resulting induced velocities yields a system of eigenvalue equations for the admissible characteristics of these perturbations.

2.3 DEVELOPMENT

2.3.1 Mathematical Definition of Infinite Helical Vortices

Referring to Figure 1, which makes use of a left-handed Cartesian coordinate system, the parametric equation of a circular helix of radius r and pitch k is

$$x = r\cos\theta \quad , \quad y = r\sin\theta \quad , \quad z = kr\theta \quad ; \quad -\infty < \theta < \infty$$

To mathematically define n coaxial vortices of radius r and pitch k, one can define an azimuthal separation angle between the first helix and successive helices (see Figure 1) as

$$\psi_m = \frac{(m-1)\cdot 2\pi}{n} \quad ; \quad m = 1, 2, \cdots, n$$

If θ_m represents the parameter for the m^{th} vortex, the parametric equation for the m^{th} vortex can then be written as

$$x_m = r\cos(\theta_m + \psi_m)$$

$$y_m = r\sin(\theta_m + \psi_m)$$

$$z_m = kr\theta_m$$

2.3.2 Calculations of the Induced Velocities

The kinematic relation between vorticity and velocity in an incompressible fluid is given by the well-known Biot-Savart law. This equation can be applied to the system of n vortices and results in the expression

$$\vec{U}_p = \sum_{m=1}^{n} \frac{\Gamma_m}{4\pi} \int \frac{\vec{R}_{mp} \times d\vec{L}_m}{|\vec{R}_{mp}|^3} \qquad (1)$$

where $\vec{U}_p$ = induced velocity on p^{th} vortex.

Γ_m = circulation strength of m^{th} vortex.

$d\vec{L}_m$ = elemental length vector on m^{th} vortex.

$\vec{R}_{mp}$ = relative position vector of point on p^{th} vortex relative to points on m^{th} vortex.

Referring to Figure 1, a vector representing an element of length along the m^{th} vortex can be written as

$$d\vec{L}_m = [dx'_m \ , \ dy'_m \ , \ dz'_m]$$

and

$$\vec{R}_{mp} = [(x'_m - x_p) \ , \ (y'_m - y_p) \ , \ (z'_m - z_p)]$$

Note that the integration in equation (1) must be performed for all values of m, including the case where m=p, to account for the fact that the p^{th} vortex induces velocity on itself. Primes have, therefore, been used to identify the general points involved in the space integration, as contrasted to the specific point at which the induced velocities are evaluated.

Rewriting the Cartesian coordinate description for the m^{th} and p^{th} vortex,

$$x'_m = r\cos(\theta'_m + \psi_m)$$
$$y'_m = r\sin(\theta'_m + \psi_m)$$
$$z'_m = Rr\theta'_m$$

and

$$x_p = r\cos(\theta_p + \psi_p)$$
$$y_p = r\sin(\theta_p + \psi_p)$$
$$z_p = Rr\theta_p$$

Therefore, $d\vec{L}_m = [-r\sin(\theta_m' + \psi_m),\ r\cos(\theta_m' + \psi_m),\ kr]\, d\theta_m'$

$$\vec{R}_{mp} = [\{r\cos(\theta_m' + \psi_m) - r\cos(\theta_p + \psi_p)\},\ \{r\sin(\theta_m' + \psi_m) - r\sin(\theta_p + \psi_p)\},\ \{kr(\theta_m' - \theta_p)\}]$$

In determinantal form, $\vec{R}_{mp} \times d\vec{L}_m$ can be written as

$$\vec{R}_{mp} \times d\vec{L}_m = d\theta_m' \begin{vmatrix} \vec{e}_x & \vec{e}_y & \vec{e}_z \\ \{r\cos(\theta_m' + \psi_m) - r\cos(\theta_p + \psi_p)\} & \{r\sin(\theta_m' + \psi_m) - r\sin(\theta_p + \psi_p)\} & kr(\theta_m' - \theta_p) \\ -r\sin(\theta_m' + \psi_m) & r\cos(\theta_m' + \psi_m) & kr \end{vmatrix}$$

where $\vec{e}_x$, $\vec{e}_y$, $\vec{e}_z$ are unit vectors in the Cartesian x, y and z directions, respectively.

Therefore, the expressions for the induced velocities are

$$\vec{U}_p \cdot \vec{e}_x = \sum_{m=1}^{n} \frac{\Gamma_m}{4\pi} \int_{\theta_m' = -\infty}^{\theta_m' = +\infty} \frac{kr^2[\sin(\theta_m' + \psi_m) - \sin(\theta_p + \psi_p) - (\theta_m' - \theta_p)\cos(\theta_m' + \psi_m)]}{[2r^2 - 2r^2\cos(\theta_m' - \theta_p + \psi_m - \psi_p) + k^2 r^2(\theta_m' - \theta_p)^2]^{3/2}} d\theta_m'$$

$$\vec{U}_p \cdot \vec{e}_y = \sum_{m=1}^{n} \frac{\Gamma_m}{4\pi} \int_{\theta_m' = -\infty}^{\theta_m' = +\infty} \frac{kr^2[\cos(\theta_p + \psi_p) - \cos(\theta_m' + \psi_m) - (\theta_m' - \theta_p)\sin(\theta_m' + \psi_m)]}{[2r^2 - 2r^2\cos(\theta_m' - \theta_p + \psi_m - \psi_p) + k^2 r^2(\theta_m' - \theta_p)^2]^{3/2}} d\theta_m'$$

$$\vec{U}_p \cdot \vec{e}_z = \sum_{m=1}^{n} \frac{\Gamma_m}{4\pi} \int_{\theta_m' = -\infty}^{\theta_m' = +\infty} \frac{r^2[1 - \cos(\theta_m' - \theta_p + \psi_m - \psi_p)]}{[2r^2 - 2r^2\cos(\theta_m' - \theta_p + \psi_m - \psi_p) + k^2 r^2(\theta_m' - \theta_p)^2]^{3/2}} d\theta_m'$$

The following simple transformation can be used to transform the Cartesian (x, y, z) velocities into cylindrical-polar (r, ϕ, z) velocities:

$$[\vec{U}_p \cdot \vec{e}_r] = [\vec{U}_p \cdot \vec{e}_x]\cos(\theta_p + \psi_p) + [\vec{U}_p \cdot \vec{e}_y]\sin(\theta_p + \psi_p)$$

$$[\vec{U}_p \cdot \vec{e}_\phi] = -[\vec{U}_p \cdot \vec{e}_x]\sin(\theta_p + \psi_p) + [\vec{U}_p \cdot \vec{e}_y]\cos(\theta_p + \psi_p)$$

The cylindrical-polar (r, ϕ, z) velocity components thus can

be written as

$$[\vec{U}_p \cdot \vec{e}_r] = \sum_{m=1}^{n} \frac{\Gamma_m}{4\pi} \int_{\theta'_m=-\infty}^{\theta'_m=+\infty} \frac{kr^2[\sin(\theta'_m - \theta_p + \psi_m - \psi_p) - (\theta'_m - \theta_p)\cos(\theta'_m - \theta_p + \psi_m - \psi_p)]}{[2r^2 - 2r^2\cos(\theta'_m - \theta_p + \psi_m - \psi_p) + k^2 r^2 (\theta'_m - \theta_p)^2]^{3/2}} d\theta'_m$$

$$[\vec{U}_p \cdot \vec{e}_\phi] = \sum_{m=1}^{n} \frac{\Gamma_m}{4\pi} \int_{\theta'_m=-\infty}^{\theta'_m=+\infty} \frac{kr^2[1 - \cos(\theta'_m - \theta_p + \psi_m - \psi_p) - (\theta'_m - \theta_p)\sin(\theta'_m - \theta_p + \psi_m - \psi_p)]}{[2r^2 - 2r^2\cos(\theta'_m - \theta_p + \psi_m - \psi_p) + k^2 r^2 (\theta'_m - \theta_p)^2]^{3/2}} d\theta'_m$$

$$[\vec{U}_p \cdot \vec{e}_z] = \sum_{m=1}^{n} \frac{\Gamma_m}{4\pi} \int_{\theta'_m=-\infty}^{\theta'_m=+\infty} \frac{r^2[1 - \cos(\theta'_m - \theta_p + \psi_m - \psi_p)]}{[2r^2 - 2r^2\cos(\theta'_m - \theta_p + \psi_m - \psi_p) + k^2 r^2 (\theta'_m - \theta_p)^2]^{3/2}} d\theta'_m$$

If, now, we define $x_{mp} \triangleq (\theta'_m - \theta_p)$

and $\psi_{mp} \triangleq (\psi_m - \psi_p)$

and transform the variable of integration, remembering that θ_p is constant, there results

$$[\vec{U}_p \cdot \vec{e}_r] = \sum_{m=1}^{n} \frac{\Gamma_m}{4\pi} \int_{-\infty}^{\infty} \frac{kr^2[\sin(x_{mp} + \psi_{mp}) - x_{mp}\cos(x_{mp} + \psi_{mp})]}{[2r^2 - 2r^2\cos(x_{mp} + \psi_{mp}) + k^2 r^2 x_{mp}^2]^{3/2}} dx_{mp}$$

$$[\vec{U}_p \cdot \vec{e}_\phi] = \sum_{m=1}^{n} \frac{\Gamma_m}{4\pi} \int_{-\infty}^{+\infty} \frac{kr^2[1 - \cos(x_{mp} + \psi_{mp}) - x_{mp}\sin(x_{mp} + \psi_{mp})]}{[2r^2 - 2r^2\cos(x_{mp} + \psi_{mp}) + k^2 r^2 x_{mp}^2]^{3/2}} dx_{mp}$$

$$[\vec{U}_p \cdot \vec{e}_z] = \sum_{m=1}^{n} \frac{\Gamma_m}{4\pi} \int_{-\infty}^{+\infty} \frac{r^2[1 - \cos(x_{mp} + \psi_{mp})]}{[2r^2 - 2r^2\cos(x_{mp} + \psi_{mp}) + k^2 r^2 x_{mp}^2]^{3/2}} dx_{mp}$$

Self Induction

Induced velocity components on any vortex, p, result from the sum of the induced velocities due to all n vortices. In each of the three expressions immediately above there is a term on the right-hand side corresponding to $m=p$. This term gives the self-induced velocity components for the p^{th} vortex. However, for $m=p$,

$$\psi_{pp} = \psi_p - \psi_p = 0$$

and at $x_{mp}=0$, the denominator becomes a zero of higher order than

the numerator, resulting in a singularity in the line integral. The difficulty is fundamental in that the Biot-Savart law is invalid in a vortex core, i.e., where viscous forces predominate.

Removal of the Singularity

If we assume that the vortex has a finite core of radius ε, the singularity in the Biot-Savart integral can be removed in several possible ways developed to a considerable extent in the literature. S. C. Crow [Reference 17] in his work with fixed wing trailing vortices eliminated the singularity by cutting the integral off at some arc length α_c on either side of the point where $|\vec{R}_{mp}| = 0$. He then subsequently determined α by taking it proportional to the radius ε of the vortex core and evaluating the constant of proportionality by reference to two similar problems whose solutions are known by other means. A similar technique has been used by Hama [References 18 and 19] for determining the progressive deformation of vortex filaments with initial curvature without and with, respectively, several kinds of initial perturbations. More recently, Widnall [Reference 16] used the method of matched asymptotic expansions to remove the singularity in the self-induction integrals by relating the problem for helices to that for two-dimensional circular vortex rings. Yet another method is to replace the denominator $[|\vec{R}_{pp}|^2]^{3/2}$ by $[|\vec{R}_{pp}|^2 + \varepsilon^2]^{3/2}$; this approach was used by Levy and Forsdyke [Reference 15] in their early work and more recently by P. C. Parks [Reference 20].

For this study a procedure similar to that of P. C. Parks was selected because a comparison with the Widnall results would provide some insights into the equivalence of different approaches and because complications are avoided in this approach when multiple interdigitated helices are considered. Thus, $[|\vec{R}_{pp}|^2]^{3/2}$ will be replaced by $[|\vec{R}_{pp}|^2 + \varepsilon^2]^{3/2}$ when self-induced velocities are calculated and subsequently in the perturbation equations.

Even with the treatment of singularities described above, another problem remains in the process of numerical integration, because the integrals behave almost as though they are singular so far as numerical evaluation is concerned. The evaluation and interpretation of integrals are therefore done by rewriting the integrand, adding and subtracting functions which have the same singularities numerically but which can be more easily treated analytically. This procedure will be discussed further in chapter 3 in connection with integration of the perturbation equations.

2.4 VORTICITY TRANSPORT THEOREM

In this analysis we have assumed a fluid of uniform density and zero viscosity and that elements of the vortex line move with fluid particles. If $\vec{r}$ denotes the position of points on a vortex line, the total derivative (Eulerian) of $\vec{r}$ is equal to the fluid velocity at that point.

If one is considering only those fluid velocities induced by the presence of vortices, then, mathematically, the vorticity transport theorem can be expressed as $\frac{d}{dt}(\vec{r}) = \vec{U}$ for points $\vec{r}$ on the vortex filaments.

A description of vorticity transport theorem can be found, for example, in the fluid dynamics book by G. K. Batchelor [Reference 21].

2.5 PERTURBATION EQUATIONS

Let the point (x_m, y_m, z_m) on the m^{th} vortex helix be perturbed to the positions $x_m+\delta x_m$, $y_m+\delta y_m$, $z_m+\delta z_m$. Here δx_m, δy_m and δz_m are considered to be first-order perturbations; i.e., their products, squares and higher powers can be neglected. The functional relationships for these perturbations can be written as

$$\delta x_m = \delta x_m(\theta_m, t)$$

$$\delta y_m = \delta y_m(\theta_m, t)$$

$$\delta z_m = \delta z_m(\theta_m, t)$$

where t is the time variable.

Now writing $\vec{r}_m = (x_m, y_m, z_m)$

and $\delta\vec{r}_m = (\delta x_m, \delta y_m, \delta z_m)$

the vorticity transport theorem thus gives, for the perturbed p^{th} vortex, $\frac{d}{dt}(\vec{r}_p + \delta\vec{r}_p) = \vec{U}_p(\vec{r}_p + \delta\vec{r}_p)$

where $\vec{U}_p(\vec{r}_p + \delta\vec{r}_p)$ is the induced velocity at point $\vec{r}_p + \delta\vec{r}_p$ on the perturbed p^{th} vortex.

The induced velocity, $\vec{U}_p$, is obtained by using the Biot-Savart law at the point $\vec{r}_p + \delta\vec{r}_p$ due to the system of vortex helices as modified by the perturbation displacements.

$$\vec{U}_p(\vec{r}_p + \delta\vec{r}_p) = \sum_{m=1}^{n} \frac{\Gamma_m}{4\pi} \int \frac{\vec{R}_{mp} \times d\vec{L}_m(\vec{r}_m + \delta\vec{r}_m)}{|\vec{R}_{mp}|^3}$$

where $$\vec{R}_{mp} = \vec{r}_m' - \vec{r}_p' + \delta\vec{r}_m' - \delta\vec{r}_p'$$

$$d\vec{L}_m = d\vec{L}_m(\vec{r}_m + \delta\vec{r}_m)$$

$$= [dx_m' + d(\delta x_m'),\ dy_m' + d(\delta y_m'),\ dz_m' + d(\delta z_m')]$$

The zeroth and first-order cross products are

$$[\vec{R}_{mp} \times d\vec{L}_m]_0 = (\vec{r}_m' - \vec{r}_p') \times \frac{\partial}{\partial\theta_m'}(\vec{r}_m')\, d\theta_m'$$

$$[\vec{R}_{mp} \times d\vec{L}_m]_1 = (\vec{r}_m' - \vec{r}_p') \times \frac{\partial}{\partial\theta_m'}(\delta\vec{r}_m')\, d\theta_m' + (\delta\vec{r}_m' - \delta\vec{r}_p') \times \frac{\partial}{\partial\theta_m'}(\vec{r}_m')\, d\theta_m'$$

We may now write

$$|\vec{R}_{mp}|^{-3} = [(x_m' - x_p + \delta x_m' - \delta x_p)^2 + (y_m' - y_p + \delta y_m' - \delta y_p)^2 + (z_m' - z_p + \delta z_m' - \delta z_p)^2]^{-3/2}$$

Defining the zeroth-order term expression as

$$|\vec{R}_{mp}|_0^{-3} = [(x_m' - x_p)^2 + (y_m' - y_p)^2 + (z_m' - z_p)^2]^{-3/2}$$

$$\triangleq J_{mp}^{-3/2}$$

and the first order term expression as

$$|\vec{R}_{mp}|_1^{-3} \triangleq J_{mp}^{-3/2}\left[1 + 2J_{mp}^{-1}\{(x_m' - x_p)(\delta x_m' - \delta x_p) + (y_m' - y_p)(\delta y_m' - \delta y_p) + (z_m' - z_p)(\delta z_m' - \delta z_p)\}\right]^{-3/2}$$

and expanding, retaining only first-order terms, yields

$$|\vec{R}_{mp}|_1^{-3} = -3 J_{mp}^{-5/2} K_{mp}$$

where K_{mp} is defined as

$$K_{mp} \triangleq (x_m' - x_p)(\delta x_m' - \delta x_p) + (y_m' - y_p)(\delta y_m' - \delta y_p) + (z_m' - z_p)(\delta z_m' - \delta z_p)$$

The corresponding zero and first-order induced velocity vectors(denoted by 0 and 1 subscripts) can be written as

$$[\vec{U}_p]_0 = \sum_{m=1}^{n} \frac{\Gamma_m}{4\pi} \int_{\theta_m'=-\infty}^{\theta_m'=+\infty} J_{mp}^{-3/2} [(\vec{r}_m' - \vec{r}_p) \times \frac{\partial}{\partial \theta_m'}(\vec{r}_m')] \, d\theta_m'$$

$$[\vec{U}_p]_1 = \sum_{m=1}^{n} \frac{\Gamma_m}{4\pi} \int_{\theta_m'=-\infty}^{\theta_m'=+\infty} J_{mp}^{-3/2} [(\vec{r}_m' - \vec{r}_p) \times \frac{\partial}{\partial \theta_m'}(\delta \vec{r}_m') + (\delta \vec{r}_m' - \delta \vec{r}_p) \times \frac{\partial}{\partial \theta_m'}(\vec{r}_m')] \, d\theta_m'$$

$$+ \sum_{m=1}^{n} \frac{\Gamma_m}{4\pi} \int_{\theta_m'=-\infty}^{\theta_m'=+\infty} -3 K_{mp} J_{mp}^{-5/2} [(\vec{r}_m' - \vec{r}_p) \times \frac{\partial}{\partial \theta_m'}(\vec{r}_m')] \, d\theta_m'$$

It will be convenient to carry out the calculations in terms of the helical coordinates, r and θ. Since the parametric equation for the m^{th} vortex helix is

$$x_m' = r \cos(\theta_m' + \psi_m)$$

$$y_m' = r \sin(\theta_m' + \psi_m)$$

$$z_m' = k r \theta_m'$$

the first-order displacement perturbation expressions can be written as

$$\delta x_m' = \delta r_m \cos(\theta_m' + \psi_m) - r \sin(\theta_m' + \psi_m) \delta \phi_m$$

$$\delta y_m' = \delta r_m \sin(\theta_m' + \psi_m) + r \cos(\theta_m' + \psi_m) \delta \phi_m$$

$$\delta z_m' = \delta z_m$$

The zeroth and first order terms of the numerator of the integrand in the x, y and z directions also can be written as

Zeroth order terms in the x direction

$$(y_m' - y_p)\frac{\partial}{\partial \theta_m'}(z_m') - (z_m' - z_p)\frac{\partial}{\partial \theta_m'}(y_m') = \{r\sin(\theta_m' + \psi_m) - r\sin(\theta_p + \psi_p)\}.kr$$

$$- kr^2(\theta_m' - \theta_p)\cos(\theta_m' + \psi_m)$$

First order terms in the x direction

$$(\delta y_m' - \delta y_p)\frac{\partial}{\partial \theta_m'}(z_m') - (\delta z_m' - \delta z_p)\frac{\partial}{\partial \theta_m'}(y_m') =$$

$$kr\left[\delta r_m \sin(\theta_m' + \psi_m) - \delta r_p \sin(\theta_p + \psi_p) + r\delta\phi_m \cos(\theta_m' + \psi_m) - r\delta\phi_p \cos(\theta_p + \psi_p)\right]$$

$$- (\delta z_m - \delta z_p).r\cos(\theta_m' + \psi_m)$$

$$(y_m' - y_p)\frac{\partial}{\partial \theta_m'}(\delta z_m') - (z_m' - z_p)\frac{\partial}{\partial \theta_m'}(\delta y_m') =$$

$$r\frac{\partial}{\partial \theta_m'}(\delta z_m)\left[\sin(\theta_m' + \psi_m) - \sin(\theta_p + \psi_p)\right] - kr(\theta_m' - \theta_p)\left[\frac{\partial}{\partial \theta_m'}(\delta r_m)\sin(\theta_m' + \psi_m)\right.$$

$$\left. + \delta r_m \cos(\theta_m' + \psi_m) + r\cos(\theta_m' + \psi_m)\frac{\partial}{\partial \theta_m'}(\delta\phi_m) - r\delta\phi_m \sin(\theta_m' + \psi_m)\right]$$

Zeroth order terms in the y direction

$$(z_m' - z_p)\frac{\partial}{\partial \theta_m'}(x_m') - (x_m' - x_p)\frac{\partial}{\partial \theta_m'}(z_m') =$$

$$- kr^2(\theta_m' - \theta_p)\sin(\theta_m' + \psi_m) - kr^2\{\cos(\theta_m' + \psi_m) - \cos(\theta_p + \psi_p)\}$$

First-order terms in the y direction

$$(\delta z_m' - \delta z_p)\frac{\partial}{\partial \theta_m'}(x_m') - (\delta x_m' - \delta x_p)\frac{\partial}{\partial \theta_m'}(z_m') =$$

$$-r(\delta z_m - \delta z_p)\sin(\theta_m' + \psi_m) - Rr[\delta r_m \cos(\theta_m' + \psi_m) - \delta r_p \cos(\theta_p + \psi_p)$$

$$-r\delta\phi_m \sin(\theta_m' + \psi_m) + r\delta\phi_p \sin(\theta_p + \psi_p)]$$

$$(z_m' - z_p)\frac{\partial}{\partial \theta_m'}(\delta x_m') - (x_m' - x_p)\frac{\partial}{\partial \theta_m'}(\delta z_m') =$$

$$Rr(\theta_m' - \theta_p)\left[\frac{\partial}{\partial \theta_m'}(\delta r_m)\cos(\theta_m' + \psi_m) - \delta r_m \sin(\theta_m' + \psi_m) - r\delta\phi_m \cos(\theta_m' + \psi_m)\right.$$

$$\left. - r\sin(\theta_m' + \psi_m)\frac{\partial}{\partial \theta_m'}(\delta\phi_m)\right] - r\frac{\partial}{\partial \theta_m'}(\delta z_m)[\cos(\theta_m' + \psi_m) - \cos(\theta_p + \psi_p)]$$

Zeroth-order terms in the z direction

$$(x_m' - x_p)\frac{\partial}{\partial \theta_m'}(y_m') - (y_m' - y_p)\frac{\partial}{\partial \theta_m'}(x_m') =$$

$$r^2\cos(\theta_m' + \psi_m)\{\cos(\theta_m' + \psi_m) - \cos(\theta_p + \psi_p)\} - r^2\sin(\theta_m' + \psi_m)\{\sin(\theta_m' + \psi_m) - \sin(\theta_p + \psi_p)\}$$

First-order terms in the z direction

$$(\delta x_m' - \delta x_p)\frac{\partial}{\partial \theta_m'}(y_m') - (\delta y_m' - \delta y_p)\frac{\partial}{\partial \theta_m'}(x_m') =$$

$$r\cos(\theta_m' + \psi_m)[\delta r_m \cos(\theta_m' + \psi_m) - \delta r_p \cos(\theta_p + \psi_p) - r\delta\phi_m \sin(\theta_m' + \psi_m)$$

$$+ r\delta\phi_p \sin(\theta_p + \psi_p)] + r\sin(\theta_m' + \psi_m)[\delta r_m \sin(\theta_m' + \psi_m)$$

$$- \delta r_p \sin(\theta_p + \psi_p) + r\delta\phi_m \cos(\theta_m' + \psi_m) - r\delta\phi_p \sin(\theta_p + \psi_p)]$$

$$(x'_m - x_p)\frac{\partial}{\partial \theta'_m}(\delta y'_m) - (y'_m - y_p)\frac{\partial}{\partial \theta'_m}(\delta x'_m) =$$

$$r[\cos(\theta'_m + \psi_m) - \cos(\theta_p + \psi_p)].\left[\frac{\partial}{\partial \theta'_m}(\delta r_m)\sin(\theta'_m + \psi_m) + \delta r_m \cos(\theta'_m + \psi_m)\right.$$

$$\left. - r\delta\phi_m \sin(\theta'_m + \psi_m) + r\cos(\theta'_m + \psi_m)\frac{\partial}{\partial \theta'_m}(\delta\phi_m)\right] - r[\sin(\theta'_m + \psi_m) - \sin(\theta_p + \psi_p)]$$

$$\left[\frac{\partial}{\partial \theta'_m}(\delta r_m)\cos(\theta'_m + \psi_m) - \delta r_m \sin(\theta'_m + \psi_m) - r\delta\phi_m \cos(\theta'_m + \psi_m) - r\sin(\theta'_m + \psi_m)\frac{\partial}{\partial \theta'_m}(\delta\phi_m)\right]$$

$$J^2_{mp} = 2r^2 - 2r^2\cos(\theta'_m - \theta_p + \psi_m - \psi_p) + k^2 r^2(\theta'_m - \theta_p)^2$$

$$K_{mp} = r\delta r_m\{1 - \cos(x_{mp} + \psi_{mp})\} + r\delta r_p\{1 - \cos(x_{mp} + \psi_{mp})\}$$

$$+ r^2\delta\phi_m \sin(x_{mp} + \psi_{mp}) - r^2\delta\phi_p \sin(x_{mp} + \psi_{mp})$$

$$+ kr\, x_{mp}\delta z_m - kr\, x_{mp}\delta z_p$$

Calculation of Terms on the Left Side of the Vortex Transport Perturbation Equation

$$x_p + \delta x_p = r\cos(\theta_p + \psi_p) + \delta r_p \cos(\theta_p + \psi_p) - r\sin(\theta_p + \psi_p)\delta\phi_p$$

$$\frac{d}{dt}(x_p + \delta x_p) = \dot{r}_p \cos(\theta_p + \psi_p) - r\dot{\phi}_p \sin(\theta_p + \psi_p) + \delta\dot{r}_p \cos(\theta_p + \psi_p)$$

$$- \delta r_p \dot{\phi}_p \sin(\theta_p + \psi_p) - \dot{r}_p \delta\phi_p \sin(\theta_p + \psi_p)$$

$$- r\dot{\phi}_p \delta\phi_p \cos(\theta_p + \psi_p) - r\delta\dot{\phi}_p \sin(\theta_p + \psi_p) \qquad (2)$$

$$y_p + \delta y_p = r\sin(\theta_p + \psi_p) + \delta r_p \sin(\theta_p + \psi_p) + r\delta\phi_p \cos(\theta_p + \psi_p)$$

$$\frac{d}{dt}(y_p + \delta y_p) = \dot{r}_p \sin(\theta_p+\psi_p) + r\dot{\phi}_p \cos(\theta_p+\psi_p) + \delta\dot{r}_p \sin(\theta_p+\psi_p)$$

$$+ \delta r_p \dot{\phi}_p \cos(\theta_p+\psi_p) + \dot{r}_p \delta\phi_p \cos(\theta_p+\psi_p)$$

$$+ r\delta\dot{\phi}_p \cos(\theta_p+\psi_p) - r\dot{\phi}_p \delta\phi_p \sin(\theta_p+\psi_p) \qquad (3)$$

$$\frac{d}{dt}(z_p + \delta z_p) = \frac{dz_p}{dt} + \delta\dot{z}_p \qquad (4)$$

We now resolve the velocity radially, circumferentially, and axially (i.e., in r, ϕ and z directions); these components will be defined as $\dot{\xi}_p$, $\dot{\eta}_p$ and $\dot{\zeta}_p$ respectively.

Multiplying equation (2) by $\cos(\theta_p+\psi_p+\delta\phi_p)$ and equation (3) by $\sin(\theta_p+\psi_p+\delta\phi_p)$ and remembering that

$$\cos(\theta_p+\psi_p+\delta\phi_p) = \cos(\theta_p+\psi_p) - \delta\phi_p \sin(\theta_p+\psi_p)$$

$$\sin(\theta_p+\psi_p+\delta\phi_p) = \delta\sin(\theta_p+\psi_p) + \delta\phi_p \cos(\theta_p+\psi_p)$$

we obtain the total radial velocity of the perturbed helix at P; thus:

$$\dot{\xi}_p = \dot{r}_p + \delta\dot{r}_p - r\dot{\phi}_p \delta\phi_p + r\dot{\phi}_p\delta\phi_p = \dot{r}_p + \delta\dot{r}_p$$

where $\dot{r}_p$ = zeroth-order radial velocity at P.

$\delta\dot{r}_p$ = first-order radial velocity at P.

Similarly, multiplying equation (2) by $-\sin(\theta_p+\psi_p+\delta\phi_p)$ and equation (3) by $\cos(\theta_p+\psi_p+\delta\phi_p)$, we obtain

$$\dot{\eta}_p = r\dot{\phi}_p - \dot{r}_p\delta\phi_p + \delta r_p\dot{\phi}_p + \dot{r}_p\delta\phi_p + r\delta\dot{\phi}_p$$

$$= r\dot{\phi}_p + \delta r_p\dot{\phi}_p + r\delta\dot{\phi}_p$$

where $r\dot{\phi}_p$ is the zeroth-order velocity and the remaining terms on the right-hand side represent first-order circumferential velocity.

Finally, $\dot{\zeta}_p = \dot{z}_p + \delta\dot{z}_p$

where $\dot{z}_p$ = zeroth-order axial velocity.

$\delta\dot{z}_p$ = first-order axial velocity.

Transformation of the Induced Velocities to Polar Form

The zeroth-order velocity in the x, y and z directions which result when the right side of equation (1) is expanded will be called U_{xp}, U_{yp} and U_{zp}, respectively, and the corresponding first-order velocity terms will be called δU_{xp}, δU_{yp} and δU_{zp}. Expressing the induced velocities also in terms of radial, circumferential, and axial components, and equating the left sides and right sides of equation (1) component by component yields

$$\dot{\xi}_p = \dot{r}_p + \delta\dot{r}_p = (U_{xp} + \delta U_{xp}) \cos(\theta_p + \psi_p + \delta\phi_p) + (U_{yp} + \delta U_{yp}) \sin(\theta_p + \psi_p + \delta\phi_p)$$

$$\dot{\eta}_p = r\dot{\phi}_p + \delta r_p\dot{\phi}_p + r\delta\dot{\phi}_p = -(U_{xp} + \delta U_{xp}) \sin(\theta_p + \psi_p + \delta\phi_p) + (U_{yp} + \delta U_{yp}) \cos(\theta_p + \psi_p + \delta\phi_p)$$

$$\dot{\zeta}_p = \dot{z}_p + \delta\dot{z}_p = U_{zp} + \delta U_{zp}$$

Now, separating zeroth-order and first-order terms, the vortex transport equations are obtained in terms of helical coordinates for unperturbed and first-order perturbed motion, as follows:

Zeroth-order (unperturbed) transport relations

$$\dot{r}_p = U_{xp} \cos(\theta_p + \psi_p) + U_{yp} \sin(\theta_p + \psi_p)$$

$$r\dot{\phi}_p = -U_{xp}\sin(\theta_p+\psi_p) + U_{yp}\cos(\theta_p+\psi_p)$$

$$\dot{z}_p = U_{zp}$$

First-order perturbation transport equations

$$\delta\dot{r}_p = -U_{xp}\,\delta\phi_p\sin(\theta_p+\psi_p) + U_{yp}\,\delta\phi_p\cos(\theta_p+\psi_p)$$

$$+ \delta U_{xp}\cos(\theta_p+\psi_p) + \delta U_{yp}\sin(\theta_p+\psi_p)$$

$$= r\dot{\phi}_p\,\delta\phi_p + \delta U_{xp}\cos(\theta_p+\psi_p) + \delta U_{yp}\sin(\theta_p+\psi_p)$$

$$\delta r_p\dot{\phi}_p + r\delta\dot{\phi}_p = -U_{xp}\,\delta\phi_p\cos(\theta_p+\psi_p) - U_{yp}\,\delta\phi_p\sin(\theta_p+\psi_p)$$

$$- \delta U_{xp}\sin(\theta_p+\psi_p) + \delta U_{yp}\cos(\theta_p+\psi_p)$$

$$= -\dot{r}_p\,\delta\phi_p - \delta U_{xp}\sin(\theta_p+\psi_p) + \delta U_{yp}\cos(\theta_p+\psi_p)$$

or

$$\delta\dot{r}_p = r\dot{\phi}_p\delta\phi_p + \delta U_{xp}\cos(\theta_p+\psi_p) + \delta U_{yp}\sin(\theta_p+\psi_p) \qquad (5)$$

$$r\delta\dot{\phi}_p = -\delta r_p\dot{\phi}_p - \dot{r}_p\,\delta\phi_p - \delta U_{xp}\sin(\theta_p+\psi_p) + \delta U_{yp}\cos(\theta_p+\psi_p) \qquad (6)$$

$$\delta\dot{z}_p = \delta U_{zp} \qquad (7)$$

Substituting for induced velocities and time rates of displacement, the unperturbed relations become

$$\dot{r}_p = \sum_{m=1}^{n}\frac{\Gamma_m}{4\pi}\int_{-\infty}^{\infty} kr^2\left\{\sin(x_{mp}+\psi_{mp}) - x_{mp}\cos(x_{mp}+\psi_{mp})\right\}J_{mp}^{-3/2}\,dx_{mp}$$

$$r\dot{\phi}_p = \sum_{m=1}^{n}\frac{\Gamma_m}{4\pi}\int_{-\infty}^{\infty} kr^2\left\{1-\cos(x_{mp}+\psi_{mp}) - x_{mp}\sin(x_{mp}+\psi_{mp})\right\}J_{mp}^{-3/2}\,dx_{mp}$$

$$\dot{z}_p = \sum_{m=1}^{n}\frac{\Gamma_m}{4\pi}\int_{-\infty}^{\infty} r^2\left\{1-\cos(x_{mp}+\psi_{mp})\right\}J_{mp}^{-3/2}\,dx_{mp}$$

Similarly, the first-order perturbation equations can be written as

$$\delta\dot{r}_p = \sum_{m=1}^{n} \frac{\Gamma_m}{4\pi} \int_{-\infty}^{\infty} J_{mp}^{-3/2} \Big[\{ -kr\, x_{mp} \sin(x_{mp}+\psi_{mp}) \frac{\partial}{\partial \theta_m'}(\delta r_m) - kr\, x_{mp}\, \delta r_m \cos(x_{mp}+\psi_{mp}) + kr\, \delta r_m \sin(x_{mp}+\psi_{mp}) \} + kr^2 \{ \delta\phi_m \cos(x_{mp}+\psi_{mp}) + x_{mp}\, \delta\phi_m \sin(x_{mp}+\psi_{mp}) - x_{mp} \frac{\partial}{\partial \theta_m'}(\delta\phi_m) \cos(x_{mp}+\psi_{mp}) - \delta\phi_p \cos(x_{mp}+\psi_{mp}) \} + r \{ -\delta\epsilon_m \cos(x_{mp}+\psi_{mp}) + \delta\epsilon_p \cos(x_{mp}+\psi_{mp}) + \frac{\partial}{\partial \theta_m'}(\delta t_m) \sin(x_{mp}+\psi_{mp}) \} \Big] dx_{mp}$$

$$- 3 \sum_{m=1}^{n} \frac{\Gamma_m}{4\pi} \int_{-\infty}^{\infty} J_{mp}^{-5/2} kr^2 \{ \sin(x_{mp}+\psi_{mp}) - x_{mp} \cos(x_{mp}+\psi_{mp}) \} K_{mp}\, dx_{mp} \qquad (8)$$

$$r\delta\dot{\phi}_p = \sum_{m=1}^{n} \frac{\Gamma_m}{4\pi} \int_{-\infty}^{\infty} J_{mp}^{-3/2} \Big[kr \{ x_{mp} \frac{\partial}{\partial \theta_m'}(\delta r_m) \cos(x_{mp}+\psi_{mp}) - \delta r_m \cos(x_{mp}+\psi_{mp}) - x_{mp}\, \delta r_m \sin(x_{mp}+\psi_{mp}) + \delta r_p \cos(x_{mp}+\psi_{mp}) + x_{mp}\, \delta r_p \sin(x_{mp}+\psi_{mp}) \} + kr^2 \{ -x_{mp} \frac{\partial}{\partial \theta_m'}(\delta\phi_m') \sin(x_{mp}+\psi_{mp}) - x_{mp}\, \delta\phi_m \cos(x_{mp}+\psi_{mp}) + \delta\phi_m \sin(x_{mp}+\psi_{mp}) - \delta\phi_p \sin(x_{mp}+\psi_{mp}) + x_{mp}\, \delta\phi_p \cos(x_{mp}+\psi_{mp}) \} + r \{ -\delta\epsilon_m \sin(x_{mp}+\psi_{mp}) + \delta\epsilon_p \sin(x_{mp}+\psi_{mp}) - \frac{\partial}{\partial \theta_m'}(\delta\epsilon_m) \cos(x_{mp}+\psi_{mp}) + \frac{\partial}{\partial \theta_m'}(\delta t_m) \} \Big] dx_{mp}$$

$$- 3 \sum_{m=1}^{n} \frac{\Gamma_m}{4\pi} \int_{-\infty}^{\infty} kr^2 J_{mp}^{-5/2} \cdot K_{mp} \left[1 - \cos(x_{mp}+\psi_{mp} - x_{mp} \sin(x_{mp}+\psi_{mp}) \right] dx_{mp} \qquad (9)$$

$$\delta\dot{z}_p = \sum_{m=1}^{n} \frac{\Gamma_m}{4\pi} \int_{-\infty}^{\infty} J_{mp}^{-3/2} \Big[r \Big\{ \frac{\partial}{\partial \theta_m'} (\delta r_m) \sin(x_{mp} + \psi_{mp}) + 2\delta r_m$$

$$- \delta r_m \cos(x_{mp} + \psi_{mp}) - \delta r_p \cos(x_{mp} + \psi_{mp}) \Big\}$$

$$+ r^2 \Big\{ \frac{\partial}{\partial \theta_m'} (\delta\phi_m) + \delta\phi_m \sin(x_{mp} + \psi_{mp}) - \cos(x_{mp} + \psi_{mp}) \frac{\partial}{\partial \theta_m'} (\delta\phi_m)$$

$$- \delta\phi_p \sin(x_{mp} + \psi_{mp}) \Big\} \Big] dx_{mp}$$

$$- \sum_{m=1}^{n} \frac{\Gamma_m}{4\pi} \int_{-\infty}^{\infty} J_{mp}^{-5/2} r^2 \{ 1 - \cos(x_{mp} + \psi_{mp}) \} K_{mp} \, dx_{mp} \qquad (10)$$

Removal of Singularities

As explained in Section 2.3.2, the integrand that provides the self-induced contribution to induced velocity becomes singular at $x_{mp} = 0$. This singularity is eliminated by changing the expression for J_{mp} from $\{2r^2 - 2r^2 \cos(x_{mp} + \psi_{mp}) + R^2 r^2 x_{mp}^2\}^{1/2}$

to $\{2r^2 - 2r^2 \cos(x_{mp} + \psi_{mp}) + R^2 r^2 x_{mp}^2 + \varepsilon_o^2\}^{1/2}$

when $m = p$. Here ε_o is the vortex core radius and is small compared to the radius r of the helix. Note, however, that when $m \neq p$, the expression for J_{mp} remains unmodified.

2.6 TYPE OF PERTURBATIONS AND EIGENVALUE EQUATIONS

The integro-differential perturbation equations derived in Section 2.5 admit solutions of the exponential type, for perturbations $\delta\vec{r}_m$; that is,

$$\delta\vec{r}_m = \hat{\delta\vec{r}}_m e^{\alpha t + i\omega\theta'_m} \tag{11}$$

or in component form

$$\delta r_m = \hat{\delta r}_m e^{\alpha t + i\omega\theta'_m}$$

$$\delta\phi_m = \hat{\delta\phi}_m e^{\alpha t + i\omega\theta'_m}$$

$$\delta z_m = \hat{\delta z}_m e^{\alpha t + i\omega\theta'_m}$$

where $\delta\vec{r}_m$ = vector perturbation of the m^{th} vortex having δr_m, $\delta\phi_m$ and δz_m as its components in the r, ϕ and z directions.

α = exponential growth rate factor, complex.

ω = wave number* of the perturbation.

In principle, no generality is lost in considering such solutions, since an arbitrary perturbation can be synthesized from these by Fourier Integration. In practice, the numerical work will, of course, deal with a limited number of wavelengths. The exponential form assumed in the solutions of perturbation equations (8), (9), and (10) allows this set of integro-differential equations to be written as a set of linear algebraic equations in the amplitudes of the perturbation components $\hat{\delta r}_m$, $\hat{\delta\phi}_m$, $\hat{\delta z}_m$. The spatial derivatives of the solution forms are given by

$$\frac{\partial}{\partial\theta'_m}(\delta r_m) = \frac{\partial}{\partial\theta'_m}\left[\hat{\delta r}_m e^{\alpha t + i\omega\theta'_m}\right] = i\omega\,\delta r_m$$

---

* The inverse of the wavelength, i.e., number of waves per helix turn.

and

$$\frac{\partial}{\partial \theta_m'}(\delta\phi_m) = i\omega\,\delta\phi_m$$

$$\frac{\partial}{\partial \theta_m'}(\delta t_m) = i\omega\,\delta t_m$$

Also, the first-order displacement perturbation components can be rewritten as

$$\delta r_m = \delta\hat{r}_m e^{\alpha t + i\omega\theta_m'} = \delta\hat{r}_m e^{\alpha t + i\omega\theta_m' - i\omega\theta_p + i\omega\theta_p}$$

$$= \delta\hat{r}_m e^{\alpha t + i\omega\theta_p} e^{i\omega x_{mp}}$$

$$\delta\phi_m = \delta\hat{\phi}_m e^{\alpha t + i\omega\theta_p} e^{i\omega x_{mp}}$$

$$\delta t_m = \delta\hat{t}_m e^{\alpha t + i\omega\theta_p} e^{i\omega x_{mp}} \qquad (12)$$

Substituting equations (12) into the perturbation equations (8), (9) and (10) and defining $y_{mp} \triangleq x_{mp} + \psi_{mp}$ yields the following eigenvalue equations:

$$\frac{4\pi\alpha\,\delta\hat{r}_p}{\Gamma} = \sum_{m=1}^{n} \int_{-\infty}^{\infty} J_{mp}^{-3/2} \Big[kr\,\delta\hat{r}_m \{\omega x_{mp} \sin y_{mp} \sin \omega x_{mp} - x_{mp} \cos y_{mp} \cos \omega x_{mp} + \sin y_{mp} \cos \omega x_{mp}\} + ikr\,\delta\hat{r}_m \{-\omega x_{mp} \sin y_{mp} \cos \omega x_{mp} - x_{mp} \cos y_{mp} \sin \omega x_{mp} + \sin y_{mp} \sin \omega x_{mp}\} + kr^2 \delta\hat{\phi}_m \{\cos y_{mp} \cos \omega x_{mp} + x_{mp} \sin y_{mp} \cos \omega x_{mp} + \omega x_{mp} \cos y_{mp} \sin \omega x_{mp}\} + ikr^2 \delta\hat{\phi}_m \{\cos y_{mp} \sin \omega x_{mp} + x_{mp} \sin y_{mp} \sin \omega x_{mp} - \omega x_{mp} \cos y_{mp} \cos \omega x_{mp}\} + r\,\delta\hat{t}_m \{-\cos y_{mp} \cos \omega x_{mp} - \omega \sin y_{mp} \sin \omega x_{mp}\} + ir\,\delta\hat{t}_m \{-\cos y_{mp} \sin \omega x_{mp} + \omega \sin y_{mp} \cos \omega x_{mp}\} + kr^2 \delta\hat{\phi}_p \{-\cos y_{mp} - x_{mp} \sin y_{mp}\}$$

$$+ r\delta\hat{z}_p \cos x_{mp}\Big] dx_{mp}$$

$$-3\sum_{m=1}^{n}\int_{-\infty}^{\infty} J_{mp}^{-5/2}\Big[kr^2\{\sin y_{mp} - x_{mp}\cos y_{mp}\}\Big].\Big[r\delta r_m$$

$$\{(1-\cos y_{mp})\cos\omega x_{mp} + i(1-\cos y_{mp})\sin\omega x_{mp}\}$$

$$+ r^2\delta\hat{\phi}_m\{\sin y_{mp}\cos\omega x_{mp} + i\sin y_{mp}\sin\omega x_{mp}\}$$

$$+ kr\delta\hat{z}_m\{+ x_{mp}\cos\omega x_{mp} + ix_{mp}\sin\omega x_{mp}\}$$

$$+ r\delta\hat{r}_p\{1-\cos y_{mp}\} - r^2\delta\hat{\phi}_p\{\sin y_{mp}\} - kr\delta\hat{z}_p x_{mp}\Big] dx_{mp}$$

— (13)

Similarly,

$$\frac{4\pi r\alpha\delta\hat{\phi}_p}{\Gamma} = \sum_{m=1}^{n}\int_{-\infty}^{\infty} J_{mp}^{-3/2}\Big[kr\delta\hat{r}_m\{-\omega x_{mp}\cos y_{mp}\sin\omega x_{mp}$$

$$- \cos y_{mp}\cos\omega x_{mp} - x_{mp}\sin y_{mp}\cos\omega x_{mp}\}$$

$$+ ikr\delta\hat{r}_m\{\omega x_{mp}\cos y_{mp}\cos\omega x_{mp} - \cos y_{mp}\sin\omega x_{mp}$$

$$- x_{mp}\sin y_{mp}\sin\omega x_{mp}\} + kr\delta\hat{r}_p\{\cos y_{mp} + x_{mp}\sin y_{mp}\}$$

$$+ kr^2\delta\hat{\phi}_m\{\omega x_{mp}\sin y_{mp}\sin\omega x_{mp} - x_{mp}\cos y_{mp}\cos\omega x_{mp}$$

$$+ \sin y_{mp}\cos\omega x_{mp}\} + ikr^2\delta\hat{\phi}_m\{-\omega x_{mp}\sin y_{mp}\cos\omega x_{mp}$$

$$- x_{mp}\cos y_{mp}\sin\omega x_{mp} + \sin y_{mp}\sin\omega x_{mp}\}$$

$$- kr^2\delta\hat{\phi}_p\{\sin y_{mp} - x_{mp}\cos y_{mp}\} + r\delta\hat{z}_m\{-\sin y_{mp}\cos\omega x_{mp}$$

$$+ \omega\cos y_{mp}\sin\omega x_{mp} - \omega\sin\omega x_{mp}\} + ir\delta\hat{z}_m$$

$$\{-\sin y_{mp}\sin\omega x_{mp} - \omega\cos y_{mp}\cos\omega x_{mp} + \omega\cos\omega x_{mp}\}$$

$$+ r\delta\hat{z}_p\sin y_{mp}\Big] dx_{mp}$$

$$-3\sum_{m=1}^{n}\int_{-\infty}^{\infty} J_{mp}^{-5/2}\Big[kr^2\{1-\cos y_{mp} - x_{mp}\sin y_{mp}\}\Big].\Big[r\delta\hat{r}_m$$

$$\{+(1-\cos y_{mp})\cos\omega x_{mp} + i(1-\cos y_{mp})\sin\omega x_{mp}\} + r^2\delta\hat{\phi}_m$$

$$\{+\sin y_{mp}\cos\omega x_{mp} + i\sin y_{mp}\sin\omega x_{mp}\} + kr\delta\hat{z}_m$$

$$\{+ x_{mp}\cos\omega x_{mp} + ix_{mp}\sin\omega x_{mp}\} + r\delta\hat{r}_p$$

$$\{+1-\cos y_{mp}\} + r^2\delta\hat{\phi}_p\{\sin y_{mp}\} - kr\delta\hat{z}_p x_{mp}\Big] dx_{mp} \quad — (14)$$

$$\frac{4\pi\alpha\delta\hat{z}_p}{\Gamma} = \sum_{m=1}^{n}\int_{-\infty}^{\infty}\Big[r\delta\hat{r}_m\{\omega\sin y_{mp}\sin\omega x_{mp} + 2\cos\omega x_{mp} - \cos y_{mp}\cos\omega x_{mp}\}$$

$$+ ir\delta\hat{r}_m\{-\omega\sin y_{mp}\cos\omega x_{mp} + 2\sin\omega x_{mp} - \cos y_{mp}\sin\omega x_{mp}\}$$

$$- r\delta\hat{r}_p\cos y_{mp} + r^2\delta\hat{\phi}_m\{-\omega\sin\omega x_{mp} + \sin y_{mp}\cos\omega x_{mp}$$

$$+ \omega\cos y_{mp}\sin\omega x_{mp}\} + ir^2\delta\hat{\phi}_m\{\omega\cos\omega x_{mp}$$

$$+ \sin y_{mp}\sin\omega x_{mp} - \omega\cos y_{mp}\cos\omega x_{mp}\}$$

$$+ r^2\delta\hat{\phi}_p\{-\sin y_{mp}\}\Big]\, dx_{mp}\cdot J_{mp}^{-3/2}$$

$$-3\sum_{m=1}^{n}\int_{-\infty}^{\infty} J_{mp}^{-5/2}\left[r^2(1-\cos y_{mp})\right].\left[r\delta r_m\{(1-\cos y_{mp})\cos\omega x_{mp}\right.$$

$$+ i(1-\cos y_{mp})\sin\omega x_{mp}\} + r^2\delta\hat{\phi}_m\{$$

$$+ \sin y_{mp}\cos\omega x_{mp} + i\sin y_{mp}\sin\omega x_{mp}\}$$

$$+ Rr\delta\hat{z}_m\{x_{mp}\cos\omega x_{mp} + ix_{mp}\sin\omega x_{mp}\} + r\delta\hat{r}_p$$

$$\{1-\cos y_{mp}\} - r^2\delta\hat{\phi}_p\{\sin y_{mp}\}$$

$$\left. - Rr\delta\hat{z}_p x_{mp}\right] dx_{mp} \qquad \text{——} \qquad (15)$$

2.7 STABILITY ANALYSIS

Equations (13) through (15) can be written for integer values of p ranging from 1 to n, where n corresponds to the number of interdigitated helices. After numerically evaluating the set of self and mutual induction integrals, a system of $3n$ eigenvalue equations is obtained. The limits of integration are from $-\infty$ to $+\infty$. The integrals in the perturbation equations are convergent, since both $J_{mp}^{-3/2}$ and $J_{mp}^{-5/2}$ vary as x_{mp}^{-3} and x_{mp}^{-5}, respectively, in the limit as x_{mp} approaches infinity.

Nevertheless, these integrals must be calculated numerically with some care and with proper treatment of the singularities. These techniques are discussed in the next chapter in more detail.

2.8 SYMMETRY CONSIDERATIONS FOR $n=2$

For two-bladed rotors, it is possible to separate symmetric and antisymmetric perturbation modes since the resulting eigenmatrix is symmetric. No such simple reduction in the order of the problem can be made for rotors with more than two blades, as the symmetry of the eigenmatrix is lost. The procedure is as follows: define $\underline{x}_1$ and $\underline{x}_2$ as the perturbation vectors for the first and second helix, respectively;

that is, $\underline{x}_1 \triangleq \begin{bmatrix} \delta\hat{r}_1 \\ r\delta\hat{\phi}_1 \\ \delta\hat{z}_1 \end{bmatrix}$ and $\underline{x}_2 \triangleq \begin{bmatrix} \delta\hat{r}_2 \\ r\delta\hat{\phi}_2 \\ \delta\hat{z}_2 \end{bmatrix}$

and $\underline{x} \triangleq \begin{bmatrix} \underline{x}_1 \\ \underline{x}_2 \end{bmatrix}$ as the perturbation vector of the matrix equation $\lambda \underline{x} = \underline{\underline{A}}\,\underline{x}$. Equations 13, 14, and 15 show that $\lambda \triangleq \frac{2\pi\alpha r^2}{\Gamma}$.

The eigenmatrix $\underline{\underline{A}}$ can be written in the form

$$\underline{\underline{A}} = \begin{bmatrix} \underline{\underline{A}}_{11} & \underline{\underline{A}}_{12} \\ \underline{\underline{A}}_{21} & \underline{\underline{A}}_{22} \end{bmatrix}$$

where $\underline{\underline{A}}_{11}$ and $\underline{\underline{A}}_{22}$ are 3x3 matrices and represent self induction for the first and second helix, respectively. $\underline{\underline{A}}_{12}$ and $\underline{\underline{A}}_{21}$ are the 3x3 matrices representing the mutual-inductance effects.

The eigenvalue equations can be expanded in the form

$$\lambda \underline{x}_1 = \underline{\underline{A}}_{11} \underline{x}_1 + \underline{\underline{A}}_{12} \underline{x}_2$$

$$\lambda \underline{x}_2 = \underline{\underline{A}}_{21} \underline{x}_1 + \underline{\underline{A}}_{22} \underline{x}_2$$

Consider a class of perturbations in which disturbance motions in one helix are repeated on another, but not necessarily at the same time. This kind of disturbance can be investigated by imposing the relationship $\underline{x}_1 = e^{i\Phi} \underline{x}_2$. In these circumstances, the above two equations remain compatible, since $\underline{\underline{A}}_{11} = \underline{\underline{A}}_{22}$ and $\underline{\underline{A}}_{12} = \underline{\underline{A}}_{21}$. Three eigenvalues can then be solved from

$$\lambda \underline{x}_2 = e^{i\Phi} \underline{\underline{A}}_{21} \underline{x}_2 + \underline{\underline{A}}_{22} \underline{x}_2 = (e^{i\Phi} \underline{\underline{A}}_{21} + \underline{\underline{A}}_{22}) \underline{x}_2$$

These eigenvalues will give maximum and minimum amplification rates for certain values of Φ. In Figure 2, divergence rates are plotted against the phase difference Φ. For $\Phi = 0$ or 2π, $\underline{x}_1 = \underline{x}_2$; for $\Phi = \pi$, $\underline{x}_1 = -\underline{x}_2$. Thus, these are cases of special symmetry: in the first case, perturbations in the two helices are of same magnitude and occur in same direction simultaneously; in the second case, they are of the same magnitude but occur in opposite directions at the same time.

These special cases have been incorporated in the computer program for the increased efficiency afforded by that option. The full eigenmatrix, which does not involve the special symmetry combinations described above, has also been calculated for the two helix cases, and the results are identical.

CHAPTER 3

COMPUTER PROGRAM

3.1 GENERAL DESCRIPTION

The computer program for the stability analysis consists of a main program and integration and eigenvalue-analysis subroutines. The main program has three significant subparts, which can be described as follows. The first part deals with treatment of singularities for the self-induction integrals. The second part deals with integration and with obtaining the perturbation equations. The third part is that used for eigenvalue and eigenfunction determination and printout. The three subparts of the main program and the subroutines will be described separately in more detail in subsequent sections.

The program is written in FORTRAN IV language and has been run on an IBM360/65 computer. Double precision, i.e., operation with 16 significant digits, has been used in the integration and in the portion of the program eliminating the singularity. The rest of the program and subroutines are in single precision, i.e., operations in which 8 significant digits are carried. Wherever a "substitute function" approximation has been made, numerical checks have been made to insure that a more complete approximation would not change the eigenvalues to within the last 5 significant digits. A block diagram for the computer program is shown in Figure 3.

3.2 TREATMENT OF SINGULARITIES IN THE SELF-INDUCTION INTEGRALS

As explained in Section 2.3.2, the singularities in self-induction integrals have been eliminated by considering that the vortex cores have a finite size. That is, the term

$$J_{pp}^{-3/2} = [2r^2 - 2r^2\cos(\alpha_{pp} + \psi_{pp}) + k^2 r^2 x_{pp}^2]^{-3/2}$$

has been changed to $J_{pp}^{-3/2} = [2r^2 - 2r^2\cos(\alpha_{pp} + \psi_{pp}) + k^2 r^2 x_{pp}^2 + \varepsilon_0^2]^{-3/2}$.

Although classical singular behavior of the integral has been eliminated by this modification, the integral is still quite sensitive to numerical evaluation. Figures 4 and 5 show some of the integrands which occur in the perturbation equations. The former exhibits near singular behavior at $\alpha_{mp} = 0$.

As noted earlier, numerical evaluation of the integrals has been accomplished by adding or subtracting functions which can eliminate the troublesome near-singular behavior of the integrands and which can themselves be integrated in closed form. The following are eight such integrals which have been found useful in dealing with numerical difficulties, together with their analytically integrated values.

Denote $$a^2 \triangleq \frac{\varepsilon^2}{(1+k^2)}$$

and $$z \triangleq \sinh^{-1}\left(\frac{xU}{a}\right)$$

where xU = some upper limit to be chosen.

$$I_1 = (1+k^2)^{-3/2}\int_0^{xU}\frac{dx}{(x^2+a^2)^{3/2}} = \frac{(1+k^2)^{-3/2}}{a^2}\tanh z = \frac{1}{\varepsilon^2\sqrt{1+k^2}}\tanh z$$

$$I_2 = (1+k^2)^{-3/2}\int_0^{xU}\frac{x\,dx}{(x^2+a^2)^{3/2}} = \frac{1}{(1+k^2)}\left[\frac{1}{\varepsilon} - \frac{1}{\{(1+k^2)(xU)^2+\varepsilon^2\}^{1/2}}\right]$$

$$I_3 = (1+k^2)^{-3/2}\int_0^{xU}\frac{x^2dx}{(x^2+a^2)^{3/2}} = (1+k^2)^{-3/2}\left[z - \tanh z\right]$$

$$I_4 = (1+k^2)^{-5/2}\int_0^{xU}\frac{dx}{(x^2+a^2)^{5/2}} = \frac{1}{\varepsilon^4(1+k^2)^{1/2}}\left[\tanh z - \tfrac{1}{3}\tanh^3 z\right]$$

$$I_5 = (1+k^2)^{-5/2}\int_0^{xU}\frac{x\,dx}{(x^2+a^2)^{5/2}} = \frac{1}{3(1+k^2)}\left[\frac{1}{\varepsilon^3} - \frac{1}{\{(1+k^2)(xU)^2+\varepsilon^2\}^{3/2}}\right]$$

$$I_6 = (1+k^2)^{-5/2}\int_0^{xU}\frac{x^2dx}{(x^2+a^2)^{5/2}} = \frac{1}{3a^2}\left[\tanh^3 z\right]$$

$$I_7 = (1+k^2)^{-5/2}\int_0^{xU}\frac{x^3dx}{(x^2+a^2)^{5/2}} = \frac{1}{(1+k^2)^2}\left[\frac{2}{3\varepsilon} - \frac{1}{\{(1+k^2)(xU)^2+\varepsilon^2\}^{3/2}} + \frac{\varepsilon^2}{3\{(1+k^2)(xU)^2+\varepsilon^2\}^{3/2}}\right]$$

$$I_8 = (1+k^2)^{-5/2}\int_0^{xU}\frac{x^4dx}{(x^2+a^2)^{5/2}} = \frac{1}{(1+k^2)^2}\left[z - \tanh z - \tfrac{1}{3}\tanh^3 z\right]$$

In Figure 6, the dashed curve II shows the plot of one of the singular integrals plotted after subtracting these analytical functions in the range 0 to 2π. Since x_0 is an arbitrary upper limit on the above integrals, it is chosen such that the addition and subtraction mentioned above will be carried out only in the region where the original integrand is nearly singular.

It can be seen that, for small values of x_{pp}, the modified function

$$J_{pp} \cong [2r^2 - 2r^2(1 - \tfrac{x_{pp}^2}{2}) + k^2 r^2 x_{pp}^2 + \varepsilon_0^2]$$

$$\cong [(1+k^2) r^2 x_{pp}^2 + \varepsilon_0^2] = (1+k^2)[r^2 x_{pp}^2 + \frac{\varepsilon_0^2}{(1+k^2)}]$$

Similarly, if in the numerator one makes the approximation $\cos x_{pp} \cong 1$ and $\sin x_{pp} \cong x_{pp}$, the perturbation integrals take the form of one of the integrals I_1 to I_6. Therefore, the perturbation integrals behave like integrals I_1 to I_8 in the neighborhood of $x_{pp} = 0$. Some idea of the errors involved in this approximation is gained by the comparison of perturbation integrand and modified perturbation integrand plotted in Figure 6.

The analytical integrals used to remove near-singular behavior labeled I_1 to I_8 and mentioned in the previous section have been denoted by symbols CO(1) to CO(8) in the computer program. The integrand of the perturbation integrals is thus modified by subtracting CO(1) to CO(8) from the appropriate integrands. The upper limit, XU, on the integrals I_1 to I_8 has been chosen to be 2π; beyond this, the perturbation integrals behave sufficiently smoothly to be amenable to standard numerical techniques.

M is the parameter which selects the overall integration limits on the perturbation integrals; M = 1 corresponds to semi-infinite integration limits, while M = 2 corresponds to doubly infinite integration limits.

The process of integrating the modified nonsingular expressions was tested by calculating some sample integrands against increasing x_{mp}, to determine a reasonable cutoff upper limit for infinite integrals. This limit is dependent upon the pitch of the helix. For a pitch of less than 0.2 radian, the integration has been performed up to $100\pi \approx 314$ radians. For pitch values between 0.2 and 0.4 radian, the cutoff upper limit was set at 70π. Finally, the cutoff limit for values of pitch ranging between 0.4 and 1.0 is 50π. Increasing the cutoff limit beyond the values specified above does not change eigenvalues to within five digits.

A combination of two numerical integration methods has been

used to balance accuracy and computer time. Since the major contributions to the integral are made when x_{mp} is small, a double precision Simpson's rule [see, for example, Hildebrand, Reference 22] has been used with an interval size limit of 14π. Between 14π and the appropriate cutoff upper limit, a double precision quadrature integration has been used. The quadrature integration technique is much faster, although less accurate. Parameter LI of the main program preselects between the two separate sets of integration subroutines. Also, the parameter LLI of the main program stops modifying the singular integrals beyond an upper limit of $XU = 2\pi$.

A short note regarding the quadrature integration technique is perhaps of some value. To compute

$$y = \int_{a_0}^{b_0} f(x)\,dx$$

by Gaussian quadrature formula, an n point expansion in terms of Legendre polynomials is used. First, transforming the range $x = a_0$ to b_0 into $\tau = -1$ to $+1$ by defining

$$\tau \triangleq \frac{2x-(a_0+b_0)}{(b_0-a_0)} \qquad \text{or} \qquad x = \frac{b_0-a_0}{2}\tau + \frac{b_0+a_0}{2}$$

there results

$$y = \frac{b_0-a_0}{2}\int_{-1}^{+1}\phi(\tau)d\tau \qquad \text{with} \qquad \phi(\tau) = f\left(\frac{b_0-a_0}{2}\tau + \frac{b_0+a_0}{2}\right)$$

Using

$$\int_{-1}^{1}\phi(\tau)d\tau = \sum_{k=1}^{n}\left[A_k^{(n)}\,\phi(t_k^{(n)})\right]$$

for some given n with coefficients $A_k^{(n)}$ and nodes $t_k^{(n)}$ (note that $t_k^{(n)}$ are the roots of Legendre polynomials of degree n), the result is the approximation

$$y_n = (b_0-a_0)\sum_{k=1}^{n}\left\{\frac{A_k^{(n)}}{2} f\left[(b_0-a_0)\frac{t_k^{(n)}}{2} + \frac{b_0+a_0}{2}\right]\right\}$$

which is exact whenever f(x) is a polynomial up to the degree $2n-1$.

In the present program the subroutine QG9 evaluates the integrals by means of a 12-point Gaussian quadrature formula which integrates polynomials up to degree 23 exactly. This subroutine is based on DQG12 taken from IBM publication System/360 Scientific Subroutine Package, Version III, Programmer's Manual. The nodes $t_k^{(n)}$ and coefficients $A_k^{(n)}$ used in QG9 are listed in Krylov [Reference 23]. IBM-supplied Scientific Subroutine Package DQG12 has been modified to collaborate with subroutine INTG, which supplies the integrand functions.

Test programs were run to check the convergence of integrated values. The upper limit on Simpson's rule, integration, the range of integration in one step of the Gaussian quadrature formula, the interval size in Simpson's rule, and the upper cut-off limits for the infinite integrals were all varied till the eigenvalues converged to five-digit accuracy for the range of parameters in the program.

3.3 FORMULATION OF EIGENVALUE EQUATIONS

The perturbation equations of Section 2.6 are a set of eigenvalue equations consisting of the growth rate terms on some p^{th} vortex. These growth rate terms are dependent upon the self-induced velocities due to perturbations in the position of the p^{th} vortex and the velocities induced by the remaining $(n - 1)$ vortices. Note that mutual-inductance terms influence the p^{th} vortex in two ways: first, by affecting the growth rate of perturbations on the p^{th} vortex due to velocity changes induced by deformations of the vortices other than the p^{th} vortex; and second, by inducing zeroth-order velocities on the p^{th} vortex which affects growth rate terms involving perturbations of the p^{th} vortex itself.

The terms associated with the m^{th} vortices and contributing to the growth rate of the p^{th} vortex differ from each other through the constant $\psi_{mp} = \psi_m - \psi_p$; values of this constant are

tabulated for each p and m in Table I. Each value of p and m corresponds to contributions of the perturbations of the m^{th} vortex to the growth rate of the p^{th} vortex. This contribution is accounted for in terms of a 3x3 matrix. It will not, however, be necessary to obtain, numerically, all $n \times n$ sets of 3x3 matrices.

Since the effect of some m^{th} vortex on the p^{th} vortex is dependent only upon the difference $\psi_m - \psi_p = \psi_{mp}$ rather than either ψ_m or ψ_p, the resulting symmetry considerations reduced the numerical work considerably. All the diagonal elements in Table I correspond to $\psi_{mp} = 0$; therefore, there is one such 3x3 matrix, representing self-induction effects in the three coordinate directions. All the super-diagonal elements correspond to the mutual inductance terms [$p=1$, $m=2$; $p=2$, $m=3$; . . .; $p = n-1$, $m=n$] and have $\psi_{mp} = \frac{2\pi}{n}$. These also need only be evaluated once instead of $(n-1)$ times. It follows that in order to obtain the complete system of eigenvalue equations, only $(2n-1)$ set of separate calculations need be made.

All of these reductions in the number of additional evaluations of eigenmatrix elements occur whether semi-infinite or doubly infinite vortices are considered. Further reductions in the number of calculations which must be performed are possible for the doubly infinite case, i.e., where $M = 2$, and such simplifications have been taken advantage of in the present investigation. Where the integration is from $-\infty$ to $+\infty$, all odd terms* drop out. Thus, for the $M=2$ case, calculations for $-\psi_{mp}$ and result in the same 3x3 matrix. In all the analyses in this report, therefore, the eigenvalue matrices are psuedosymmetric; that is, they are symmetric if one considers that the 3x3 submatrices are the eigenvalue matrix elements.

This set of n calculations is carried out by the computer program in terms of n values of the parameter K, as shown in Table II; the value of K corresponds to the number of matrix elements that must be calculated.

---

* Here "odd terms" refer to those which change sign in crossing zero on the axis of integration.

TABLE I. VALUES OF $\psi_{mp} = \psi_m - \psi_p$, THE PHASE DIFFERENCE CONSTANT FOR n-BLADED ROTOR

	m=1	m=2	m=3	---	m=n-1	m=n
p=1	0	$2\pi/n$	$4\pi/n$	---	$\frac{2\pi}{n}(n-2)$	$\frac{2\pi}{n}(n-1)$
p=2	$-2\pi/n$	0	$2\pi/n$	---	$\frac{2\pi}{n}(n-3)$	$\frac{2\pi}{n}(n-2)$
p=3	$-4\pi/n$	$-2\pi/n$	0	---	$\frac{2\pi}{n}(n-4)$	$\frac{2\pi}{n}(n-3)$
⋮	⋮	⋮	⋮	↖ 0 ↘	⋮	⋮
p=n-1	$-\frac{2\pi}{n}(n-2)$	$-\frac{2\pi}{n}(n-3)$	$-\frac{2\pi}{n}(n-4)$	---	0	$2\pi/n$
p=n	$-\frac{2\pi}{n}(n-1)$	$-\frac{2\pi}{n}(n-2)$	$-\frac{2\pi}{n}(n-3)$	---	$-2\pi/n$	0

$\psi_m = \frac{2\pi(m-1)}{n}$; m = 1 to n

$\psi_p = \frac{2\pi(p-1)}{n}$; p = 1 to n and $\psi_{mp} = \psi_m - \psi_p$

TABLE II. NO. OF MATRIX ELEMENTS RESULTING FROM EACH CALCULATION K

K	ψ_{mp}	p	m	No. of matrix elements resulting from this set of calculations
1	$\frac{2\pi(n-1)}{n}$	1	n	1
2	$\frac{2\pi(n-2)}{n}$	1 2	n-1 n	2
n-1	$\frac{2\pi}{n}$	1 2 ⋮ n-1	2 3 ⋮ n	n-1
n	0	1 2 ⋮ n	1 2 ⋮ n	n

3.4 EIGENVALUE ANALYSIS

For a set of n vortex helices, the perturbation equations are a set of $n \times n$ self- and mutual-inductance effects. Each of these $n \times n$ components in turn is a 3x3 matrix involving perturbations in the r, ϕ and z directions. The resulting perturbation equations, therefore, constitute a $3n \times 3n$ eigenmatrix, which must be solved to conduct the stability analysis. Each 3x3 matrix has complex elements. As suggested by use of the term "psuedo-symmetric" in the previous section, although the $n \times n$ array of matrix elements is symmetric, when the 3x3 matrix elements are inserted, the $3n \times 3n$ stability matrix is not symmetric.

The eigenmatrix equation which expresses the conditions for solution of admissible perturbation growth rates can be written as

$$\lambda \underline{x} = \underline{\underline{A}} \underline{x}$$

where $\underline{x}$ = $3n \times 1$ vector corresponding to the $3n$ perturbation displacement components.

$\underline{A}$ = nonsymmetric $3n \times 3n$ matrix with complex elements.

λ = eigenvalues of the above matrix equation; a set of $3n$ complex quantities, related to the dimensional growth rates and wave velocities of the perturbations, i.e., the complex quantity, α, by $\lambda = \frac{2\pi\alpha r^2}{\Gamma}$.

Solving this perturbation equation is a substantial task even with the help of a digital computer. $\underline{A}$ is nonsymmetric, has complex elements, and has the order 18x18 for a six-bladed rotor.

Considerable effort was expended in attempts to simplify the above matrix equation. Section 2.8 describes one such simplification for a two-bladed rotor. This, however, cannot be generalized for three-, four-, five-, and six-bladed rotors, since the structure of the eigenvalue matrix, $\underline{A}$, does not permit a transformation of the type

$$\underline{y}_p = \sum_{k=1}^{n} q_{kp} \underline{x}_k$$

where $\underline{y}_p$ = a new perturbation vector $(\delta r_p, r\delta\phi_p, \delta z_p)$ for the vortex.

$\underline{x}_k$ = a perturbation vector $(\delta r_k, r\delta\phi_k, \delta z_k)$ for the vortex.

q_{kp} = a set of scalars.

The subroutine labled 'ALLMAT' has been used to determine eigenvalues and eigenvectors. 'ALLMAT' is a FORTRAN IV subprogram that calculates the right eigenvalues* and/or eigenvectors of arbitrary complex matrices, using the QR algorithm and the Wielandt inverse power method for vectors.

Some discussion concerning the suitability of this subroutine, the technique used for calculations, and its numerical stability seems pertinent. The theoretical background for the QR algorithm may be found in numerical analysis texts, for example, Ralston [Reference 24] and Acton [Reference 25]. The function of the QR algorithm is to decompose an arbitrary, nonsymmetric complex matrix $\underline{A}$ into a product $\underline{Q}\underline{U}$, where $\underline{Q}$ is unitary and $\underline{U}$ is upper triangular. Since this method utilizes unitary

---

* If $\underline{A}$ is a nonsymmetric complex matrix and $\underline{A}^H$ denotes its Hermitian transpose, right eigenvectors $\underline{x}_i$ and left eigenvectors $\underline{y}_j$ are defined by relations $\underline{A}\underline{x}_i = \lambda_i \underline{x}_i$ and $\underline{y}_j^H \underline{A} = \lambda_j \underline{y}_j^H$ respectively.

transformations, as opposed to triangular decomposition, it tends to be numerically stable. An alternate approach to treating the complex matrix eigenvalue problem is to reduce the problem to one involving real matrices. This technique, however, doubles the order of the matrix, and for large-order matrices it is generally preferable to treat a complex matrix directly.

The complex subroutine 'ALLMAT' calculates the full set of eigenvalues ($3n$ in number), after the eigenmatrix elements have been evaluated for the specified values of the parameters k (pitch), ω (wave number of the perturbations) and ε (vortex core size specified as a fraction of helix diameter or radius) for an n-bladed rotor. These eigenvalues, in general, are complex. The real part of the eigenvalues determines the decay or the growth rates of the perturbations, thereby showing stability or instability, respectively. Positive real eigenvalues are, of course, unstable while negative real eigenvalues are stable. Eigenvalues with zero real parts are "neutrally stable". It is sufficient, therefore, to examine the eigenvalue with maximum real part to determine stability. The imaginary parts of the eigenvalues define the direction of propagation of the disturbances. An eigenvalue with a negative imaginary part corresponds to disturbances propagating in the positive θ direction.

The stability analysis results obtained in this study indicate that there are in all cases disturbances travelling in several directions with positive, negative and zero growth rates. In a linear stability analysis such as this, the unstable modes with the largest divergence rates very quickly dominate the disturbance shapes and determine the shape of the resulting distorted helices.

CHAPTER 4

RESULTS

4.1 GENERAL

This chapter presents three distinct kinds of material. The first consists of a discussion of the selection of cases and a physical description of the modal deflections. These are contained in Sections 4.2 and 4.3. The second consists of the results for special cases which were selected to help verify the theory and increase confidence in the numerical methods used in the present investigation. This material is contained in Sections 4.4 through 4.6. The third kind of material is comprised of results for two-, three-, four-, five-, and six-bladed rotors for various specific values of parameters of interest, such as the pitch of the helix, the wave number of perturbations, and core size. These results are presented in Sections 4.7 and 4.8 .

There is very little experimental evidence against which to check the predictions carried out in the present investigation of wake stability. However, some qualitative experimental results have been reported by Landgrebe [Reference 11] using a rotor model hover test facility. The object of Landgrebe's experiment was to measure the effect of parameters such as number of blades, blade linear twist, blade aspect ratio, rotor tip speed and collective pitch on rotor hover performance and the associated wake geometry characteristics. Flow visualization data were obtained by injecting smoke, and wake photographs and high-frame-speed movies were taken. Examination of the photographic results leads to the qualitative conclusion that the far-wake region of a hovering rotor is unstable or, at best, neutrally stable. These conclusions do not, at least, contradict the results of the present investigation.

4.2 SELECTION OF CASES TO BE RUN

In this section representative values of the pitch of the helix have been calculated under hovering conditions. Glauert, for example [Reference 1], and Payne [Reference 26] give the following equation for the induced velocity at the rotor in vertical flight.

$$(V_c + v_i)\, v_i = \frac{D/L}{2\rho}$$

where V_c = climb velocity.

v_i = increase in velocity at the actuator disc (induced velocity).

D/L = disc loading.

ρ = mass density of air = 0.0023 slug/ft^3 (sea level, std. day).

In hover, $V_c = 0$; therefore, $v_i = \sqrt{\frac{D/L}{2\rho}}$. The downward axial velocity in a fully developed slipstream V_t is given by

$$V_t = 2v_i = \sqrt{\frac{2D/L}{\rho}}$$

Typical helicopter disc loadings vary from 2 to 10 lb/ft^2, and typical tip speeds range from 500 to 700 ft/sec.

Thus, since average axial downwash velocity is given by

$$V_t = \sqrt{\frac{2(D/L)}{\rho}}$$

typical values vary from 40 ft/sec to 95 ft/sec.

A period for one rotor revolution is $T = \frac{2\pi}{\Omega}$, and axial displacement for one turn of the helix is $z = kr\theta = kr(2\pi)$.

Therefore,

$$\frac{2\pi}{\Omega} V_t = kr2\pi$$

or

$$k = \frac{V_t}{\Omega r} = \frac{\text{axial downwash speed}}{\text{tip speed of rotor}}$$

Thus values of pitch of the wake helix corresponding to typical disc loadings and tip speeds will vary from

$$\frac{40}{700} \cong 0.05 \quad \text{to} \quad \frac{95}{500} \cong 0.20$$

Although, as shown above, the pitch of the vortex helices corresponding to the normal extremes of hovering rotor operating conditions lies approximately between 0.05 and 0.20, the majority of results obtained here are for pitch equal to 0.1 radian. The ratio of vortex core diameter to the helix diameter, labeled in the tables given in this report as " core size", is, however, considerably more difficult to relate to reality. A paucity of experimental results or other evidence exists regarding actual vortex core size of the helices in the wake of a hovering rotor. The ratio of core radius to helix radius has been chosen here to be 0.1, following Widnall, and some cases have also been for this nondimensional core size equal to 0.33 to investigate the effect of core size on vortex stability. Perturbation wave numbers have been examined from 0.25 (long wavelengths) to 8.0 (short wavelengths), including the wave number of 0.0. Perturbation wavelengths which are very short compared to the helix diameter are likely to occur if the disturbances are concentrated and would seem to involve changes of vortex core cross section in the plane perpendicular to the helical filament centerline. Thomson [Reference 27], however, has shown that so long as the radius of the cross section of the core in the plane perpendicular to the filament centerline is small compared with the radius of curvature of that centerline, the cross section will remain approximately circular under the self-influence of the whole vortex. This same observation has been made by Widnall in her study of short wave perturbation instability modes of planar circular vortex rings [Reference 28]; however, a cutoff at rather large wave numbers was used to limit the extent of the stability curves in Reference 16. The core diameter ratio of 0.10 satisfies the assumption that the core size is small compared to helix radius; 0.33 does not. For the highest wave numbers, i.e., 8.0, even a core which is 0.1 helix diameter is hardly small compared to a wavelength of 0.393 helix diameter. Thus, in Figures 14 through 19 a wave number limit of about 8.0 is arbitrarily shown.

4.3 PHYSICAL DESCRIPTION OF MODAL DEFLECTIONS

A clear picture of modal perturbations will provide increased insight into instability mechanisms. The type of vector perturbations introduced in Section 2.6 is represented by

$$\vec{\delta r}_m = \vec{\delta \hat{r}}_m \, e^{\alpha t + i \omega \theta_m}$$

This deflection, of course, has components in r, ϕ and z directions. To visualize the deflections associated with certain wave numbers, consider a deformation of the type $\delta r = \delta \hat{r} \cos(\omega\theta) \cdot e^{\alpha t}$

where δr = perturbation in r direction.

$\delta\hat{r}$ = amplitude of the perturbation.

ω = the wave number.

The real parts of distortion modes in axial and circumferential directions can similarly be written as

$$\delta\phi = \delta\hat{\phi}\,[\cos\omega\theta]\,e^{\alpha t}$$

and

$$\delta z = \delta\hat{z}\,[\cos\omega\theta]\,e^{\alpha t}$$

Once the eigenfunctions $\delta\hat{\phi}$ and $\delta\hat{z}$ are known, the distorted shapes of the helices in these directions can be calculated for the corresponding wave number, ω .

Dilatational Mode, $\omega = 0$

For $\omega = 0$,

$$\delta r = \delta\hat{r}\,e^{\alpha t}$$

$$\delta\phi = \delta\hat{\phi}\,e^{\alpha t}$$

$$\delta z = \delta\hat{z}\,e^{\alpha t}$$

Since this perturbation is independent of θ, it is uniform throughout space. Whereas the z and ϕ coordinates simply change the position of given helix with respect to coordinate axes, the radial perturbations expand or contract the diameter of the vortex helix uniformly. The unperturbed helix is shown in Figure 1, and a dilatational mode disturbance is shown in Figure 7. Note that to simplify sketches of distorted wake shapes, in all cases, perturbations will be shown in only one direction in any one sketch. This can be done without sacrificing generality, so long as the reader keeps in mind that reference to more than one figure will generally be required to visualize a given modal deflection. Since this dilatational mode distorts the helix from its initial configuration only by uniform diameter changes, it is a disturbance which,

in a nondimensional sense, changes the helix pitch angle without changing the basic helical shape.

Deformation Mode for $\omega = 1$

For $\omega = 1$, the deformation shape can be pictured by noting that at

$$\theta = 0 \; ; \quad \delta r = \delta \hat{r} e^{\alpha t}, \quad \delta z = \delta \hat{z} e^{\alpha t}, \quad \delta \phi = \delta \hat{\phi} e^{\alpha t}$$

$$\theta = \frac{\pi}{2} \; ; \quad \delta r = 0 \quad , \quad \delta z = 0 \quad , \quad \delta \phi = 0$$

$$\theta = \pi \; ; \quad \delta r = -\delta \hat{r} e^{\alpha t}, \quad \delta z = -\delta \hat{z} e^{\alpha t}, \quad \delta \phi = -\delta \hat{\phi} e^{\alpha t}$$

$$\theta = \frac{3\pi}{2} \; ; \quad \delta r = 0 \quad , \quad \delta z = 0 \quad , \quad \delta \phi = 0$$

These deformations are sketched in Figures 8 and 9. As shown in the top and side views, there is some deformation of the initial circular shape of the helix as a result of perturbations in r direction, but in the main, it represents a relatively undistorted translation in a direction normal to the centerline axis of the helix. In the z-direction, however, these deformations amount to a tilting of the coils relative to the axis of the helix. This point has been elaborated in Section 4.4. Deformations in the ϕ or circumferential sense mainly stretch or compress the helical vortex line, and since in this analysis the cross section of the vortex core (i.e., normal to the helical axis) has been assumed to be constant, deformations in the circumferential sense can largely be ignored.

Distortion Mode Values of ω Other Than 0 or 1

Consider, for example, $\omega = 2$ at

$$\theta = 0 \; ; \quad \delta r = \delta \hat{r} e^{\alpha t}, \quad \delta z = \delta \hat{z} e^{\alpha t}, \quad \delta \phi = \delta \hat{\phi} e^{\alpha t}$$

$$\theta = \pi/2 \; ; \quad \delta r = -\delta \hat{r} e^{\alpha t}, \quad \delta z = -\delta \hat{z} e^{\alpha t}, \quad \delta \phi = -\delta \hat{\phi} e^{\alpha t}$$

$$\theta = \pi \; ; \quad \delta r = \delta \hat{r} e^{\alpha t}, \quad \delta z = \delta \hat{z} e^{\alpha t}, \quad \delta \phi = \delta \hat{\phi} e^{\alpha t}$$

$$\theta = 3\pi/2 \; ; \quad \delta r = -\delta \hat{r} e^{\alpha t}, \quad \delta z = -\delta \hat{z} e^{\alpha t}, \quad \delta \phi = -\delta \hat{\phi} e^{\alpha t}$$

The plan and side views of the helix distorted by radial and axial deformations in this mode are shown, respectively, in Figures 10 and 11. In Figure 10, the helix is shown to be distorted from circular to elliptic. In Figure 11, the distortions change the projections of the helical turns from straight lines to sickle-shaped curves, which are all either concave upward or concave downward, depending upon the sign of the deformation in the ξ direction.

Other Possible Distortion Modes

Distortion forms corresponding to higher integer and noninteger wave numbers can be similarly visualized. For example, the distorted shapes of two successive coils are quite different when $\omega = 1/2$, but such distortions are repeated after traversing every two coils of the helix. Similarly, for $\omega = 1.5$, three coils of the helix must be examined before one would expect to find a complete cycle. On the other hand, for $\omega = 3$, there will be three maximum and three minimum distortion points in one turn of helix. The $\omega = 1/2$ mode for r and ξ perturbations is shown in Figures 12 and 13a.

Extension of Modal Perturbation Modes to Multiple Interdigitated Helices

Each vortex helix in the array trailed by multibladed rotors can undergo the modal deformations discussed in the previous sections. In addition, however, the temporal phase relationship among the deformations in different helices provides three more possibilities of combinations of motions, one for each coordinate direction, for each additional helix. The actual phase and magnitude are determined by the eigen-solution. In the simplest possible example, two interdigitated helices may be undergoing a dilatational (i.e., $\omega = 0$) deformation, but with opposite sign, so that when one helix is expanding the other is contracting, and vice versa. Similarly, in a no-radial-deformation (i.e., $\omega = 1$) mode, the modal deformations for each helix of a two-bladed rotor may have the same sign, in which case the two helices would translate in the same direction, and the change in pitch angle would also be occurring in the same direction. In this case there would be no change in the relative positions of the two helices, one to the other. By contrast, if, in an $\omega = 1$ mode, the modal deformations of the two helices had opposite signs and equal magnitude, then the translation of each helix would be in opposite

directions and the effective pitch change of these helices would also be such as to reduce the axial distance between corresponding segments of the helices.

4.4 LEVY AND FORSDYKE CASE

The early Levy and Forsdyke analysis [Reference 15] cited earlier in this report concluded that a doubly infinite, constant-diameter helical vortex is unstable for the wave number = 1 mode when the helix pitch angle is less than 0.3 radian and is stable for pitch angles greater than 0.3 radian. Stability analyses for the same single helix case have also been carried out in the present study and have shown such a vortex to be stable in the wave number = 1 perturbation mode for all helix pitch angles. Some insight is gained by reference to the distortion shapes in this mode.

The $\omega = 1$ perturbation comes close to translating the whole helix to right, left, up, or down without much radial distortion. Such motion clearly is approximated by a change in the arbitrary choice of a coordinate axis system, and it cannot reasonably be expected to influence the tendency of the helix to distort. Such motion is depicted in Figure 8. However, deformations in the direction presented in Figure 9 for this mode are shown to be equivalent to tilting the coils relative to the axis of the helix. In this distortion, segments at any point on the helix always remain at the same distance from those segments in preceding or subsequent turns directly above and below them. With respect to their separation from vortex segments at different azimuthal stations on the helix, any given segment gets a bit closer to those on one "turn" and that same amount farther away from the corresponding segment on the next "turn". Thus, it is intuitively satisfying to find that such deformation modes are predicted to be stable.

Secondly, beyond those discrepancies in the Levy and Forsdyke results associated with the use of a planimeter, referred to earlier in this report, their evaluation of singular integrals expanded $\cos\omega$ and $\sin(x)$ terms in power series. Terms up to x^6 were retained in the numerators and terms up to x^2 were retained in the denominators. Since the upper and lower limits of integration are 0 to $\pi/6$ and the integrands are near singular in their behavior, considerable error is introduced by this

approximation. Table III lists cases run under the present investigation which may be compared with the results of Levy and Forsdyke [Reference 15]. In addition, selected integrals were calculated; most of the integrated values checked out, but errors as high as an order of magnitude were noted in others.

4.5 WIDNALL CASE OF SINGLE HELIX

The results recently published by Widnall [Reference 16] represent the stability of a single vortex filament of finite core for small sinusoidal displacements of its (helical) centerline. The singularity resulting from the self-induced motion of the element has been removed in Reference 16 by cutting off the integration in the region of the singularity and using a method of matched asymtotic expansions in this region. The solution in this region has been matched with the solution for a plane, circular vortex ring of the same radius of curvature. This mathematically sophisticated approach succesfully duplicated the results of Betchov [Reference 29] for the case of a vortex filament whose cross-sectional radius is very small compared to its radius of curvature. Numerical results for various pitch angles, core sizes and perturbation wave numbers have been reported by Widnall.

The special case of a single helix in the present study deals with the same physical situation as the work reported in Reference 16 but differs significantly in the treatment of singularities, as has been mentioned in chapter 2.

The results of the single helix cases run under the present study are plotted in Figure 14 and tabulated in Table IV along with the corresponding results obtained by Widnall. The table facilitates a direct comparison of the numerical results of this analysis with those of Widnall. One observes that the results are qualitatively similar, but that the numerical values of maximum divergence rates differ. In a typical case, for example, pitch = 0.1, wave number = 0.5 and core size = 0.33, Widnall predicts a divergence rate of 24.8 The corresponding value in the present analysis is 7.90. Note, however, that in the present investigation divergence rate is defined as $\frac{r^2}{\Gamma} 2\pi\alpha$, while in the Widnall study divergence rate is taken to be $\frac{r^2}{\Gamma} 4\pi\alpha$. Thus, for a comparison, the present value of 7.90 must be compared with (1/2)24.8 = 12.4. Thus, to facilitate comparisons on the same nondimensionalized basis, the divergence rates taken from the Widnall graphs have been divided

TABLE III. LEVY AND FORSDYKE CASE, COMPARISON WITH THE PRESENT STUDY

Wave Number	Core Size	Pitch	Stable or Unstable	
			Levy/Forsdyke Study	Present Study
1.00	0.10	0.10	Unstable	Stable
1.00	0.10	0.20	Unstable	Stable
1.00	0.10	0.25	Unstable	Stable
1.00	0.10	0.30	Stable or Unstable	Stable
1.00	0.10	0.40	Stable	Stable
1.00	0.10	0.60	Stable	Stable
1.00	0.10	0.80	Stable	Stable
1.00	0.10	1.00	Stable	Stable

TABLE IV. CASE OF SINGLE-BLADE, DIVERGENCE RATES OBTAINED IN THE PRESENT STUDY COMPARED WITH THE VALUES OBTAINED BY WIDNALL (Ref. 16*)

Pitch of Helix (rad)	Wave Number	Core Size = 0.1		Core Size = 0.33	
		Max. Divergence Rates in Present Study	Max. Divergence Rates Reported by Widnall	Max. Divergence Rates in Present Study	Max. Divergence Rates Reported by Widnall
0.1	0.00	~0.00	0.0 (0.0)	0.0	0.0 (0.0)
0.1	0.25	8.75	19.0 (9.5)	6.35	17.6 (8.8)
0.1	0.50	11.84	25.2 (12.6)	7.90	24.8 (12.4)
0.1	0.75	9.01	18.8 (9.4)	6.56	17.4 (8.7)
0.1	1.00	0.00	0.0 (0.0)	0.00	0.0 (0.0)
0.1	1.25	8.33	18.0 (9.0)	6.17	16.4 (8.2)
0.1	1.50	11.43	24.0 (12.0)	7.66	23.2 (11.6)
0.1	1.75	8.80	16.6 (8.3)	6.50	16.4 (8.2)
0.1	2.00	0.00	0.0 (0.0)	2.74	0.0 (0.0)
0.1	2.50	10.61	21.4 (10.7)	7.26	22.6 (11.3)
0.1	3.00	0.26	0.0 (0.0)	4.15	7.6 (3.8)
0.1	3.50	9.47	0.0 (0.0)	6.78	20.6 (10.3)
0.1	4.00	0.99	0.0 (0.0)	4.93	12.0 (6.0)
0.1	4.50	8.23	0.0 (0.0)	6.27	19.6 (9.8)
0.1	5.00	1.99	0.0 (0.0)	5.17	14.0 (7.0)
0.1	5.50	7.18	0.0 (0.0)	5.70	17.4 (8.7)
0.1	6.00	3.21	0.0 (0.0)	4.98	11.6 (5.8)
0.1	7.00	4.51	0.0 (0.0)	4.40	0.0 (0.0)
0.1	8.00	5.79	0.0 (0.0)	3.42	0.0 (0.0)

* The approximate divergence rates used in the above comparison were taken from the graphs in Ref. 16.

by a factor of 2 and written within the brackets in the same columns in Table IV. As pointed out in the previous paragraph, the results are significantly different for core size 0.33; the divergence rates compare quite closely, however, for core size 0.1. It has been noted that estimates of the core size of vortex helices in the wake of a hovering rotor are not known with any confidence, but a core diameter ratio of 0.1 would seem closer to reality than 0.33. Note that Landgrebe [Reference 11] assumed the core radius of 0.005, while Crimi [Reference 12] has used a value of 0.05 to 0.08 .

Some estimates of core size are, however, available for the vortices trailed by fixed-wing aircraft. Spreiter and Sacks [Reference 30] estimated the core diameter of vortices trailed behind elliptically loaded aircraft wings as 0.197 times the separation between the trailing vortices. The effect of curvature probably modifies the core size, but this estimate of core size falls somewhat closer to the 0.1 value used for helical vortices in the present study than it does to 0.33. For the smaller, more realistic core sizes, the present study with its different approach toward treatment of singularities in the Biot-Savart integration, appears to predict divergence rates quite comparable to the method used in the Widnall study.

4.6 S. C. CROW'S CASE (TRAILING VORTICES FROM FIXED-WING AIRCRAFT WINGS)

S. C. Crow [Reference 17] presents an analysis of the stability of a pair of straight, parallel vortices as trailed from a fixed-wing aircraft. This analysis also gives rise to an eigenvalue problem for the growth rate of sinusoidal perturbations.

If the pitch is allowed to approach infinity in the present study for the case of a two-bladed rotor, the wake should correspond to two straight, parallel infinite vortices. It is shown in Appendix I that the perturbation equations used here, taken to this limit, yield the same expressions as S. C. Crow's case, except for the differences associated with the cutoff technique to remove singularities. Incidentally, P. C. Parks [Reference 20] has duplicated S. C. Crow's results by modifying the self-induction integrals in lieu of "cutting off". Parks' integration to eliminate the effects of singular integrals yields the same expressions obtained in the present study, after the proper limits are taken, and has confirmed the essential features of Crow's theory with small numerical changes. Since the singularities in the self-induction integral have been removed in the present study by an approach similar to that used by P. C. Parks, it is reassuring that limiting expressions which are

approaching the case of trailing fixed-wing vortices do, in fact, duplicate those used by Parks.

It is a more difficult matter to attempt to duplicate S. C. Crow's quantitative results using the computer program developed in the present study, since the integration techniques used here are tailored for low values of pitch. In limiting cases where pitch is taken to be very large, the sine and cosine terms in the perturbation equations oscillate very rapidly, and the integrated values using the current numerical techniques are inappropriate for obtaining accurate results. Two cases, however, have been run, and the results are tabulated in Table V.

4.7 DISCUSSION OF RESULTS

Single Helix

The single-blade case was run primarily to check the present work against the results of Levy and Forsdyke [Reference 15] and Widnall [Reference 16]. The comparisons have been discussed in the preceding sections. Further consideration of the single helix case will be limited here to a discussion of the perturbation deflection shapes and their influence on helix stability. As shown in Figure 14, the single helix has no instabilities for wave numbers $\omega = 0$ and $\omega = 1$. Figures 7, 8, 9 and 13d show that radial and axial deflections for these two deformation modes have two characteristics in common: first, the circular cross section seen in the plan views is largely preserved, and second, axial separation between vortex segments at corresponding circumferential positions is preserved in the deformations. In terms of the Biot-Savart law of induction, it is clear that changes of the helix diameter, so long as they are uniform around the circumference, will cause uniform changes of induced effects. Further, if such deformations are repeated without change on every helix coil, then induced effects associated with changes in helix diameter will not distort the helix, but will simply cause the entire helix to translate axially. Since the choice of coordinate axes and their velocities in inertial space is completely arbitrary, it is not surprising that neither translation of the entire helix, such as exists in the plan view for $\omega = 1$, nor uniform change of the helix radius, as shown in the plan view of Figure 7 for $\omega = 0$, has any influence on the stability. Changes in the relative axial position of helix segments, however, will influence induced effects in the radial direction. For these two modes, however, there is no such change in relative position, at least among the

TABLE V. RESULTS OF THIS ANALYSIS FOR S. C. CROW'S CASE

Point 1				Point 2			
Eigenmatrix				Eigenmatrix			
0	0.92263	0	-0.91889	0	0.85992	0	-0.85935
-3.5407	0	-1.6991	0	-3.4780	0	-1.7587	0
0	+0.91889	0	-0.92263	0	0.85935	0	-0.85992
+1.6991	0	+3.5407	0	-1.7587	0	+3.4780	0

$\alpha_s = [(-0.92263 + 0.91889)(3.5407 - 1.6991)]^{1/2}$
$= [-\nu\epsilon]^{1/2}$ Stable.

$\alpha_s = [(-0.92263 - 0.91889)(3.5407 - 1.6991)]^{1/2}$
$= [-\nu\epsilon]^{1/2}$ Stable.

$\alpha_s = [(-0.85992 + 0.85935)(3.4780 - 1.7587)]^{1/2}$
$\cong 0$ Neutrally Stable.

$\alpha_s = [(-0.85992 - 0.85935)(3.4780 + 1.7587)]^{1/2}$
$= [-\nu\epsilon]^{1/2}$ Stable.

Point 1: Parameters in S. C. Crow's paper: $\beta = 2$, $\epsilon/\beta = 0.1$
Point 2: Parameters: $\beta = 0.5$, $\epsilon/\beta = 0.1$

corresponding parameters in present study

Point 1: Pitch = 1000, wave number = 1000, $\epsilon = 0.311$
Point 2: Pitch = 1000, wave number = 250, $\epsilon = 0.311$

Remarks: Numerical comparison of divergence rates with Crow's results for these points has not been shown here since the current program is not designed for such large values of pitch and wave numbers; as a result, the calculated values are not expected to be accurate. The purpose of the above run is to demonstrate the limiting behavior in the present study, which has otherwise been shown theoretically.

vortex segments closest to one another, that is, in the same circumferential position from one coil to the next. For $\omega = 1/2$, on the other hand, as shown in the side view of Figure 12, the relative axial displacements of vortex segments at the same circumferential position do, in fact, approach each other or separate from one another. Induced effects of some importance do, therefore, exist, and any initial tendency for adjacent segments to come together will be amplified still more by the increased proximity. One would certainly expect such modes to be unstable, and they are, as shown in Figure 14.

For the $\omega = 2$ mode, the plan view changes as shown in Figure 10 from circle to ellipse. Such changes induce axial velocities which are not uniform around the circumference. Furthermore, they will be such as to cause roughly the same displacement changes as seen in the side view of modal perturbations shown in Figure 10. These are not very strong effects, however, since for every pair of opposite segments which come together in the sense seen in the plan view (and thereby increase their mutually induced effects), there are two other segments which are farther apart, not just from each other, but from the first pair. Since the induced effects of the latter pair on the first pair are reduced, there are tendencies toward compensation. The separation distance is in the denominator of the Biot-Savart law, however, so that such effects are not linear. This possibly explains why the divergence rate in the $\omega = 2$ mode is less stable for the single helix whose vortex core diameter ratio is .33 than it is for the case where this parameter is .1, as shown in Figure 14.

Finally, Figure 11 shows that the modal perturbation for $\omega = 2$ preserves the axial separation between points at corresponding circumferential locations on the single helix.

Multiple-Bladed Rotors

It is important to note that the solution method for multiple-bladed rotors is identical to that for a single helix; namely, a wave number, ω, is selected, and the eigenmatrix is solved numerically for the values of λ which determine the divergence rates corresponding to the perturbation modes associated with that value of ω. There is, of course, an eigen deformation mode associated with each eigenvalue, λ. Components of the eigen mode for the single helix are the complex values of $\delta\hat{r}$, $\delta\hat{\phi}$ and $\delta\hat{z}$. Since the multibladed rotor introduces additional degrees of freedom, for the case of a rotor with n blades there are n sets of eigenvectors, $\delta\hat{r}_{i\lambda}$, $\delta\hat{\phi}_{i\lambda}$ and $\delta\hat{z}_{i\lambda}$, where $i = 1, 2, \ldots n$, for every eigenvalue, λ. The phase relationship between motions of the blades i = 1 and i = 2 is

embodied in the complex values, say, of $\hat{\delta z}_{1\lambda}$ and $\hat{\delta z}_{2\lambda}$; this phase relationship will determine whether the helix trailed from the number 1 blade will move toward or away from the helix trailed from the number 2 blade in the deformation eigenmode corresponding to λ . This phase relationship, between motions in the same coordinate direction at corresponding points on two different helices, cannot be known prior to solving the eigenvalue matrix. This contrasts with the case of a single helix, for which phase relations among segments at corresponding positions are known as soon as a value of ω is chosen.

Numerical results for multiple-bladed rotors are tabulated in Tables VI through X and are plotted in Figures 15 through 19. Most of these results are obtained with pitch = 0.1 and core size = 0.1. A few cases were run for pitch = 0.15 and core size = 0.33; these are also shown in the figures, although the curves vs wave number are largely extrapolated, using the curves for pitch = 0.1 and core size = 0.1 as guides.

For the case of a two-bladed rotor, the divergence rate, λ , is plotted vs wave number, ω , in Figure 15. It is noted that the maxima of the continuum of the divergence rate points decrease rather smoothly as wave number increases. Similarly the minima of the curves increase slightly and then decrease rather smoothly. For larger integer wave numbers, i.e., short wavelength perturbations, the difference between minimum and maximum divergence rates decreases as wave number increases. Figures 20 and 21 suggest that maximum divergence rates occur at integer wave numbers, because at these wave numbers the segments adjacent to each other on the two helices approach each other to the maximum extent. Minimum relative motion of this sort seems to occur with half-integer wave numbers. Imagining a helix from a second blade in Figure 13a with the most favorable phase angle possible shows how little of the vortices approach each other in such motion.

Figures 16 through 19, for three-, four-, five-, and six-bladed rotors, respectively, exhibit similar divergence rate - wave number relationships; i.e., the maximum and minimum divergence rates occur at wave numbers equal to 1/2 times even-integer multiples and 1/4 times odd-integer multiples, respectively, times the number of blades. For example, a five-bladed rotor exhibits maximum divergence rates at the wave numbers 2.5, 5.0 and 7.5, etc., which are 1/2, 1, and 3/2 times 5. Similarly, minimum divergence rates for a five-bladed rotor occur at wave numbers 1.25, 3.75 and 6.25, etc., which is 1/4, 3/4 and 5/4 times the number of blades in the rotor, namely, 5. For three-, four-, five- and six-bladed rotors, the excursion from the mean divergence rate also decreases with increasing wave numbers.

TABLE VI. MAXIMUM DIVERGENCE RATES FOR TWO-BLADED ROTOR

Pitch of Helix (rad)	Wave Number	Core Size	Max Divergence Rate
0.10	0.25	0.10	46.65
0.10	0.50	0.10	37.05
0.10	0.75	0.10	46.26
0.10	1.00	0.10	49.80
0.10	1.25	0.10	46.57
0.10	1.50	0.10	37.16
0.10	1.75	0.10	45.42
0.10	2.00	0.10	49.06
0.10	2.50	0.10	36.95
0.10	3.00	0.10	47.93
0.10	3.50	0.10	36.56
0.10	4.00	0.10	46.52
0.10	4.50	0.10	36.12
0.10	5.00	0.10	44.94
0.10	5.50	0.10	35.74
0.10	6.00	0.10	43.48
0.10	7.00	0.10	41.86
0.10	8.00	0.10	40.47
0.15	0.50	0.10	16.70
0.15	1.00	0.10	22.10
0.15	1.50	0.10	16.83
0.15	2.00	0.10	21.40
0.15	3.00	0.10	20.36
0.15	4.00	0.10	19.14
0.10	0.50	0.33	33.23
0.10	1.00	0.33	49.34
0.10	1.50	0.33	33.50
0.10	2.00	0.33	48.30
0.10	3.00	0.33	46.73
0.10	4.00	0.33	44.87

TABLE VII. MAXIMUM DIVERGENCE RATES FOR THREE-BLADED ROTOR

Pitch of Helix (rad)	Wave Number	Core Size	Max Divergence Rate
0.10	0.25	0.10	113.97
0.10	0.50	0.10	100.98
0.10	0.75	0.10	78.83
0.10	1.00	0.10	94.00
0.10	1.25	0.10	115.57
0.10	1.50	0.10	123.71
0.10	1.75	0.10	116.57
0.10	2.00	0.10	96.52
0.10	2.25	0.10	79.65
0.10	2.50	0.10	96.85
0.10	3.00	0.10	115.37
0.10	3.50	0.10	99.41
0.10	3.75	0.10	79.28
0.10	4.00	0.10	90.88
0.10	4.50	0.10	114.81
0.10	5.00	0.10	95.85
0.10	5.25	0.10	79.47
0.10	5.50	0.10	89.97
0.10	6.00	0.10	108.00
0.15	0.50	0.10	45.38
0.15	1.00	0.10	41.62
0.15	1.50	0.10	54.67
0.15	2.00	0.10	43.79
0.15	3.00	0.10	50.17
0.15	4.00	0.10	38.36
0.10	0.50	0.33	97.19
0.10	1.00	0.33	93.55
0.10	1.50	0.33	120.01
0.10	2.00	0.33	95.78
0.10	3.00	0.33	114.16
0.10	4.00	0.33	89.40

TABLE VIII. MAXIMUM DIVERGENCE RATES FOR FOUR-BLADED ROTOR

Pitch of Helix (rad)	Wave Number	Core Size	Max Divergence Rate
0.1	0.25	0.1	209.37
0.1	0.50	0.1	194.22
0.1	0.75	0.1	168.98
0.1	1.00	0.1	135.16
0.1	1.25	0.1	165.99
0.1	1.50	0.1	191.69
0.1	1.75	0.1	207.28
0.1	2.00	0.1	212.87
0.1	2.50	0.1	193.32
0.1	3.00	0.1	138.17
0.1	3.50	0.1	186.24
0.1	4.00	0.1	208.16
0.1	4.50	0.1	190.05
0.1	5.00	0.1	139.94
0.1	5.50	0.1	179.51
0.1	6.00	0.1	201.23
0.1	7.00	0.1	141.21
0.1	8.00	0.1	193.23
0.15	0.50	0.1	87.25
0.15	1.00	0.1	61.20
0.15	1.50	0.1	84.72
0.15	2.00	0.1	94.52
0.15	3.00	0.1	63.58
0.15	4.00	0.1	90.31

TABLE IX. MAXIMUM DIVERGENCE RATES FOR FIVE-BLADED ROTOR

Pitch of Helix (rad)	Wave Number	Core Size	Max Divergence Rate
0.10	0.25	0.10	332.56
0.10	0.50	0.10	315.78
0.10	0.75	0.10	288.09
0.10	1.00	0.10	250.72
0.10	1.25	0.10	219.68
0.10	1.50	0.10	252.93
0.10	1.75	0.10	282.58
0.10	2.00	0.10	307.43
0.10	2.50	0.10	340.74
0.10	3.00	0.10	311.15
0.10	3.50	0.10	256.42
0.10	3.75	0.10	220.27
0.10	4.00	0.10	242.70
0.10	4.50	0.10	302.72
0.10	5.00	0.10	327.21
0.10	5.50	0.10	307.83
0.10	6.00	0.10	253.02
0.10	6.25	0.10	220.94
0.10	7.00	0.10	290.84
0.10	7.50	0.10	316.34
0.10	8.00	0.10	298.76

TABLE X. MAXIMUM DIVERGENCE RATES FOR SIX-BLADED ROTOR

Pitch of Helix (rad)	Wave Number	Core Size	Max Divergence Rate
0.10	0.25	0.10	483.43
0.10	0.50	0.10	465.33
0.10	0.75	0.10	435.62
0.10	1.00	0.10	395.08
0.10	1.25	0.10	358.51
0.10	1.50	0.10	318.15
0.10	1.75	0.10	353.64
0.10	2.00	0.10	390.09
0.10	2.50	0.10	459.22
0.10	3.00	0.10	485.01
0.10	3.50	0.10	462.12
0.10	4.00	0.10	396.97
0.10	4.50	0.10	318.72
0.10	5.00	0.10	381.72
0.10	5.50	0.10	445.94
0.10	6.00	0.10	472.46
0.10	7.00	0.10	394.10
0.10	8.00	0.10	370.54

In short, peak values of divergence rate occur at wave numbers, ω, equal to integer multiples times one-half the number of blades, and in all cases the magnitude of the peak divergence rate decreases with wave number.

Enveloping curves can be drawn through maximum and minimum divergence rate points in all cases. There is some absolute maximum divergence rate which occurs at the maximum of the enveloping curve through the maximum divergence rate points. For two-, four- and six-bladed rotors this absolute maximum rate occurs at wave number 0.0, i.e., for the dilatational mode. For three- and five-bladed rotors the dilatational mode is still highly unstable, but the absolute maximum divergence rate occurs at wave numbers 1.5 and 2.5 respectively, i.e., where the wave number is one-half the number of blades ($\omega = n/2$).

To assess the effect of helix pitch angle, some variations in this parameter were run for two-, three-, and four-bladed rotors. For the higher pitch angles the divergence rate drops considerably, even though the characteristic variations with wave number remain. For example, an increase in pitch of helix from 0.10 to 0.15 reduces the divergence rate by a factor of almost 2. Note that the curves for pitch = 0.15 must be read on the right scales, as also pointed out in Figures 15 through 17. Physically, this behavior can be explained in terms of interaction between the neighboring coils of the helices. For higher pitch angles the neighboring helix coils are farther apart, and distortions that tend to cause neighboring coils to approach each other therefore result in lesser interactions. Absolute maximum divergence rates for different rotors are plotted against pitch in Figure 22 and are tabulated in Table XI.

The nondimensional divergence rate of multiple-bladed rotors would seem to increase with the number of blades for the same sort of reason that it increases with decreasing pitch; namely, there is a decreased separation between successive lines of vorticity. Figure 22 shows that for a helix pitch angle of .05, for example, a two-bladed rotor has a maximum divergence rate of 200 and a four-bladed rotor has a maximum divergence rate of 850. It must be noted that these rates are nondimensionalized by total vortex strength Γ, as shown in the equation for λ on pages 27 and 37. If the sum of the blades in each rotor produced the same lift (which is the case in comparing alternate designs for the same aircraft), the vortex strength, Γ, in the two-bladed case would be twice that of the four-bladed case, so that the dimensional rates would then compare as 400 to 850. Thus, in terms of the stability of the vortices in the far wake for rotors of equal lifting capacity, the fewer blades the better.

The effect of core size on stability is not so noticeable for multiple rotors. When the core size was increased from 0.1 to

TABLE XI. ABSOLUTE MAXIMUM DIVERGENCE RATES FOR MULTIBLADED ROTORS OF VARYING PITCH

Pitch of Helix (rad)	Number of Blades	Wave Number	Absolute Maximum Divergence Rates
0.05	2	0.0	199.89
0.10			50.05
0.15			22.34
0.20			12.65
0.05	3	1.5	492.11
0.10			123.71
0.15			54.67
0.20			30.47
0.05	4	0.0	853.90
0.10			214.57
0.15			96.17
0.20			54.70
0.05	5	2.5	1363.00
0.10			340.74
0.15			150.64
0.20			84.26
0.05	6	0.0	1940.50
0.10			489.65
0.15			219.78
0.20			125.26

0.33, the amplification rate dropped only about 2% for the wave numbers with highest divergence rates in all cases where $n = 1$. Core size does appear to be an important influence on stability of a single helix, i.e., where $n = 1$, as shown in Figure 14.. Its reduced effect on the stability of multiple-bladed rotors does not seem unreasonable, since the mutual inductance between different helices is a relatively important influence on the stability of interdigitated vortex systems, whereas variations in core size are felt most in self-induction effects.

4.8 COMMENTS ON ABSOLUTE MAXIMUM WAKE DIVERGENCE RATES FOR MULTIBLADED ROTORS WITH ODD AND EVEN NUMBERS OF BLADES

This section deals with a qualitative physical explanation of absolute maximum divergence rates for multibladed rotors. First, as seen in Figures 15 through 19, these absolute maxima are associated with the $\omega = 0$ and $\omega = n/2$ modes for rotors with even and odd numbers of blades respectively. Comments in most cases will be restricted to axial perturbation displacements since the effect on induced velocities of such motions is one order of magnitude higher than either radial or circumferential perturbation displacements insofar as the mutual inductance between neighboring coils is concerned. This can be explained more explicitly as follows:

The Biot-Savart law reveals that the maximum interaction occurs between those vortex elements which are nearest to each other. For helix pitch angles less than 0.20, the parallel elements which are closest to each other are on two neighboring coils at the same circumferential position, i.e., located on the same line parallel to the axial direction. This axial distance shall be denoted by d. A radial perturbation of ϵ in the radial direction will replace d by $\sqrt{d^2+\epsilon^2}$, and the integrand in the Biot-Savart law will be modified from d^{-3} to $d^{-3}[1+3\epsilon/d+\cdots]$, contributing a second-order term to the perturbation integrand. However, an axial perturbation of ϵ will modify the minimum interaction distance d to $(d-\epsilon)$, contributing $(d-\epsilon)^{-3}$ in the perturbation integrand. This corresponds to a change from d^{-3} to $d^{-3}[1+3\epsilon/d+\cdots\cdots]$ and is a first-order contribution. Therefore, the axial perturbation is the dominant factor in the interactions between the nearest parallel vortex elements. It follows that the divergence rate of a given deformation mode will be greater than another, if the normalized axial displacements which reduce the separation between vortex elements adjacent to their counterparts on neighboring coils take place over more of the arc lengths of the helix than the other deformation mode.

For the purpose of evaluating this intuitive notion pertaining to the absolute maximum wake instability of multibladed hovering rotors, an average distortion factor will be defined. This "average relative distortion" will be calculated for two- and three-bladed rotors for axial perturbations at the wave numbers where maximum instabilities occur. Subsequently, it will be used to explain why absolute maximum instability occurs at wave numbers 0.0 for rotors with an even number of blades, and at wave numbers 1.5 and 2.5 for rotors with an odd number of blades, i.e., three- and five-bladed rotors, respectively.

For the case of the three-bladed rotor, maximum instabilities occur at wave numbers 0.0 and 1.5. Eigenfunctions for the most unstable eigenvalues at these wave numbers are tabulated in Table XII, and the elevation views of the perturbed vortex system for only axial perturbations are sketched in Figures 23 and 24.

For a wave number of 0.0, eigenfunctions for helices 1, 2 and 3 are

$$\delta\hat{z}_1 = +1 \quad ; \quad \delta\hat{z}_2 = 0 \quad ; \quad \delta\hat{z}_3 = -1$$

The "average relative distortion" is defined as a line integral of the reduction in the axial displacement between vortex elements at the same circumferential position on neighboring coils evaluated around the azimuth.

Thus, the average relative distortion between the 1st and 3rd helices for period π is

$$\int_0^{\pi} d\theta + \int_0^{\pi} d\theta = 2\pi$$

The average relative distortion between the 3rd and 2nd helices for period π is

$$\int_0^{\pi} d\theta = \pi$$

and finally, the average relative distortion between the 2nd and 1st helices for period π is

$$\int_0^{\pi} d\theta = \pi$$

The total average relative distortion factor, therefore, is $4\pi = 12.57$.

For a wave number of 1.5, eigenfunctions for helices 1, 2 and 3 are

$$\delta\hat{z}_1 = +1 \quad ; \quad \delta\hat{z}_2 = -0.25 \quad ; \quad \delta\hat{z}_3 = +1$$

TABLE XII. EIGENFUNCTIONS FOR THE MOST UNSTABLE EIGENVALUES OF A THREE-BLADED ROTOR AT WAVE NUMBERS 0.0 AND 1.5, PITCH = 0.1 AND CORE SIZE = 0.1

Eigenfunction for Wave Number 0.0			Eigenfunction for Wave Number 1.5		
Label	Real	Imaginary	Label	Real	Imaginary
$\delta\hat{r}_1$	-1.000	0.000	$\delta\hat{r}_1$	-0.981	-0.005
$r\delta\hat{\phi}_1$	-0.076	0.000	$r\delta\hat{\phi}_1$	-0.073	-0.012
$\delta\hat{z}_1$	+0.996	0.000	$\delta\hat{z}_1$	+0.996	+0.004
$\delta\hat{r}_2$	0.000	0.000	$\delta\hat{r}_2$	+0.210	0.000
$r\delta\hat{\phi}_2$	0.000	0.000	$r\delta\hat{\phi}_2$	+0.016	+0.002
$\delta\hat{z}_2$	0.000	0.000	$\delta\hat{z}_2$	-0.248	+0.000
$\delta\hat{r}_3$	1.000	0.000	$\delta\hat{r}_3$	-0.981	-0.005
$r\delta\hat{\phi}_3$	0.076	0.000	$r\delta\hat{\phi}_3$	-0.073	-0.012
$\delta\hat{z}_3$	-0.996	0.000	$\delta\hat{z}_3$	+0.996	+0.004

Referring to Figure 24, the following distortion factors can be calculated.

The average relative distortion between 1st and 3rd helices for period π is

$$\int_0^{\pi/3} [\,|\sin(1.5\theta)| + |\cos(1.5\theta)|\,]\,d\theta + i\int_0^{\pi/3} [\,|\cos(1.5\theta)| + |\sin(1.5\theta)|\,]\,d\theta$$

$$+ \int_0^{\pi/3} [\,|\cos(1.5\theta)| - |\sin(1.5\theta)|\,]\,d\theta + i\int_0^{\pi/3} [\,|\cos(1.5\theta)| - |\sin(1.5\theta)|\,]\,d\theta$$

$$+ \int_0^{\pi/3} [\,|\cos(1.5\theta)| + |\sin(1.5\theta)|\,]\,d\theta + i\int_0^{\pi/3} [\,|\cos(1.5\theta)| + |\sin(1.5\theta)|\,]\,d\theta$$

$$= 4 + 4i$$

Similarly, the average relative distortion between 3rd and 2nd helices for period π is

$$\int_0^{\pi/3} [\,|\cos(1.5\theta)| + 0.25\,|\sin(1.5\theta)|\,]\,d\theta + i\int_0^{\pi/3} [\,|\cos(1.5\theta)| + 0.25\,|\sin(1.5\theta)|\,]\,d\theta$$

$$+ \int_0^{\pi/3} [\,|\sin(1.5\theta)| - 0.25\,|\cos(1.5\theta)|\,]\,d\theta + i\int_0^{\pi/3} [\,|\sin(1.5\theta)| - 0.25\,|\cos(1.5\theta)|\,]\,d\theta$$

$$+ \int_0^{\pi/3} [\,|\cos(1.5\theta)| + 0.25\,|\sin(1.5\theta)|\,]\,d\theta + i\int_0^{\pi/3} [\,|\cos(1.5\theta)| + 0.25\,|\sin(1.5\theta)|\,]\,d\theta$$

$$= 3.25 + 3.25\,i$$

Finally, the average relative distortion between 2nd and 1st helices for period π is

$$\int_0^{\pi/3} [\,0.25\,|\sin(1.5\theta)| + |\sin(1.5\theta)|\,]\,d\theta + i\int_0^{\pi/3} [\,0.25\,|\sin(1.5\theta)| + |\sin(1.5\theta)|\,]\,d\theta$$

$$+ \int_0^{\pi/3} [\,|\cos(1.5\theta)| + 0.25\,|\cos(1.5\theta)|\,]\,d\theta + i\int_0^{\pi/3} [\,|\cos(1.5\theta)| + 0.25\,|\cos(1.5\theta)|\,]\,d\theta$$

$$+ \int_0^{\pi/3} [\,0.25\,|\sin(1.5\theta)| + |\sin(1.5\theta)|\,]\,d\theta + i\int_0^{\pi/3} [\,0.25\,|\sin(1.5\theta)| + |\sin(1.5\theta)|\,]\,d\theta$$

$$= 3.75 + 3.75\,i$$

Thus, the total average relative distortion factor is 11 + 11i, and its magnitude is approximately 15.5.

Consider the case of a two-bladed rotor; maximum instabilities occur at wave numbers 0.0 and 1.0. Eigenfunctions for the most unstable eigenvalues at these wave numbers are tabulated in Table XIII.

For a wave number of 0.0, the axial distortion amplitudes for helices 1 and 2 are

$$\delta\hat{e}_1 \cong -1.00 \quad ; \quad \delta\hat{e}_2 \cong +1.00$$

The average relative distortion factor over a period π is

$$\int_0^{\pi} d\theta + \int_0^{\pi} d\theta = 2\pi \cong 6.28$$

For a wave number of 1.0, the axial distortion amplitudes for helices 1 and 2 are

$$\delta\hat{e}_1 \cong 0.812 \quad ; \quad \delta\hat{e}_2 = 0.812$$

Referring to Figure 21, the average relative distortion factor over a period π is

$$2(0.812)\int_0^{\pi/2} |\cos(\theta)|\,d\theta + 2(0.812)\int_0^{\pi/2} |\cos(\theta)|\,d\theta$$

$$+ i\left[2(0.812)\int_0^{\pi/2} |\sin(\theta)|\,d\theta + 2(0.812)\int_0^{\pi/2} |\sin(\theta)|\,d\theta\right]$$

$$= 3.25 + 3.25i$$

Thus the magnitude of the average relative distortion factor is approximately 4.60.

Results of the above calculations are tabulated in Table XIV. This shows that the relative axial displacements do, in fact, determine the stability and that those modes which have the highest average reduction of axial separation between adjacent coils around the circumference of the helix will be the most highly divergent.

TABLE XIII. EIGENFUNCTIONS FOR THE MOST UNSTABLE EIGENVALUES OF A TWO-BLADED ROTOR AT WAVE NUMBERS 0.0 AND 1.0, PITCH = 0.1 AND CORE SIZE = 0.1

Eigenfunction for Wave Number 0.0			Eigenfunction for Wave Number 1.0		
Label	Real	Imaginary	Label	Real	Imaginary
$\delta\hat{r}_1$	+0.998	0.002	$\delta\hat{r}_1$	-0.784	-0.215
$r\delta\hat{\phi}_1$	+0.065	0.000	$r\delta\hat{\phi}_1$	-0.043	-0.034
$\delta\hat{z}_1$	-0.998	-0.002	$\delta\hat{z}_1$	+0.783	+0.212
$\delta\hat{r}_2$	-0.998	-0.002	$\delta\hat{r}_2$	-0.784	-0.215
$r\delta\hat{\phi}_2$	-0.065	-0.000	$r\delta\hat{\phi}_2$	-0.043	-0.034
$\delta\hat{z}_2$	+0.998	+0.002	$\delta\hat{z}_2$	+0.783	+0.212

TABLE XIV. COMPARISON OF MAXIMUM INSTABILITY FOR TWO- AND THREE-BLADED ROTORS

Number of Blades	Wave Numbers	Amplitude of Average Distortion Factor	Max Divergence Rate	Conclusion
2	0.0	6.28	50.05	Perturbations for the wave number 0.0 are more unstable
	1.0	4.60	49.80	
3	0.0	12.57	118.42	Perturbations for the wave number 1.5 are more unstable
	1.5	15.50	123.71	

CHAPTER 5

CONCLUSIONS

1. The small-perturbation stability analysis of a doubly infinite array of interdigitated right circular helical vortices formulated here shows reasonable agreement with the recent work of Widnall [Reference 16] where vortex core to helix diameter ratios are 0.1 or less and when the number of blades is set equal to unity. The larger differences which appear in a comparison with the Reference 16 results at larger core ratios (e.g., 0.33) are attributed to differences in the methods for eliminating the self-induction singularity. While the method works best for small pitch angles, it has been shown to be the equivalent of the formulations developed by S.C. Crow and Parks [References 17 and 20] dealing with the infinite straight vortices such as trail from the tips of fixed-wing aircraft, when the pitch angle is made to approach infinity for a two-bladed rotor.

2. A continuum of instability modes has been found associated with all values of wave numbers; only modes with wave numbers 0 and 1 are so much as neutrally stable, and only for the case of a single helix. The most unstable modes involve the most axial motion of adjacent vortex segments relative to each other. By "adjacent segments" is meant vortex segments above and below each other (i.e., at the same azimuthal location) on adjacent coils of the same or neighboring helices. Furthermore, the larger the percentage of the helical arc length involved in such motion, the more rapidly the distortion will diverge. Maximum divergence rates in the unstable modes increase as the helix pitch decreases, increase as the number of helices increases, and decrease as the number of cycles of deformations in one turn of the helix (i.e., wave number) increases.

3. The effect of increasing helix filament core diameter is to make the analysis more sensitive to the means by which the singularity is eliminated. Increasing the number of blades appears to make the core diameter less influencial in determining the rates of divergence. Although it has not been demonstrated here, one would expect that reduced pitch would also reduce the dependence of the calculation on the vortex core size. Finally, a larger core diameter ratio also appears to reduce the difference between peak and minimum divergence rates as a function of wave number.

CHAPTER 6

RECOMMENDATIONS

In view of the instability of helical vortex arrays observed (a) in tests and (b) in iterative distorted wake geometry calculations and which now have been confirmed in this study, it is recommended that the stability of a semi-infinite vortex array, together with the bound vortices which generate it, be studied in a manner similar to the analyses reported here. The purpose of such a study would be twofold: first, to examine the effect of the bound vortex on helical vortex stability and the associted unstable divergence rates, and second, to develop analytical and realistic perturbation quantities to be used as forcing functions for the unstable modes of the semi-infinite vortex array typical of lifting rotors. In such a "forced" calculation, one would expect to predict the actual distorted geometry of the wake beneath lifting rotors which must be known to perform more accurate airloads analyses, for all purposes.

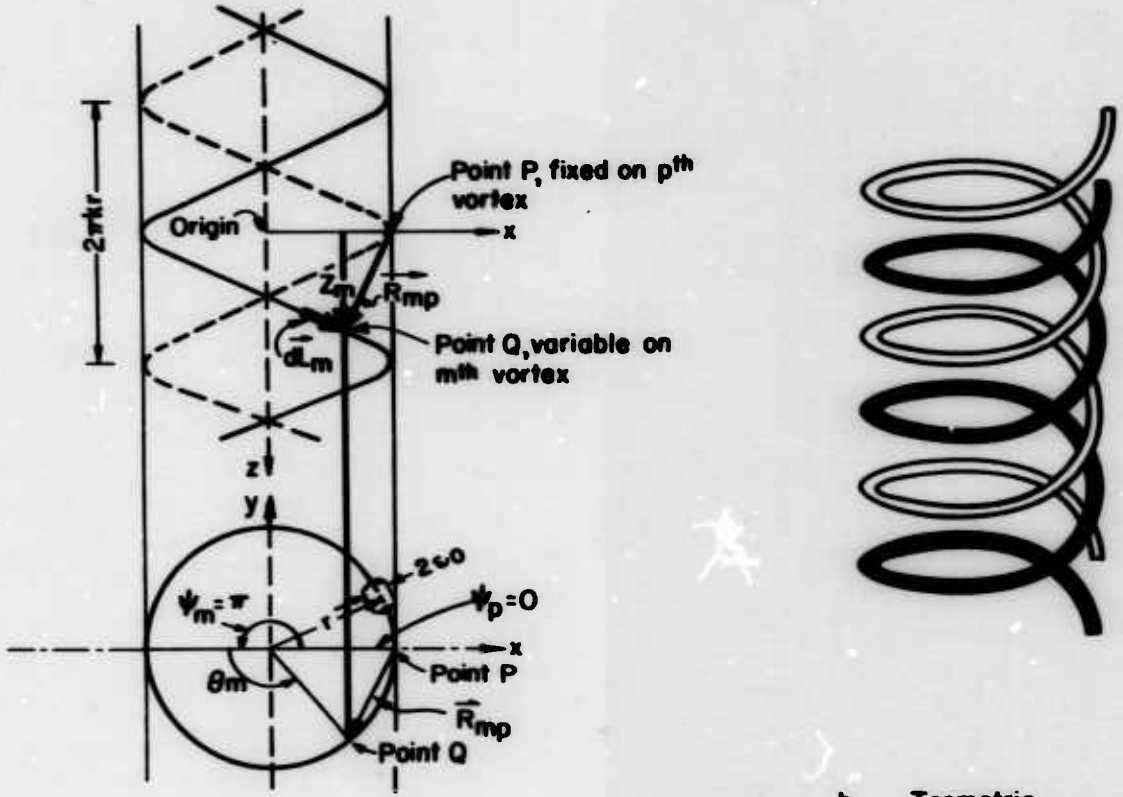

a. Plan and Elevation

b. Isometric

Figure 1. Undistorted p^{th} and m^{th} Vortex Helices of Radius r, Pitch k, and Vortex Core Diameter $2\varepsilon_o$.

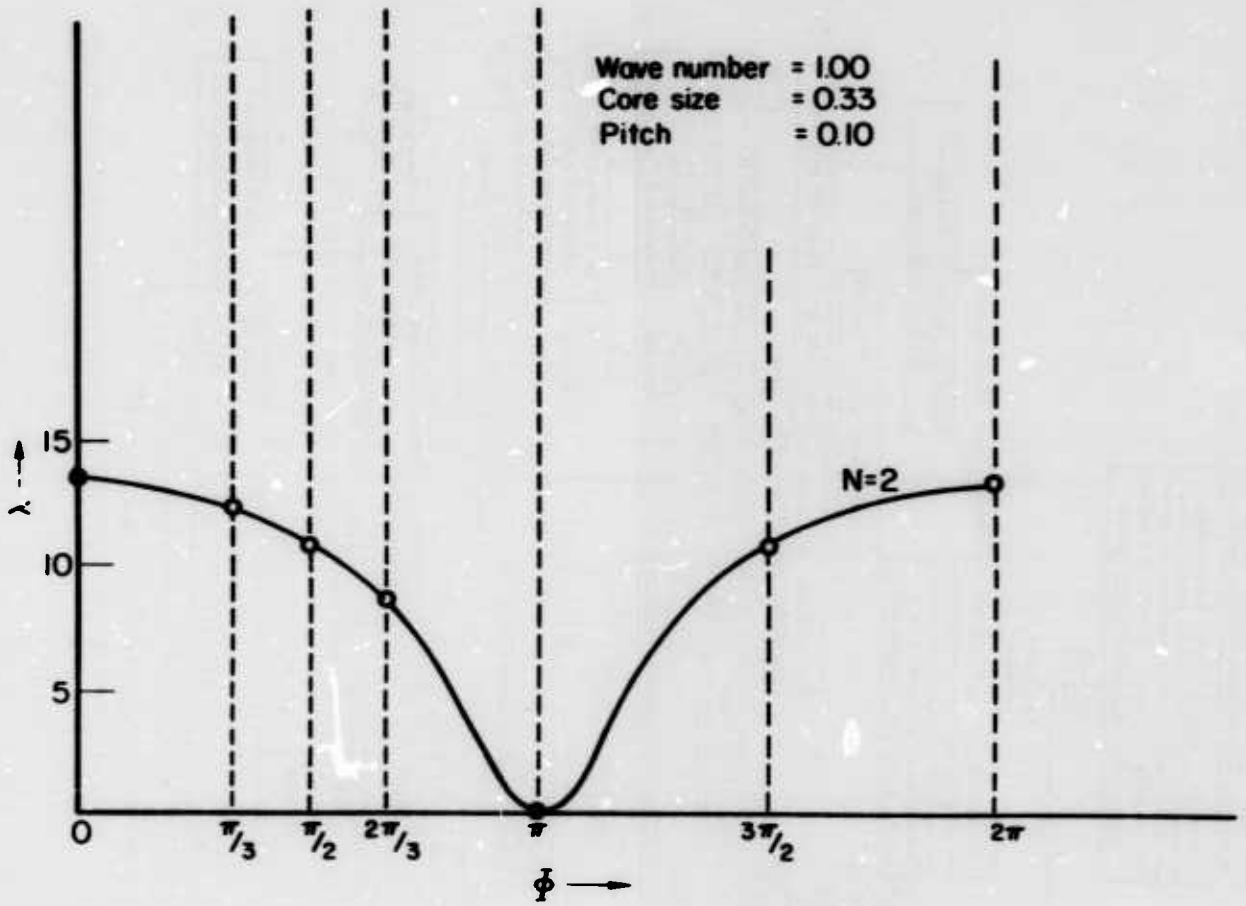

Figure 2. Plot of Divergence Rate Against Phase Difference for a Two-Bladed Rotor.

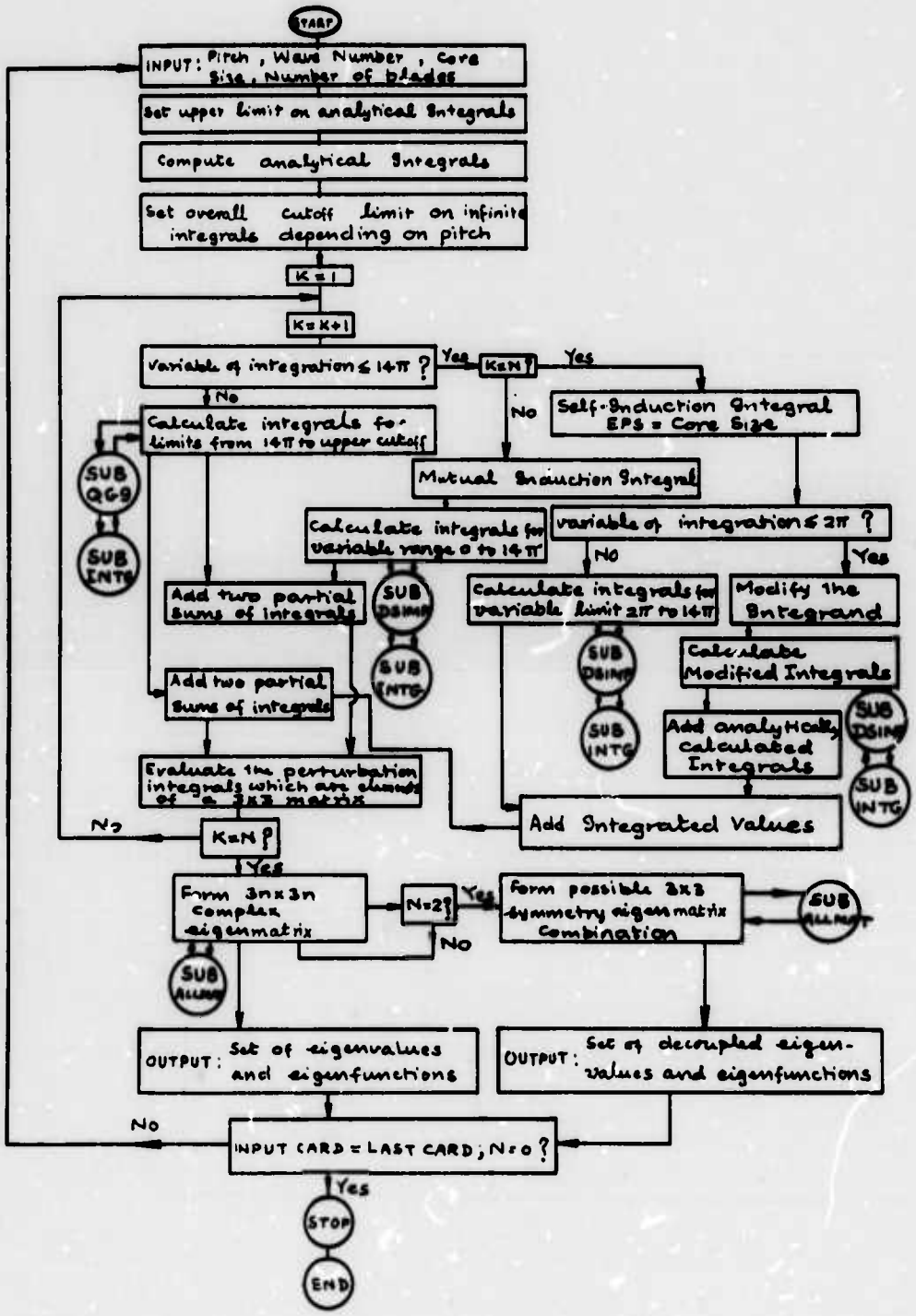

Figure 3. Major Steps in the Computer Program.

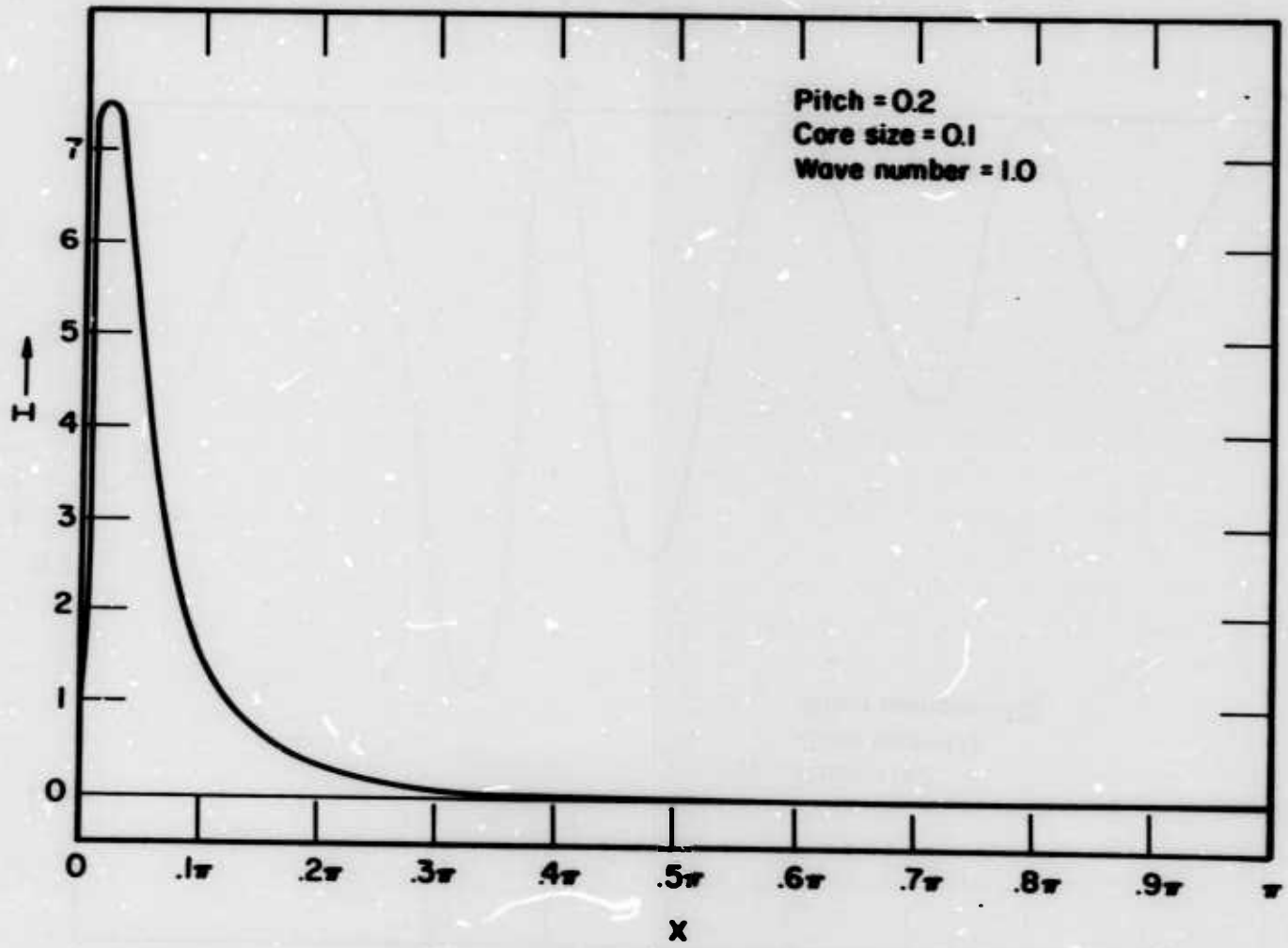

Figure 4. Perturbation Integrand $I = [kJ^{-3/2} \sin x \cos(\omega x)]$.

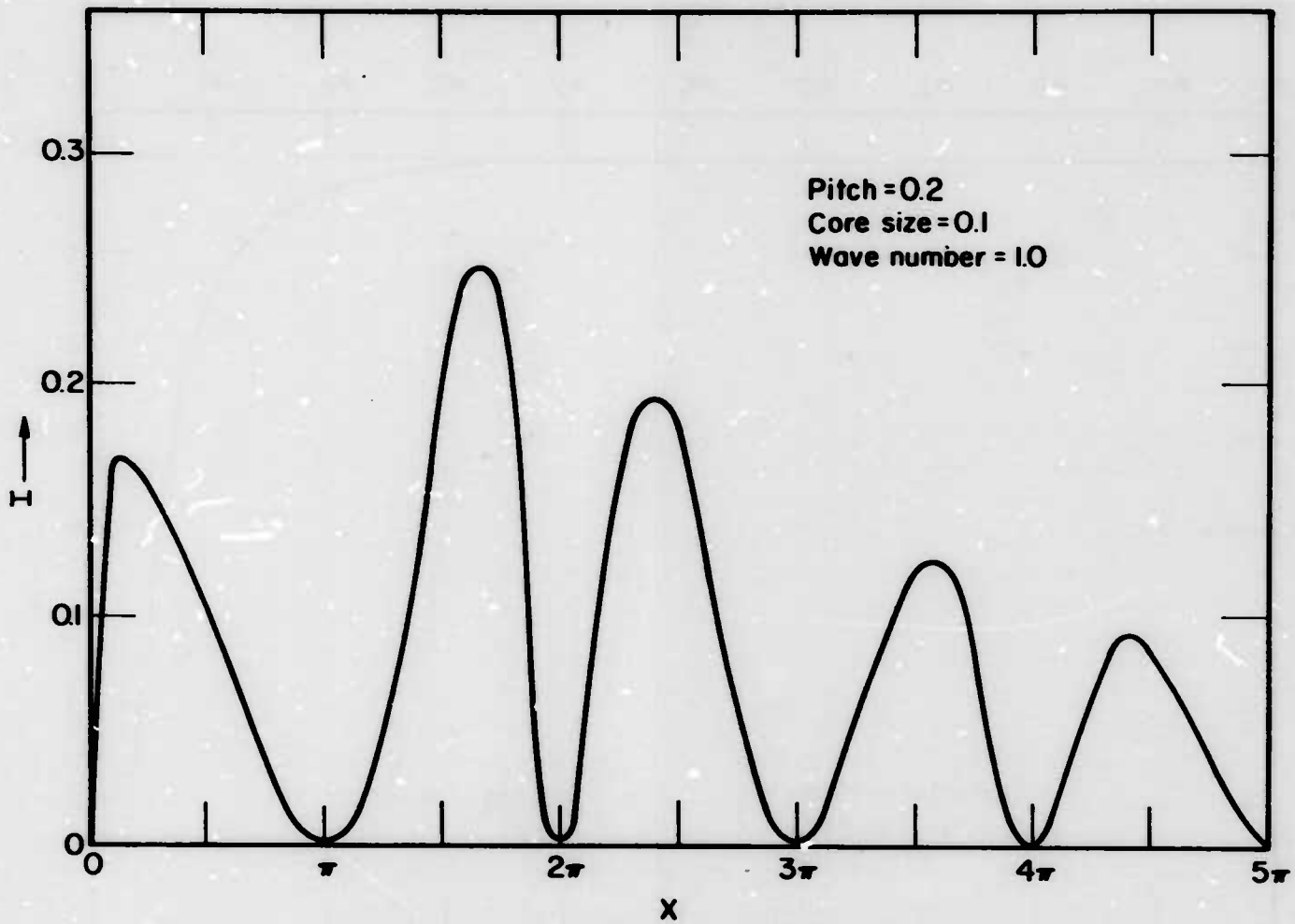

Figure 5. Perturbation Integrand $I = [k^{-3/2} x \sin x \sin(\omega x)]$.

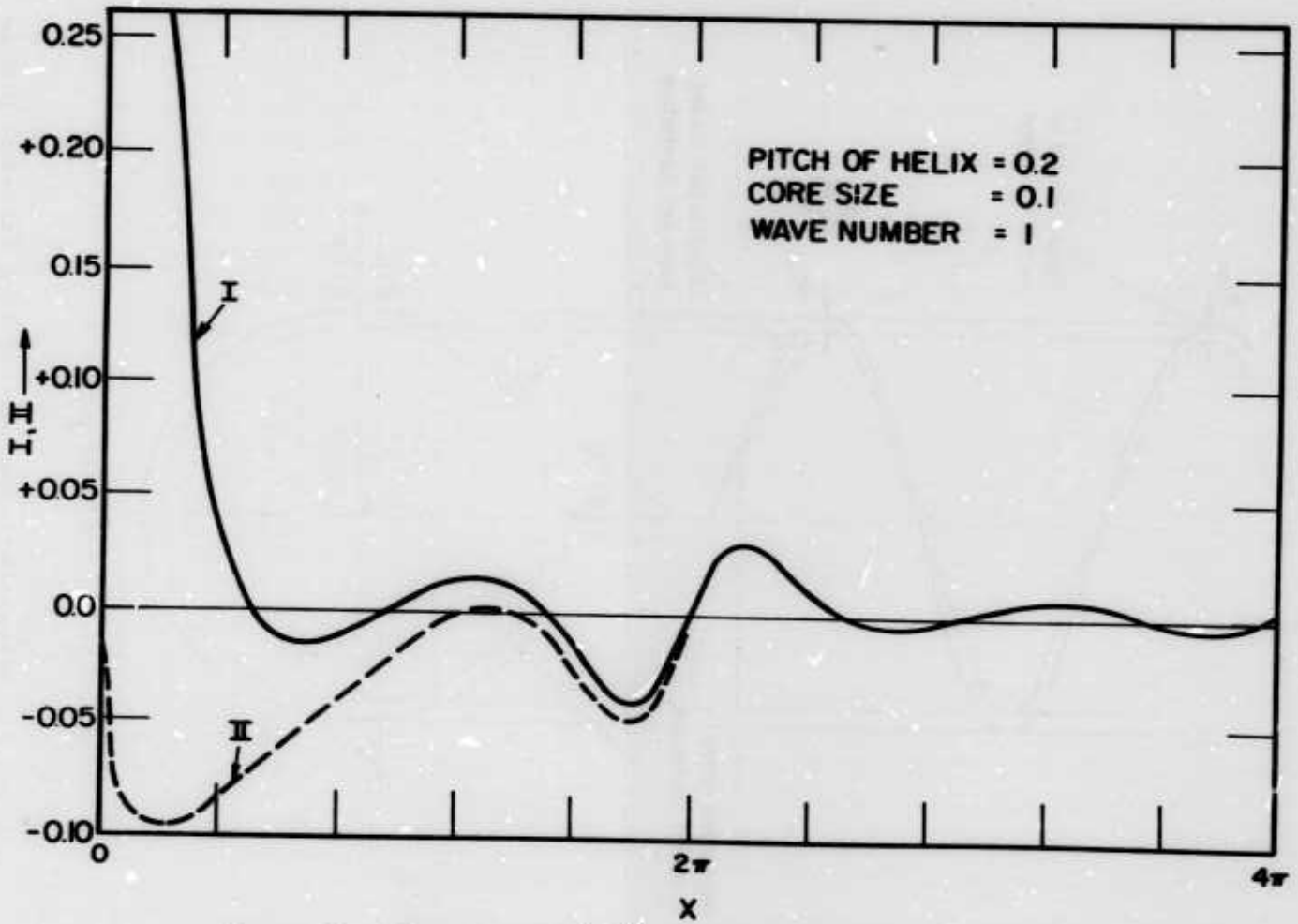

Figure 6. Plot I: $I = [k^{-3/2} \sin x \cos x]$ Against x;
Plot II: $II = [k^{-3/2} \sin x \cos x\} - kx\{(1+k^2)x^2 + \epsilon^2\}^{-3/2}]$ Against x.

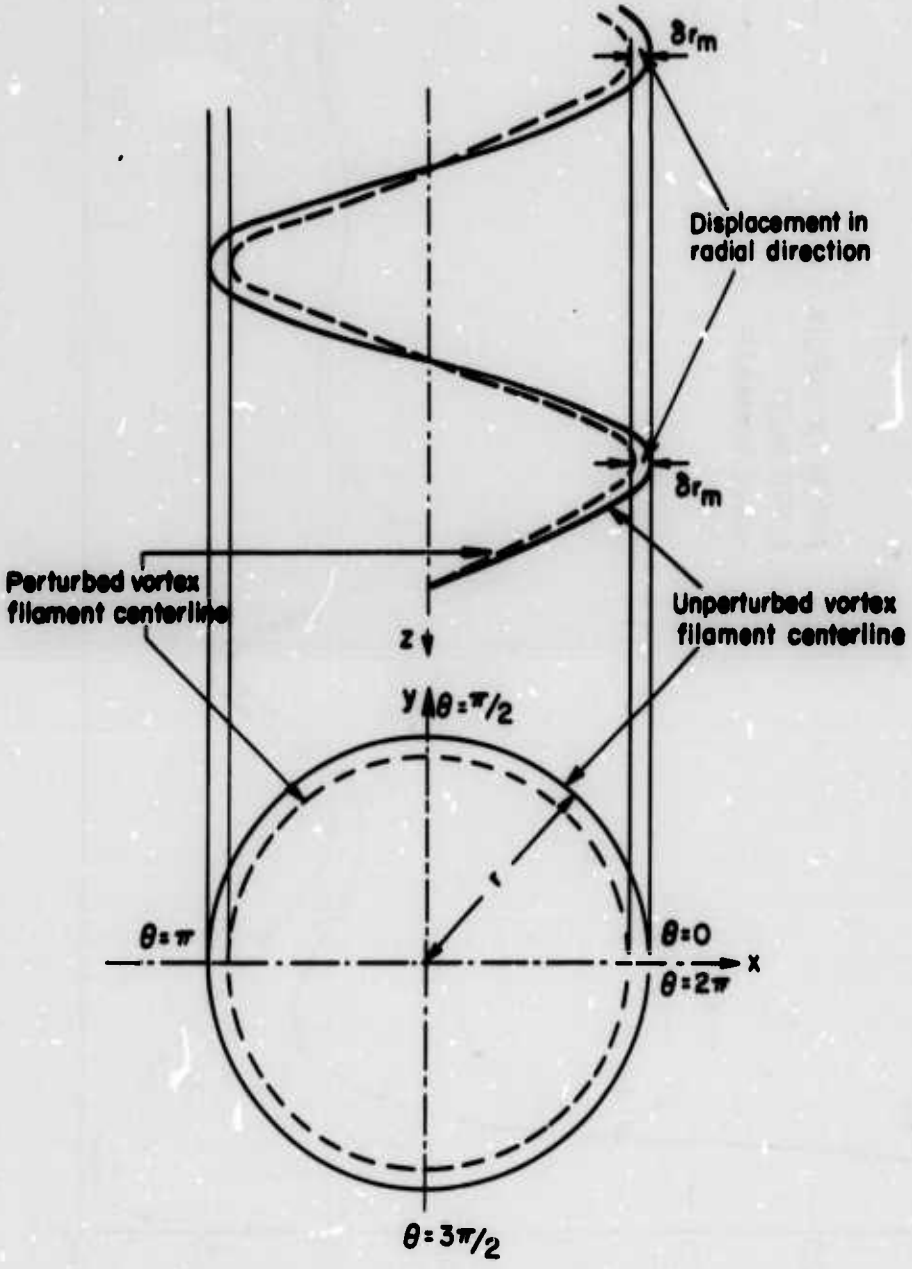

Figure 7. Radial Perturbations in Wave Number = 0 Mode (Dilatational).

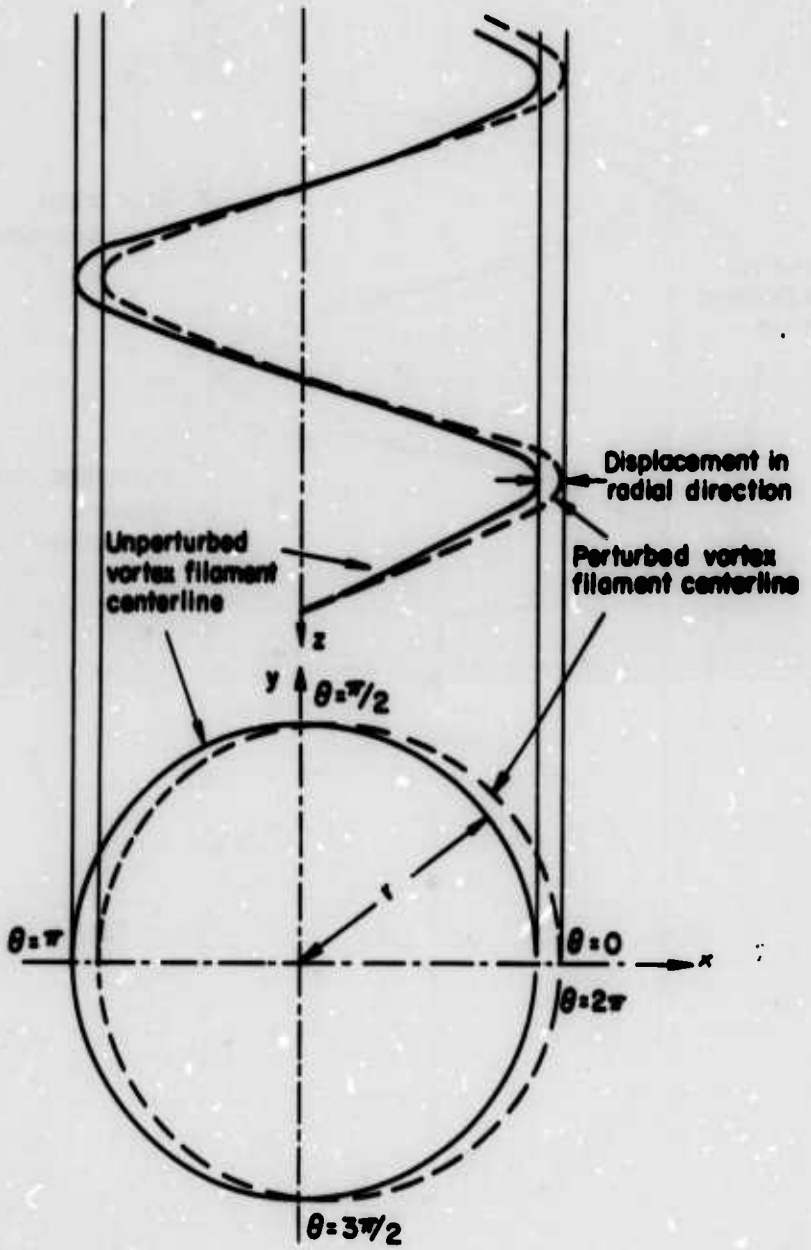

Figure 8. Radial Perturbations in Wave Number = 1 Mode.

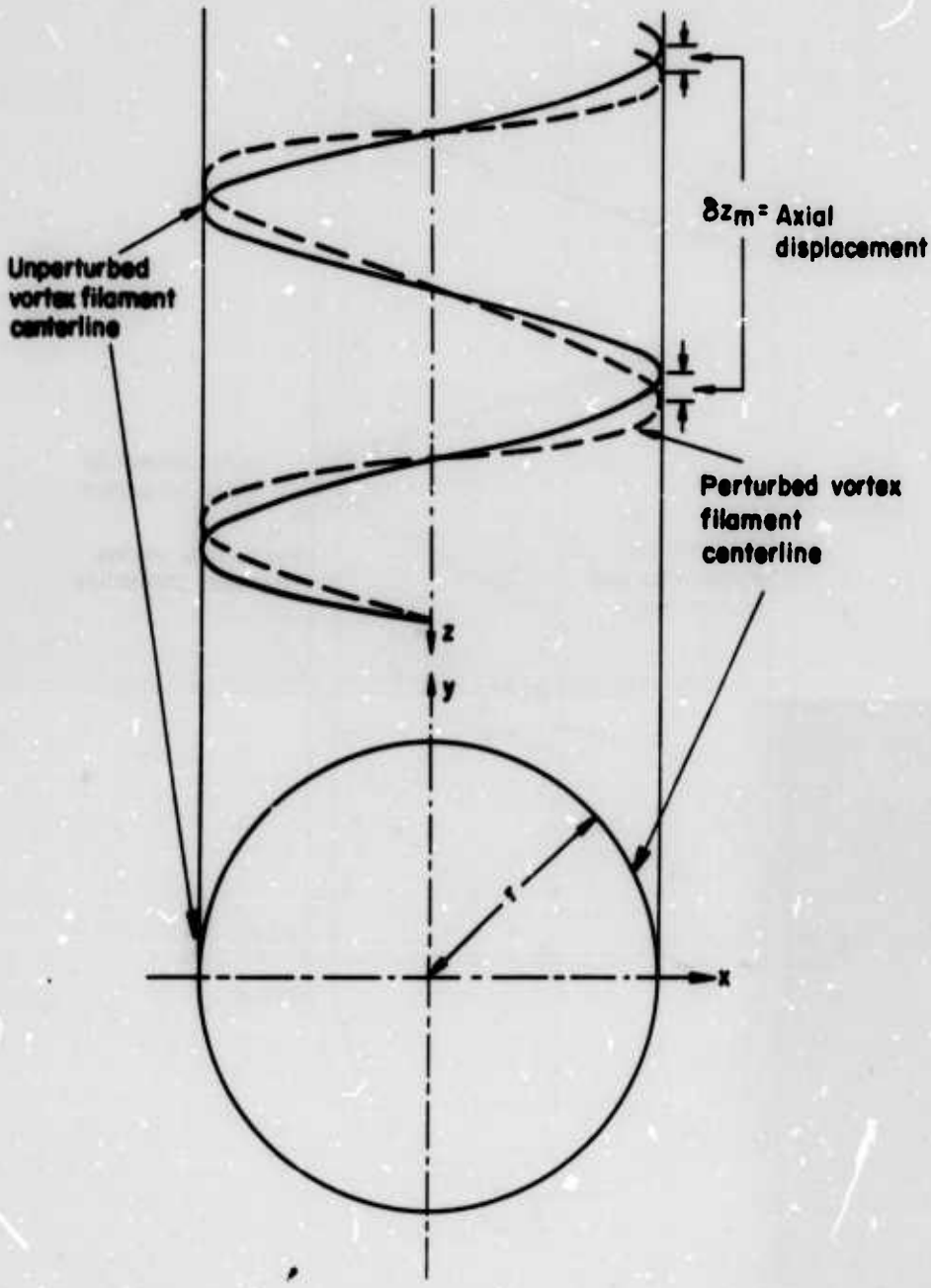

Figure 9. Axial Perturbations in Wave Number = 1 Mode.

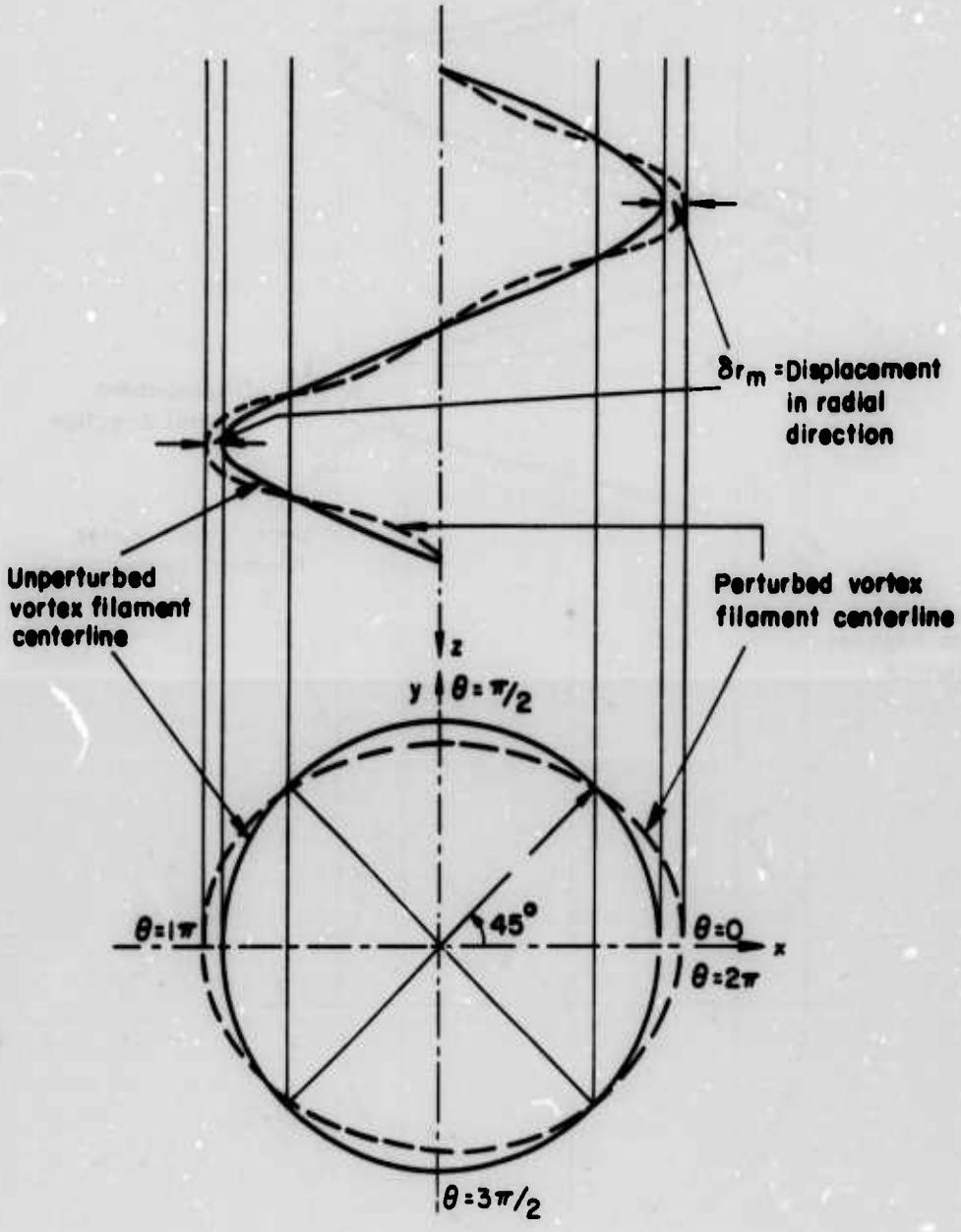

Figure 10. Radial Perturbations in Wave Number = 2 Mode.

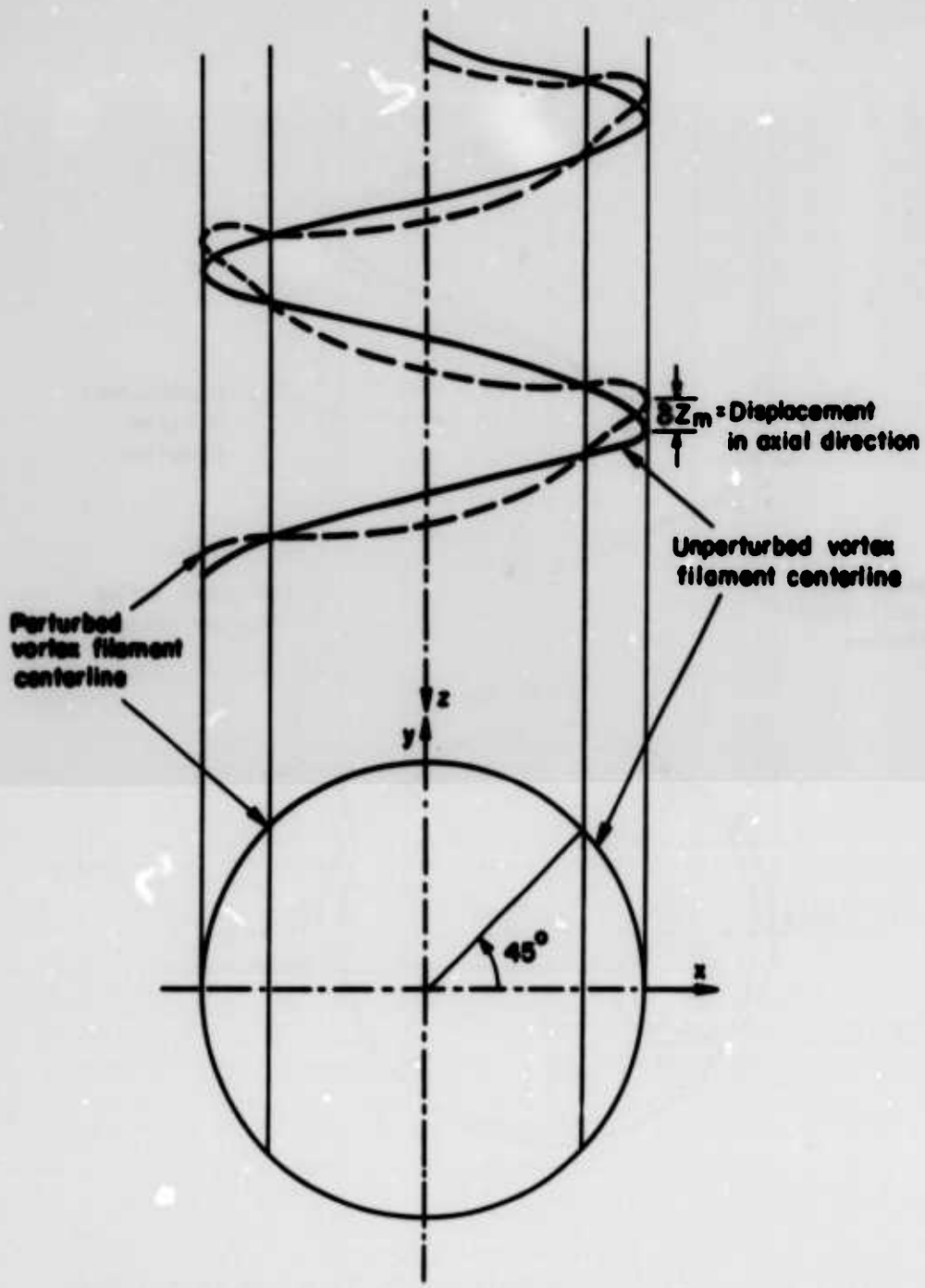

Figure 11. Axial Perturbations in Wave Number = 2 Mode.

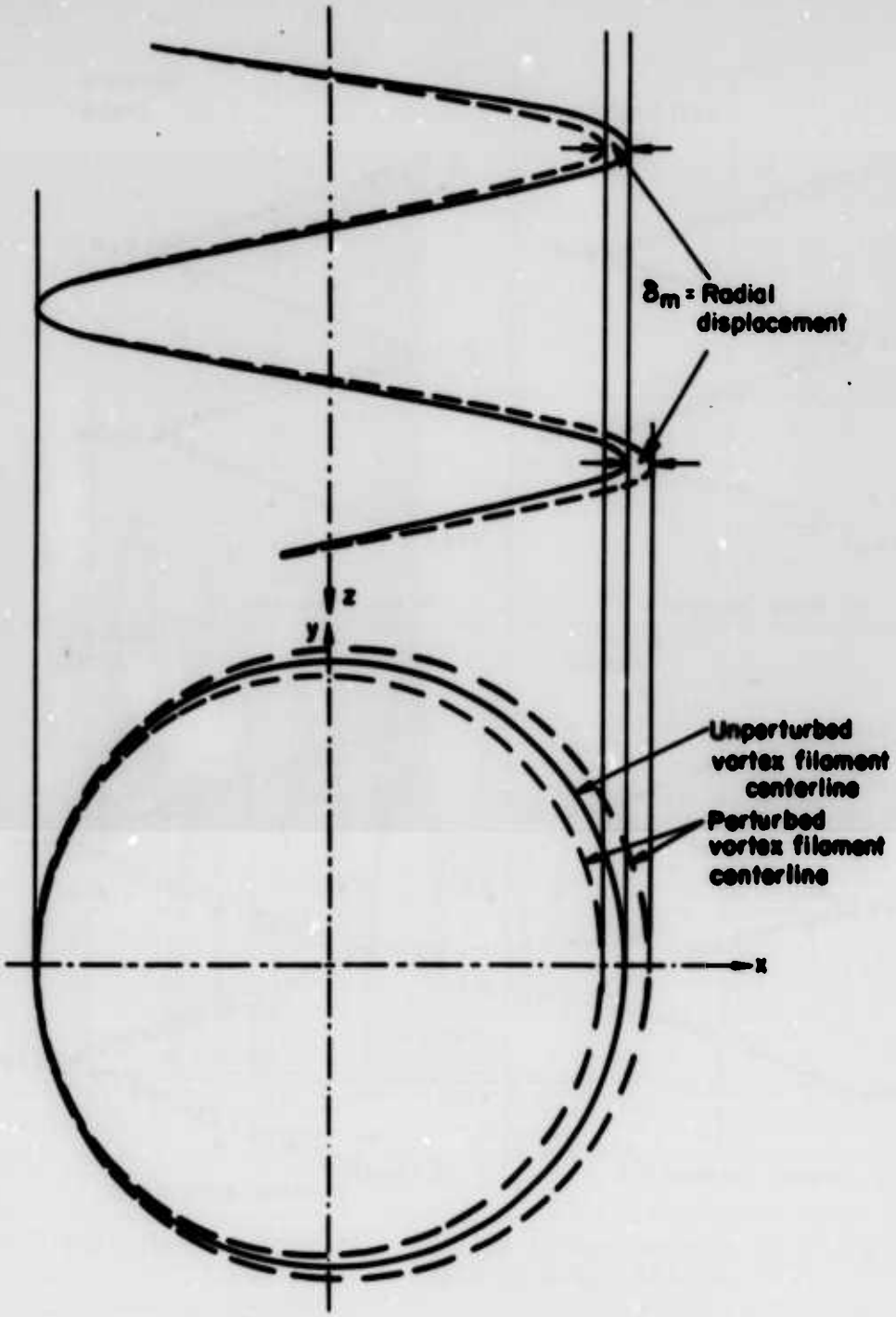

Figure 12. Radial Perturbations in Wave Number = 1/2 Mode.

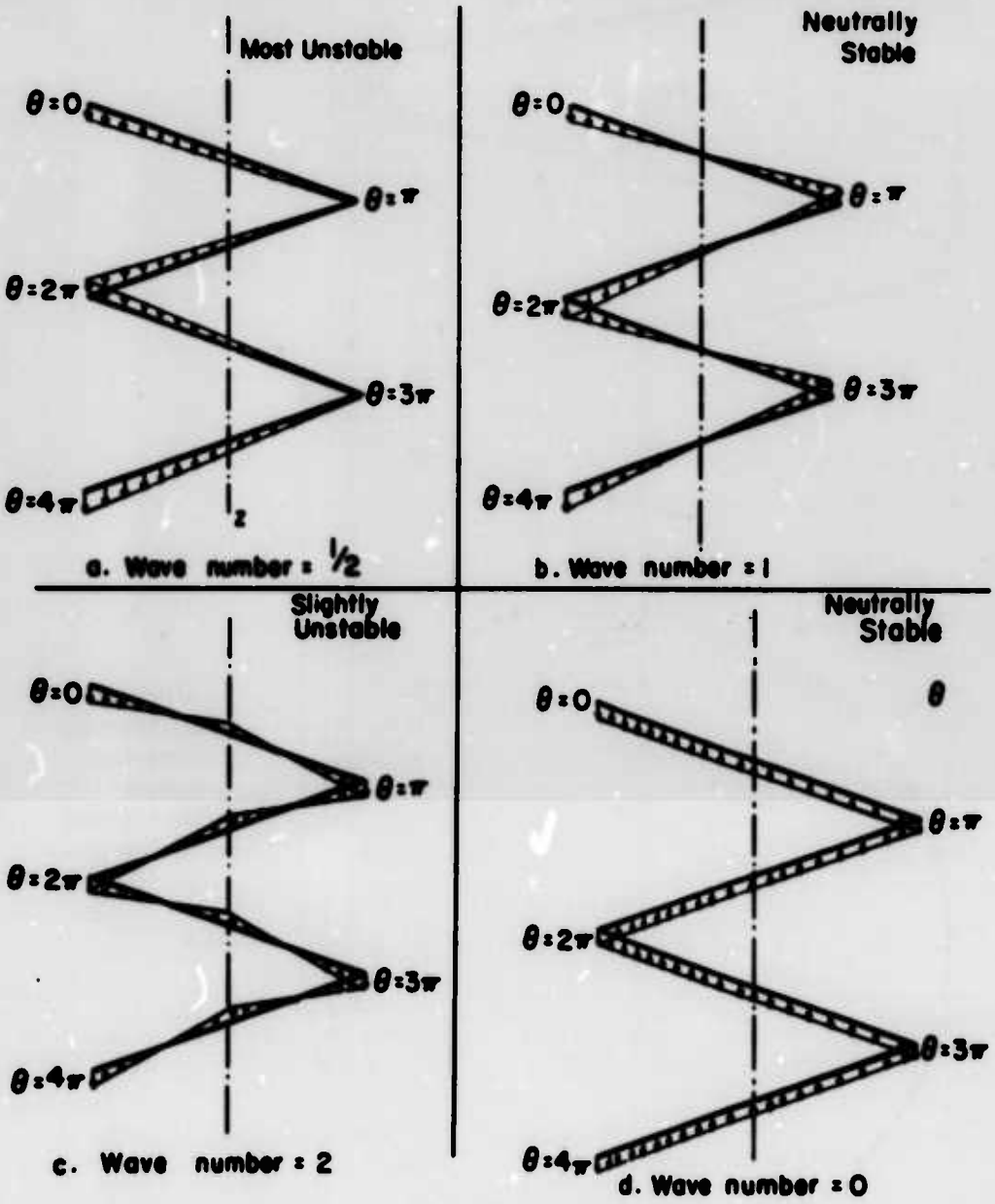

Figure 13. Comparison of Various Perturbation Modes for Single Helix in Axial Direction.

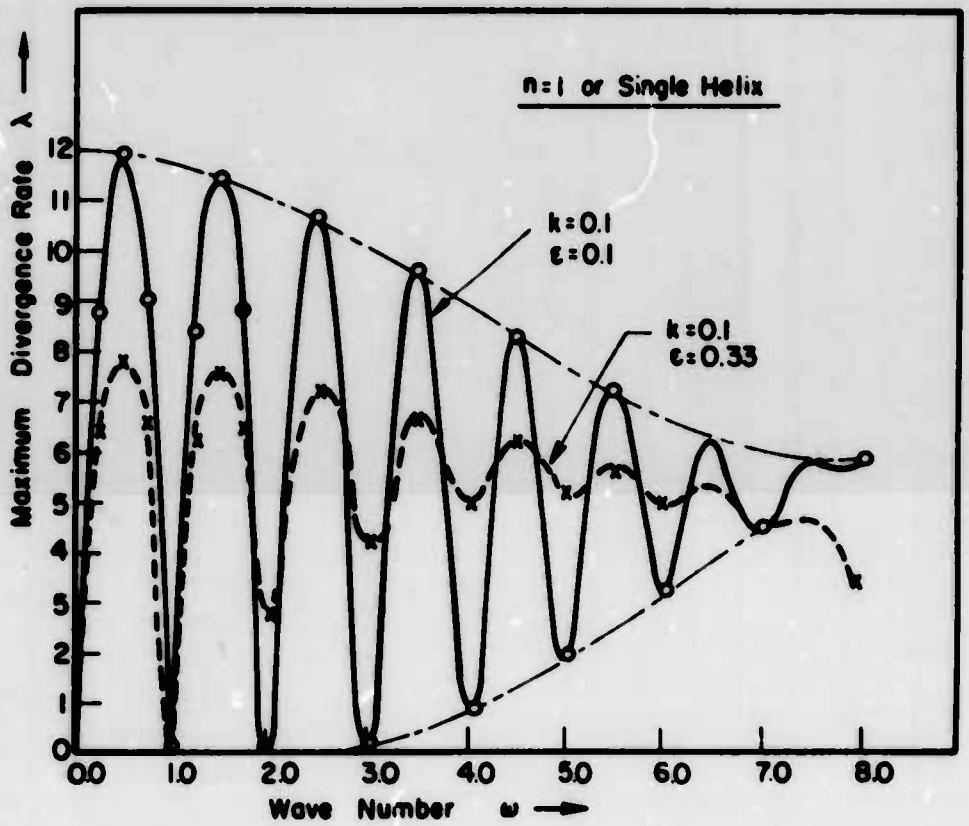

Figure 14. Plot of Maximum Divergence Rate vs Wave Number for Single Helix.

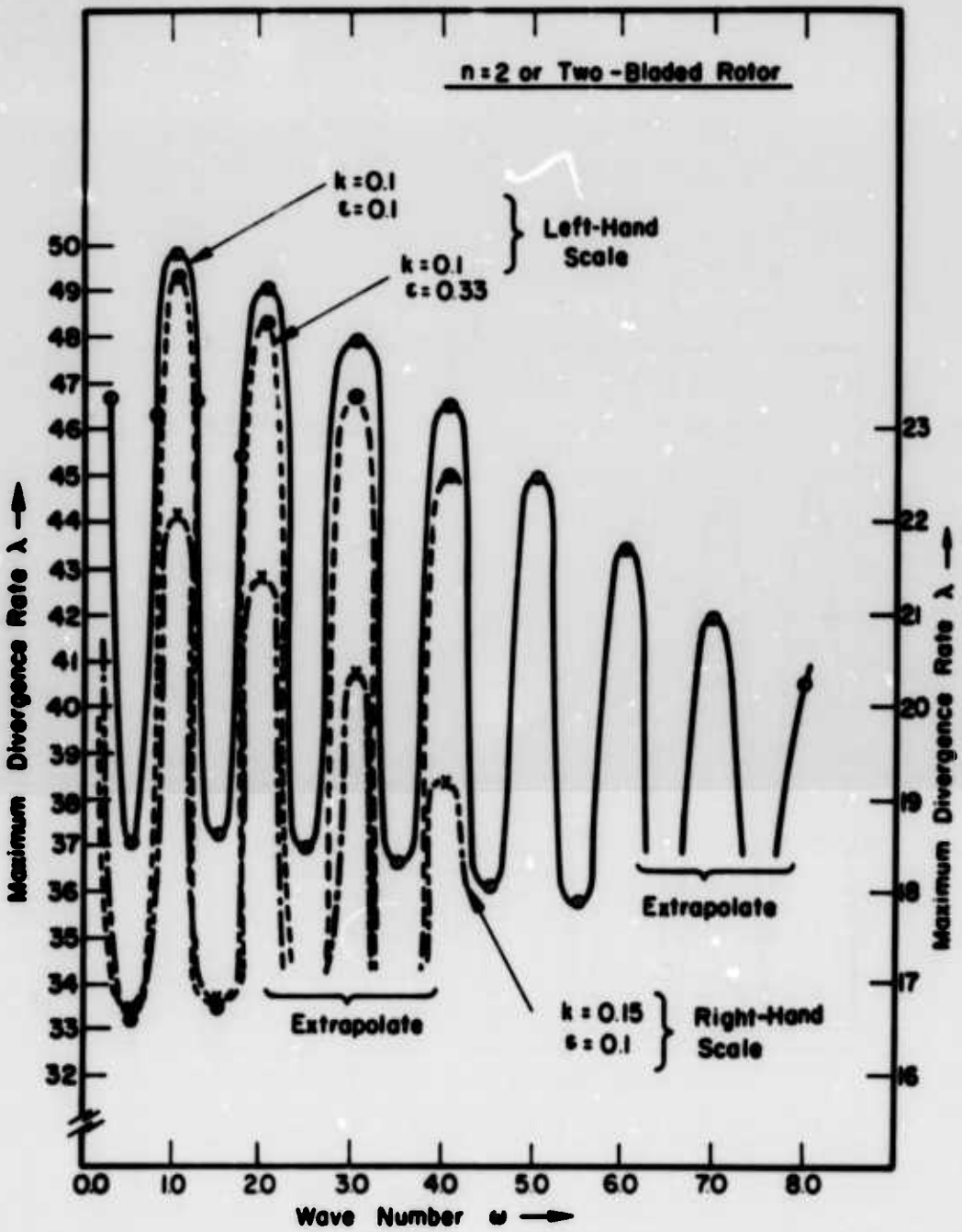

Figure 15. Plot of Maximum Divergence Rate vs Wave Number for Two-Bladed Rotor.

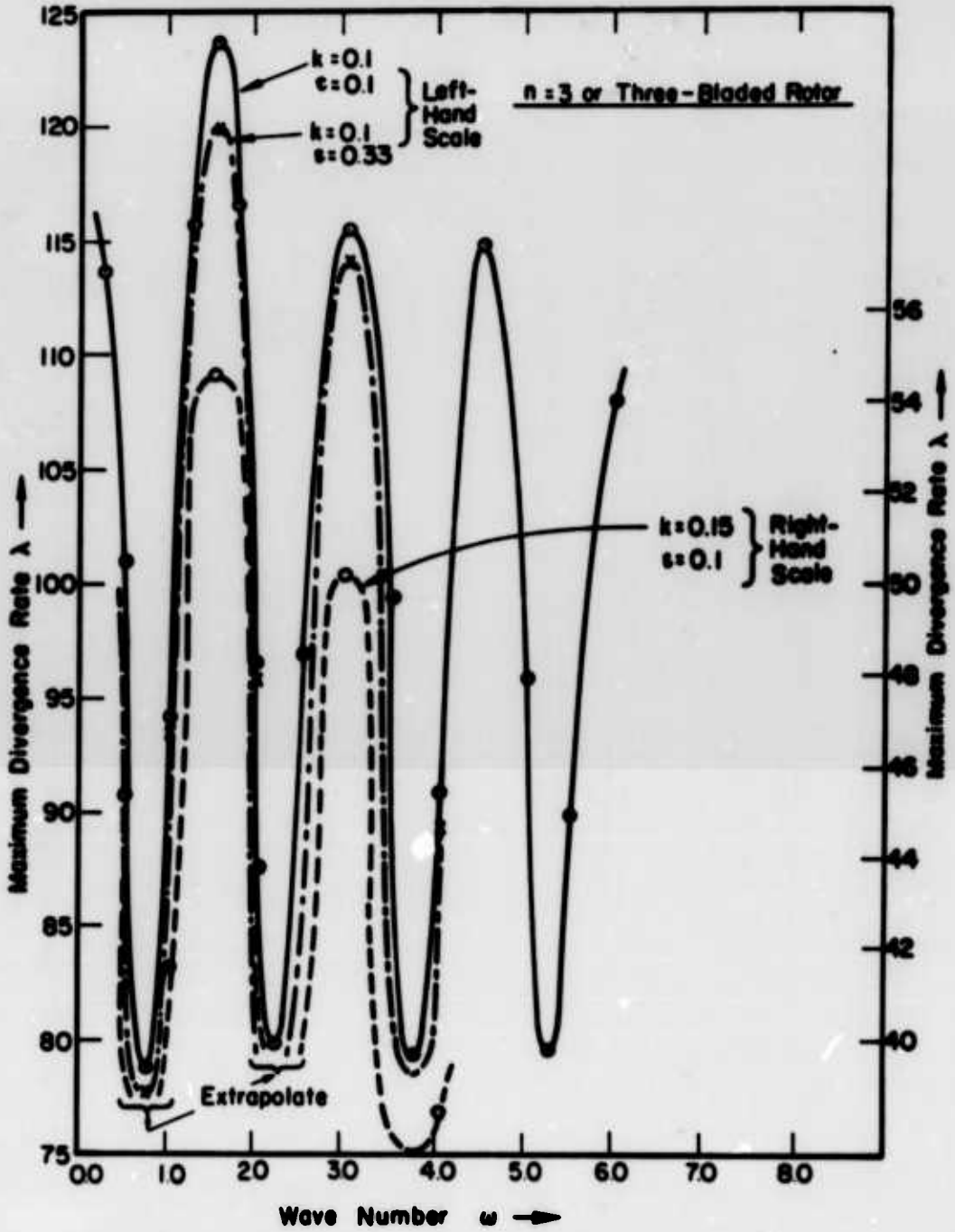

Figure 16. Plot of Maximum Divergence Rate vs Wave Number for Three-Bladed Rotor.

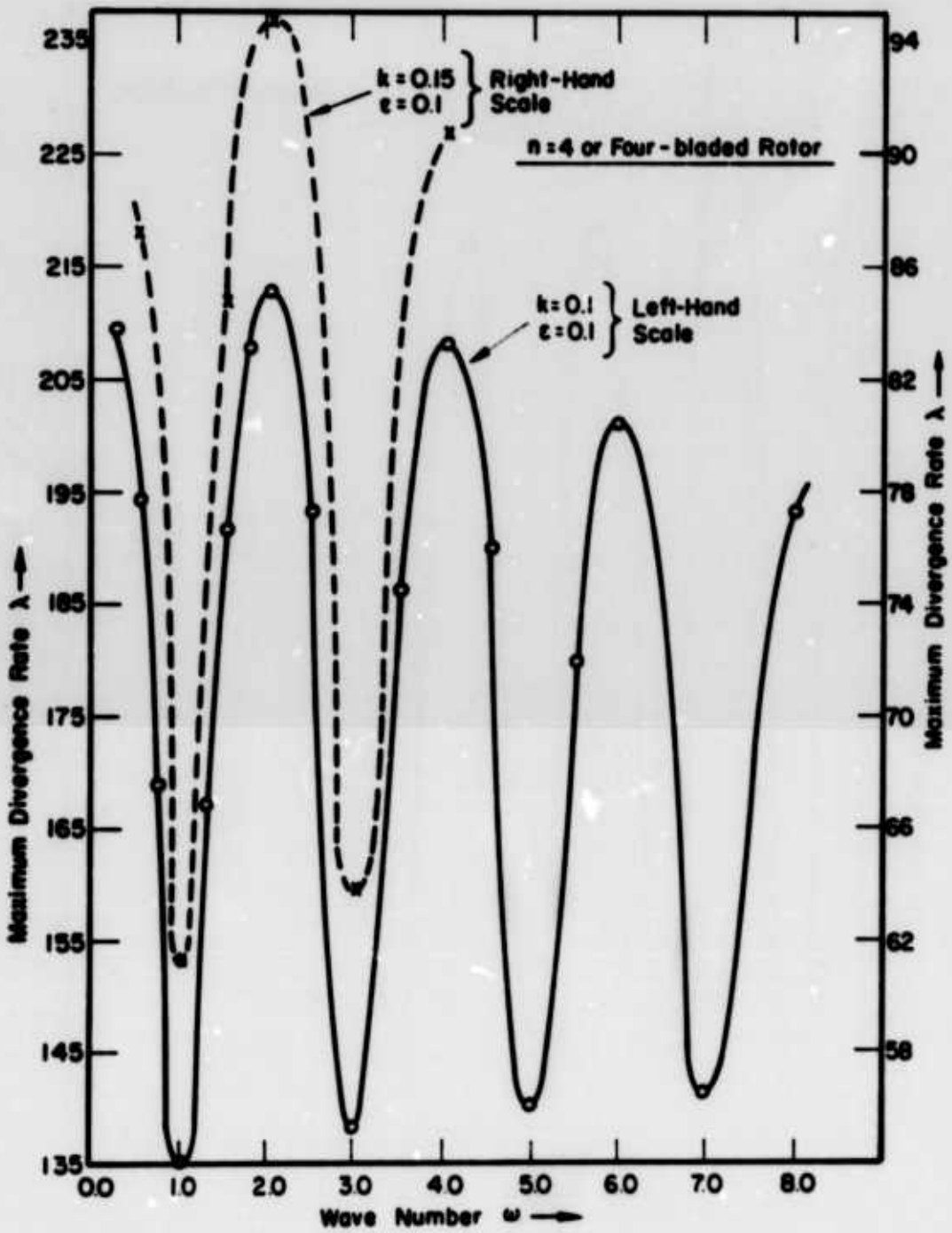

Figure 17. Plot of Maximum Divergence Rate vs Wave Number for Four-Bladed Rotor.

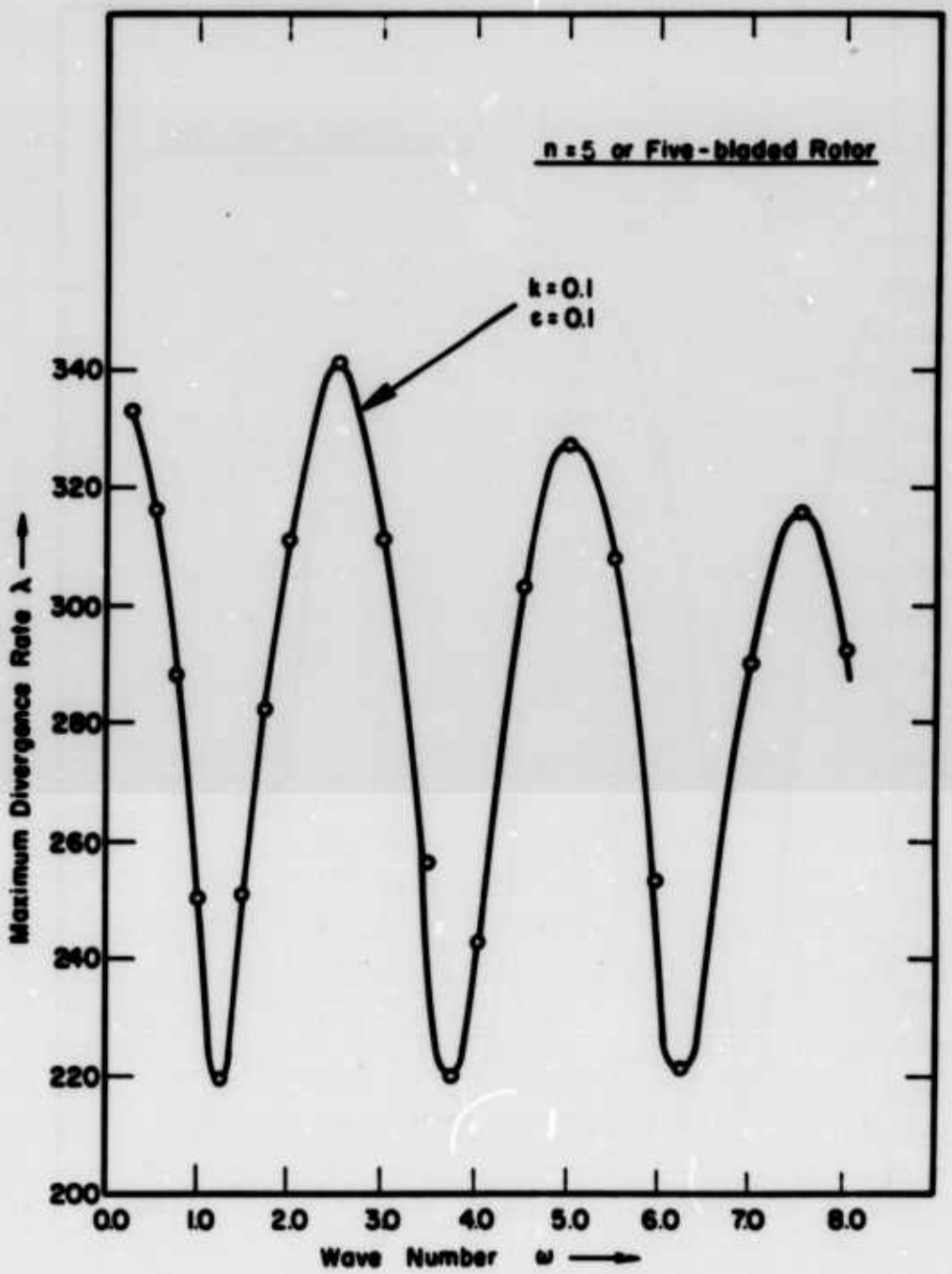

Figure 18. Plot of Maximum Divergence Rate vs Wave Number for Five-Bladed Rotor.

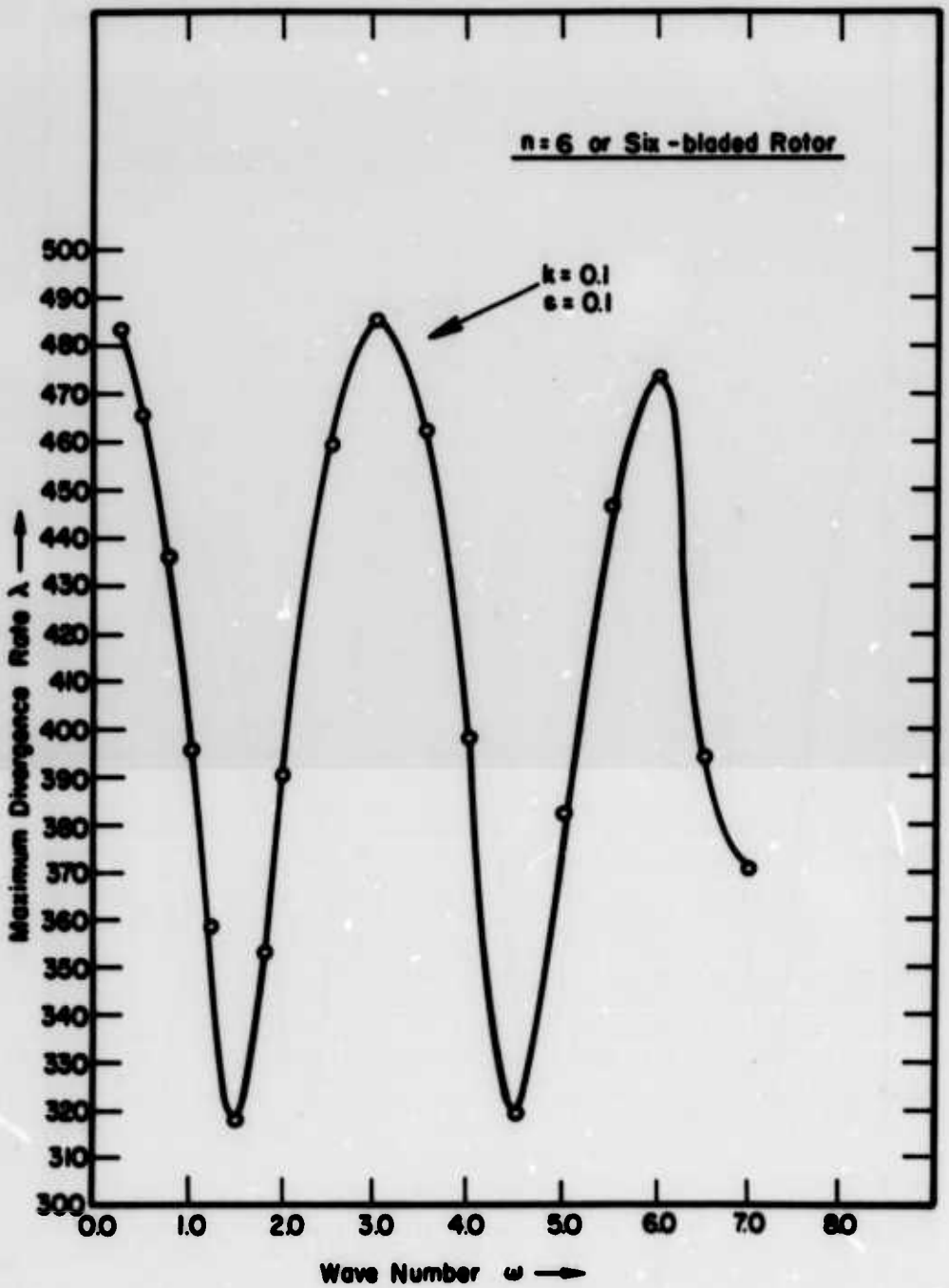

Figure 19. Plot of Maximum Divergence Rate vs Wave Number for Six-Bladed Rotor.

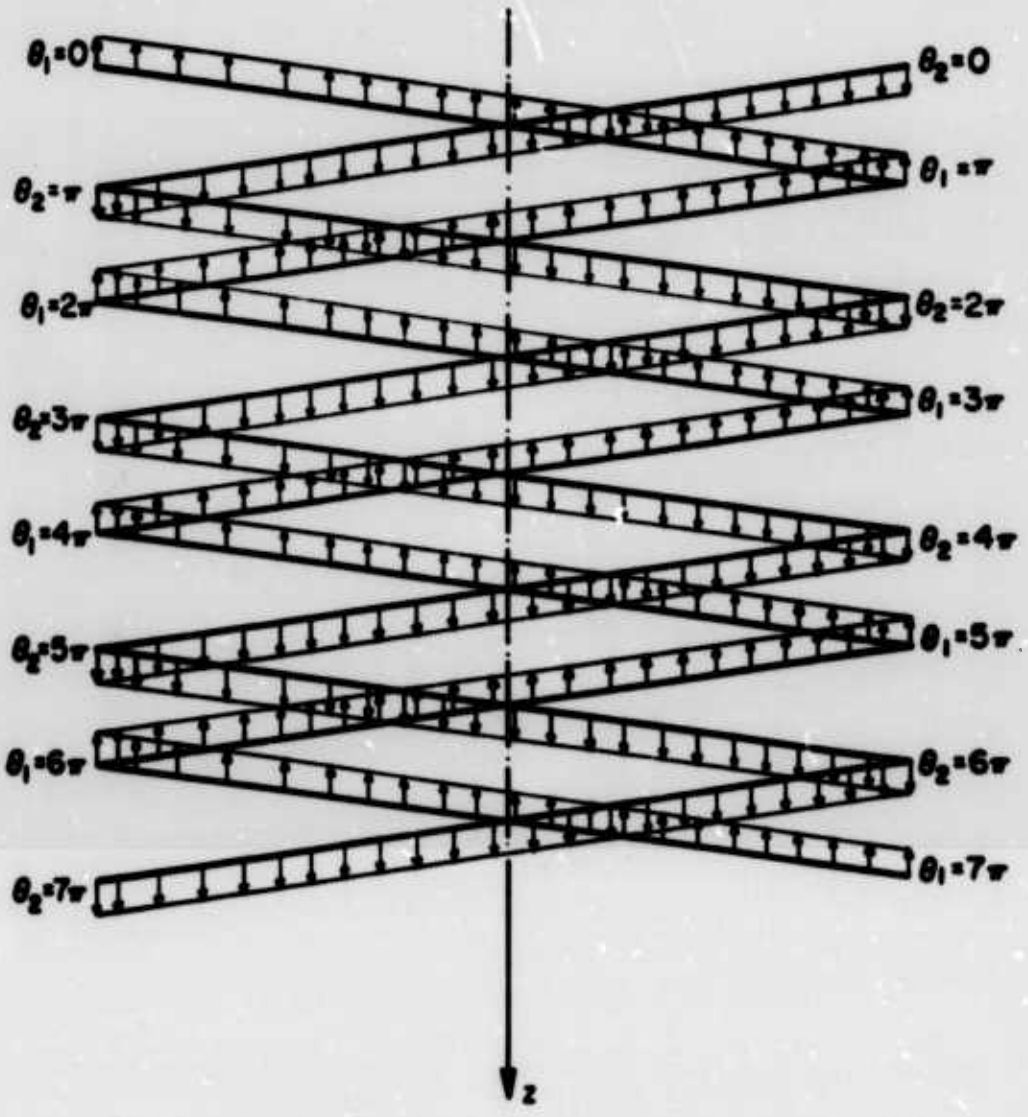

Figure 20. Real Component of Axial Perturbations for a Two-Bladed Rotor at Wave Number 0.0.

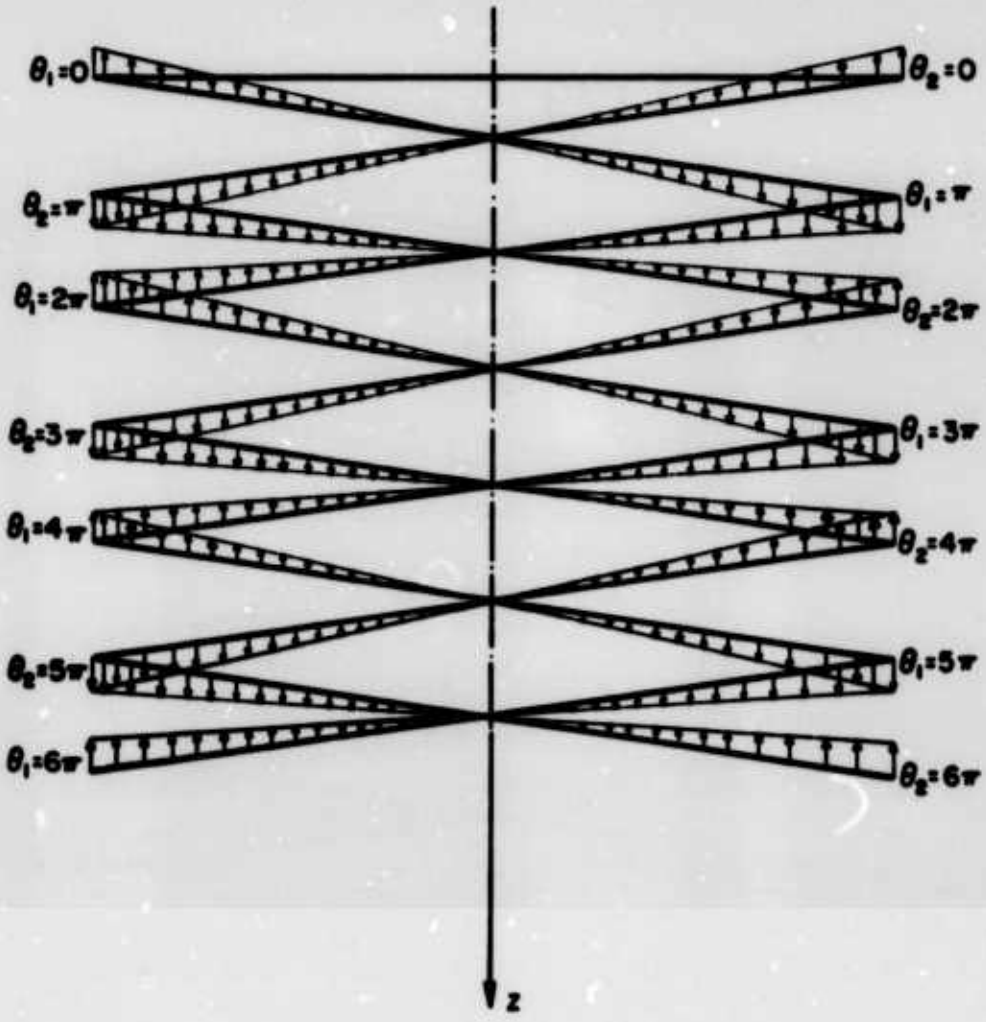

Figure 21. Real Component of Axial Perturbations for a Two-Bladed Rotor at Wave Number 1.0.

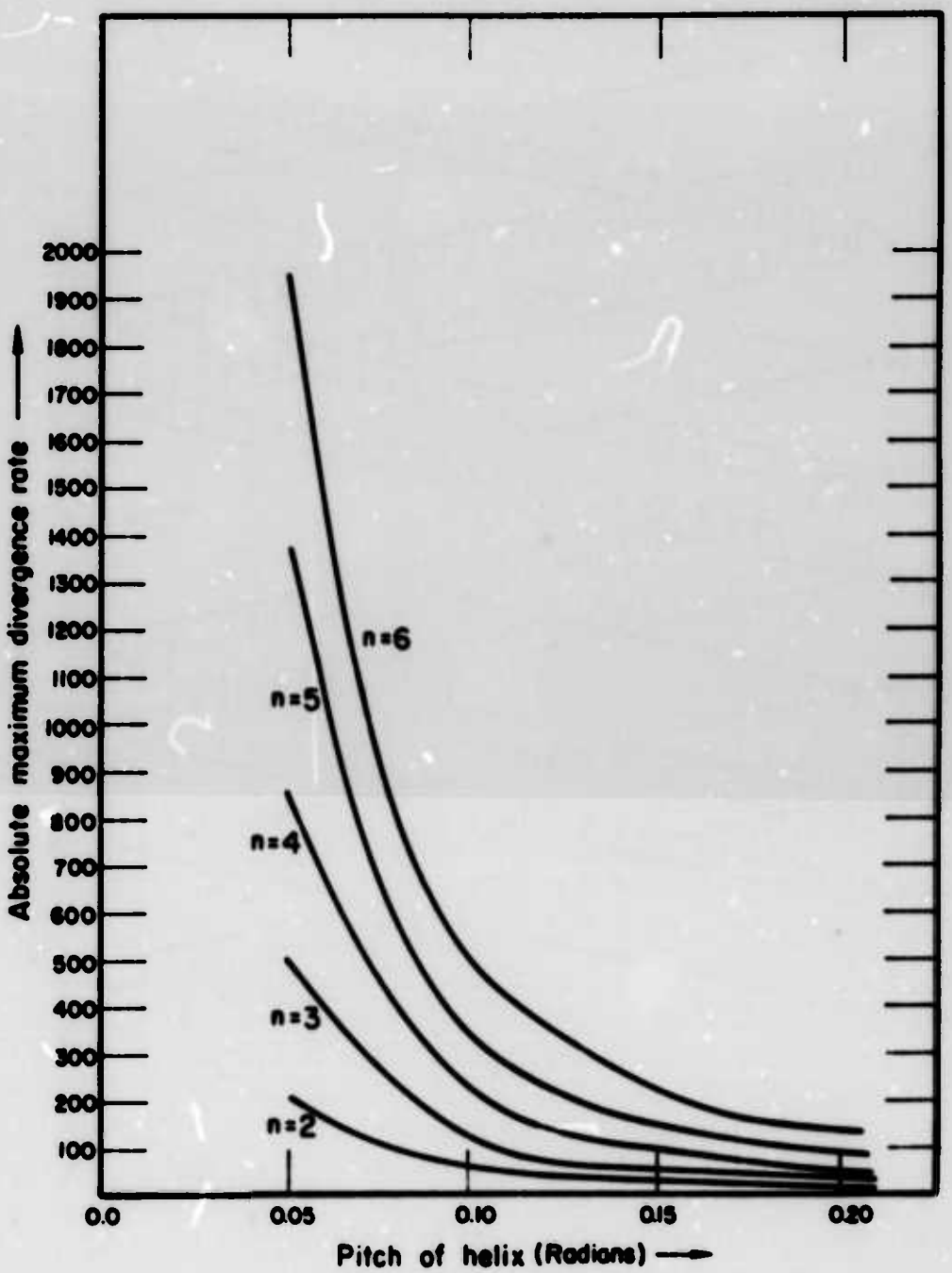

Figure 22. Absolute Maximum Divergence Rates for Multibladed Rotors of Varying Pitch.

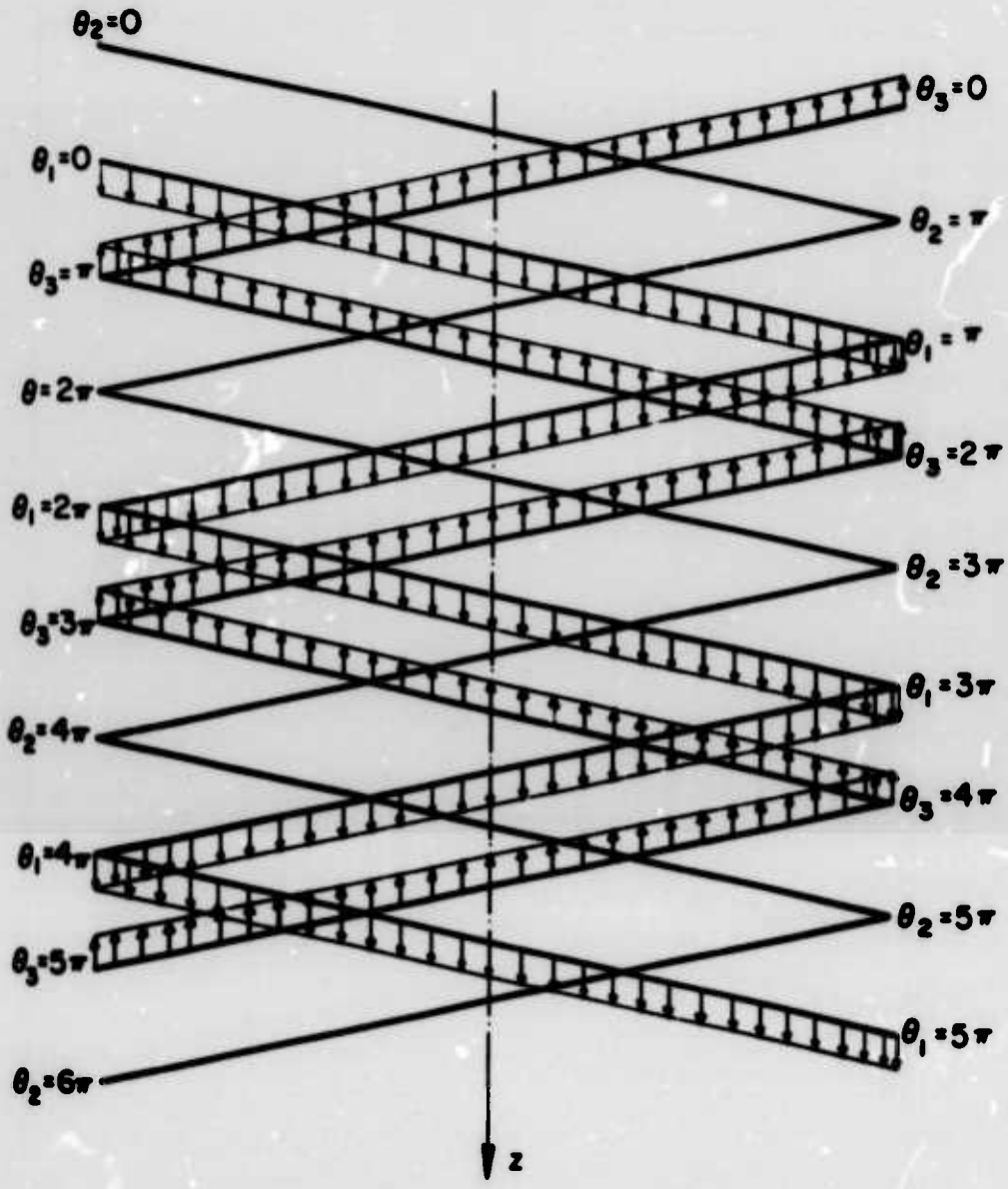

Figure 23. Real Component of Axial Perturbations for a Three-Bladed Rotor at Wave Number 0.0.

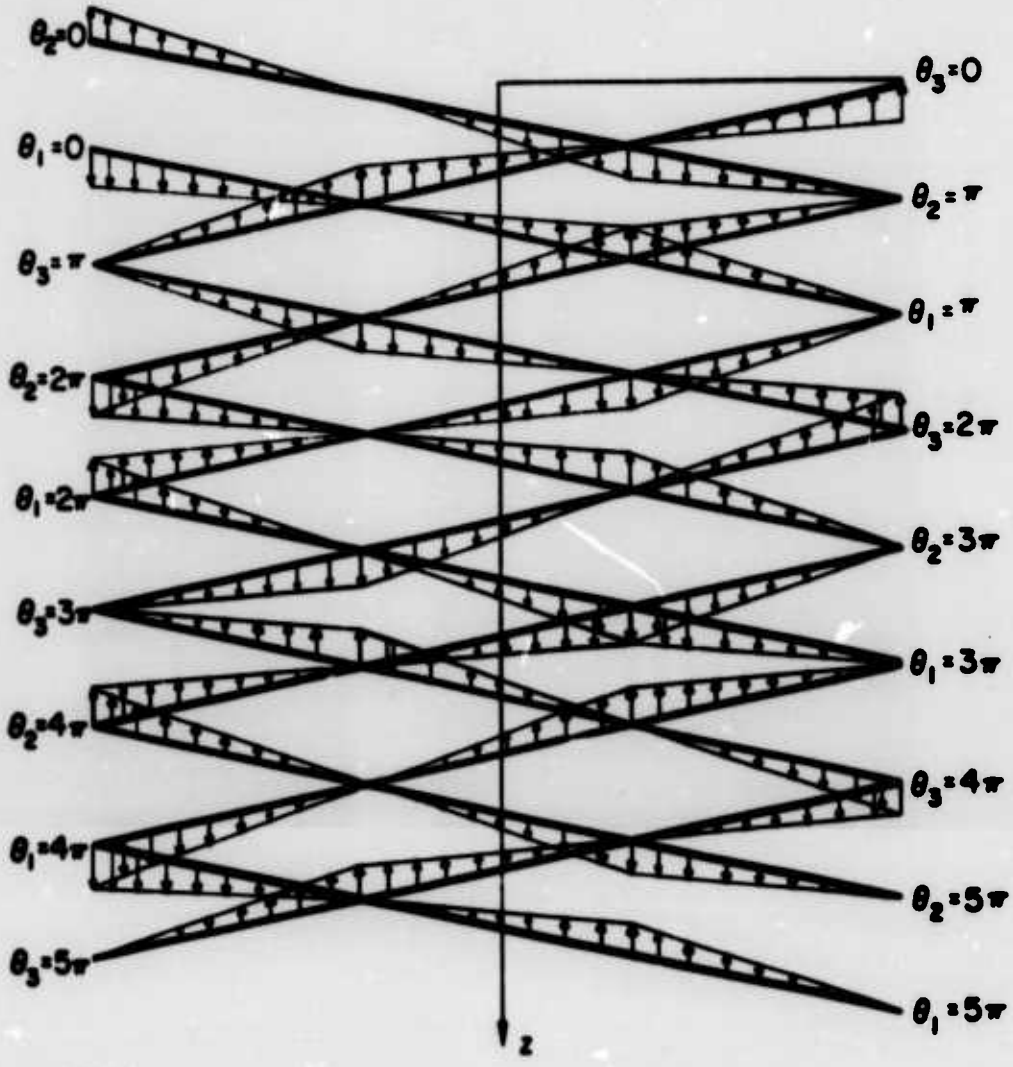

Figure 24. Real Component of Axial Perturbations for a Three-Bladed Rotor at Wave Number 1.5.

LITERATURE CITED

1. Glauert, H., AIRPLANE PROPELLERS, Aerodynamic Theory, edited by W. F. Durand, Dover Publications, New York, 1955, Chapter X, Division L, Vol. IV.

2. Shapiro, Jacob, PRINCIPLES OF HELICOPTER ENGINEERING, New York, McGraw-Hill Book Co., Inc., 1956, pp. 70-73.

3. Gessow, A.,and Myers, G. C. Jr., AERODYNAMICS OF THE HELICOPTER, New York, The MacMillan Company, 1952, pp. 46-47.

4. Mangler, K. W., CALCULATION OF INDUCED VELOCITY FIELD OF A ROTOR, Royal Aircraft Establishment Report, No. Aero.2247, 1948.

5. Loewy, R.,and Joglekar, M., AN ACTUATOR DISC ANALYSIS OF HELICOPTER WAKE GEOMETRY AND THE CORRESPONDING BLADE RESPONSE, University of Rochester; USAAVLABS Technical Report 69-66, U. S. Army Aviation Materiel Laboratories, Fort Eustis, Virginia, December 1970, AD 891981.

6. Goldstein, S., ON THE VORTEX THEORY OF SCREW PROPELLERS, Proceedings - Royal Society of London, Vol. A123, No. A792, 1929.

7. Jenny, D., Olson, J., and Landgrebe, A., A REASSESSMENT OF ROTOR HOVERING PERFORMANCE PREDICTION METHODS, Journal of the American Helicopter Society, Vol. 13, No. 2, April 1968, pp. 1-26.

8. Miller, R. H., ON THE COMPUTATION OF AIRLOADS ACTING ON ROTOR BLADES IN FORWARD FLIGHT, Journal of the American Helicopter Society, Vol. 7, No. 2, April 1962.

9. DuWaldt, F. A., Piziali, R. A., A METHOD FOR COMPUTING ROTARY WING AIRLOAD DISTRIBUTIONS IN FORWARD FLIGHT, U. S. Army TRECOM Report No. TCREC TR 62-44, November 1962.

10. Tarrarine, S., EXPERIMENTAL AND THEORETICAL STUDY OF LOCAL INDUCED VELOCITIES OVER A ROTOR DISC FOR ANALYTICAL EVALUATION OF THE PRIMARY LOADS ACTING ON HELICOPTER ROTOR BLADES, European Research Office, U. S. Army Contract, October 1960.

11. Landgrebe, A. J., AN ANALYTICAL AND EXPERIMENTAL INVESTIGATION OF HELICOPTER ROTOR HOVER PERFORMANCE AND WAKE GEOMETRY CHARACTERISTICS, United Aircraft Corporation; USAAMRDL Technical Report 71-24, U. S. Air Mobility Research and Development Laboratory, Fort Eustis, Virginia, June 1971, AD 728835.

12. Crimi, P., PREDICTION OF ROTOR WAKE FLOWS, presented at CAL/USAAVLABS symposium, Buffalo, New York, June 1966.

13. Sadler, Gene S., MAIN ROTOR FREE WAKE GEOMETRY EFFECTS ON BLADE AIR LOADS AND RESPONSE FOR HELICOPTERS IN STEADY MANEUVERS, Rochester Applied Science Associates, Inc., NASA CR-2110, National Aeronautics and Space Administration, Washington, D. C., September 1972.

14. Kármán, Theodore von, AERODYNAMICS, Ithaca, N. Y., Cornell University Press, 1954, Chapter II, pp. 31-59.

15. Levy, M. A., and Forsdyke, A. G., THE STEADY MOTION AND STABILITY OF A HELICAL VORTEX, Royal Society - Proceedings, Vol. 120, No. A786, October 1, 1928, pp. 670-690.

16. Widnall, S. E., THE STABILITY OF A HELICAL VORTEX FILAMENT, Journal of Fluid Mechanics, Vol. 54, Part 4, 1972, pp. 641-663.

17. Crow, S. C., STABILITY THEORY FOR A PAIR OF TRAILING VORTICES, American Institute of Aeronautics and Astronautics Journal, Vol. 8, No. 12, Dec. 1970, pp. 2172-2179.

18. Hama, F. R., PROGRESSIVE DEFORMATION OF A CURVED VORTEX FILAMENT BY ITS OWN INDUCTION, The Physics of Fluids, Vol. 5, No. 10, October 1962, pp. 1156-1162.

19. Hama, F. R., PROGRESSIVE DEFORMATION OF A PERTURBED LINE VORTEX FILAMENT, The Physics of Fluids, Vol. 6, No. 4, April 1963, pp. 526-534.

20. Parks, P. C., A NEW LOOK AT THE DYNAMICS OF VORTICES WITH FINITE CORES: Proceedings of Symposium on Aircraft Wake Turbulence held in Seattle, Washington, September 1970 (Included in the book AIRCRAFT WAKE TURBULENCE AND ITS DETECTION, editors, Olson, J. H., Goldberg, A., and Rogers, M., New York, Plenum Press, 1971, pp. 355-388).

21. Batchelor, G. K., AN INTRODUCTION TO FLUID DYNAMICS, Cambridge University Press, Cambridge, England, 1967, p. 264.

22. Hildebrand, F. B., INTRODUCTION TO NUMERICAL ANALYSIS, New York, McGraw-Hill Book Company, 1956, pp. 73, 141, 146.

23. Krylov, V. I., APPROXIMATE CALCULATION OF INTEGRALS, New York, The Macmillan Company, 1962, pp. 338-339.

24. Ralston, A., A FIRST COURSE IN NUMERICAL ANALYSIS, New York, McGraw-Hill Book Company, 1965, pp. 516-519.

25. Acton, F. S., NUMERICAL METHODS THAT WORK, New York, Harper and Row, 1970, p. 347.

26. Payne, P. R., HELICOPTER DYNAMICS AND AERODYNAMICS, New York, The Macmillan Company, 1959, p. 32.

27. Thomson, W., ON THE VIBRATIONS OF A COLUMNAR VORTEX, Philosophical Magazine, Serial 5, Volume 10, No. 61, Sept. 1880, pp. 155-168.

28. Widnall, S. E., and Sullivan, J., ON THE STABILITY OF VORTEX RINGS, Proceedings - Royal Society of London, Vol. A332, 1973, pp. 335-353.

29. Betchov, R., ON THE CURVATURE AND TORSION OF AN ISOLATED VORTEX FILAMENT, Journal of Fluid Mechanics, Vol. 22, Part 3, 1965, pp. 471-479.

30. Spreiter, J. R., and Sacks, A. H., THE ROLLING UP OF THE TRAILING VORTEX SHEET AND ITS EFFECT ON THE DOWNWASH BEHIND WINGS, Journal of the Aeronautical Sciences, Vol. 18, No. 1, Jan. 1951, pp. 21-32.

APPENDIX I
LIMITS FOR S. C. CROW'S CASE

The equivalence of the special case of the present work with that of Crow and Parks can be seen by noting that the direction z in the present study corresponds to the axial direction of the aircraft trailing vortex, and that the directions r and ϕ of the present study in the limit will correspond to the y and z directions, respectively, in S. C. Crow's theory. All the nondimensional parameters in Crow's work must be defined in terms of the parameters of the present study to demonstrate the correspondence. The r perturbation equation in the present study with above-mentioned restrictions can be written as

$$\alpha \delta\hat{r}_p = \sum_{m=1}^{n} \frac{\Gamma_m}{2\pi} \int_{-\infty}^{\infty} J_{mp}^{-3/2} \Big[ikr\delta\hat{r}_m \{ \omega x_{mp} \sin(x_{mp}+\psi_{mp}) \sin\omega x_{mp}$$

$$- x_{mp}\cos(x_{mp}+\psi_{mp})\cos\omega x_{mp} + \sin(x_{mp}+\psi_{mp})\cos\omega x_{mp}\}$$

$$+ ikr\delta\hat{r}_m \{-\omega x_{mp}\sin(x_{mp}+\psi_{mp})\cos\omega x_{mp} - x_{mp}\cos(x_{mp}+\psi_{mp})\sin\omega x_{mp}$$

$$+ \sin(x_{mp}+\psi_{mp})\sin\omega x_{mp}\} + ikr^2\delta\hat{\phi}_m \{\cos(x_{mp}+\psi_{mp})\cos(\omega x_{mp})$$

$$+ x_{mp}\sin(x_{mp}+\psi_{mp})\cos\omega x_{mp}$$

$$+ \omega x_{mp}\cos(x_{mp}+\psi_{mp})\sin\omega x_{mp}\} + ikr^2\delta\hat{\phi}_m$$

$$\{+\cos(x_{mp}+\psi_{mp})\sin\omega x_{mp} + x_{mp}\sin(x_{mp}+\psi_{mp})\sin\omega x_{mp}$$

$$- \omega x_{mp}\cos(x_{mp}+\psi_{mp})\cos\omega x_{mp}\} + ikr^2\delta\hat{\phi}_p\{-\cos(x_{mp}+\psi_{mp})$$

$$- x_{mp}\sin(x_{mp}+\psi_{mp})\}\Big] dx_{mp}$$

$$- 3\sum_{m=1}^{n} \frac{\Gamma_m}{4\pi} \int_{-\infty}^{\infty} J_{mp}^{-5/2} \Big[ikr^2 \{\sin(x_{mp}+\psi_{mp}) - x_{mp}\cos(x_{mp}+\psi_{mp})\}\Big] K_{mp} dx_{mp}$$

where J_{mp} and K_{mp} are defined in Section 2.6.

First the variables of the present theory will be transformed into corresponding variables used in S. C. Crow's analysis, and then the limit will be taken as helix pitch tends to infinity. All of S. C. Crow's parameters will carry the subscript 's' to avoid confusion.

From the definition of axial coordinate, $kr\chi = \chi_s$.

The perturbations in the present study are of the type $e^{\alpha t + i\omega x_{mp}}$,

and if the wave number in S. C. Crow's theory is expressed as $k_s = \frac{\omega}{k_T}$, the form of the perturbations is transformed to $e^{i k_s x_s + \alpha t}$ and the nondimensional wave number becomes $\beta_s = k_s \cdot 2r = k_s b$.

Applying the transformation described above, the self-induction term can be written as

$$\alpha \delta \hat{r}_1 = \frac{\Gamma_1}{2\pi} \int_0^\infty J_{11}^{-3/2} k_T \delta \hat{r}_1 \left[i \left\{ -\frac{\omega x_s}{k_T} \sin\left(\frac{x_s}{k_T}\right) \cos\left(\frac{\omega x_s}{k_T}\right) - \frac{x_s}{k_T} \cos\left(\frac{x_s}{k_T}\right) \sin\left(\frac{\omega x_s}{k_T}\right) \right.\right.$$

$$\left.\left. - \frac{x_s}{k_T} \cos\left(\frac{x_s}{k_T}\right) \sin\left(\frac{\omega x_s}{k_T}\right) + \sin\left(\frac{x_s}{k_T}\right) \sin\left(\frac{\omega x_s}{k_T}\right) \right\} \right] d\frac{x_s}{k_T}$$

$$+ \frac{\Gamma_1}{2\pi} \int_0^\infty J_{11}^{-3/2} k_T^2 \delta \hat{\Phi}_1 \left[\cos\left(\frac{x_s}{k_T}\right) \cos\left(\frac{\omega x_s}{k_T}\right) + \frac{x_s}{k_T} \sin\left(\frac{x_s}{k_T}\right) \cos\left(\frac{\omega x_s}{k_T}\right) \right.$$

$$\left. + \frac{\omega x_s}{k_T} \cos\left(\frac{x_s}{k_T}\right) \sin\left(\frac{\omega x_s}{k_T}\right) \right] d\frac{x_s}{k_T}$$

$$+ \frac{\Gamma_1}{4\pi} \int_{-\infty}^\infty J_{11}^{-3/2} k_T^2 \delta \hat{\Phi}_1 \left[-\cos\left(\frac{x_s}{k_T}\right) - \frac{x_s}{k_T} \sin\left(\frac{x_s}{k_T}\right) \right] d\frac{x_s}{k_T}$$

. . . . plus terms involving $J_{11}^{-5/2}$ . .

Now, $\frac{x_s}{k_T} = x \alpha \theta \to 0$ as helix pitch $\to \infty$, and one can approximate

$$\cos\left(\frac{x_s}{k_T}\right) \to 1$$

$$\sin\left(\frac{x_s}{k_T}\right) \to \frac{x_s}{k_T}$$

Neglecting $\left(\frac{x_s}{k_T}\right)^2$ terms and noting that $\frac{\omega}{k_T} \cong k_s$, it follows that $J_{11}^{-3/2} = \left[2r^2 - 2r^2 \cos\left(\frac{x_s}{k_T}\right) + \frac{k^2 x_s^2}{k^2} + \varepsilon_0^2\right] = \left[x_s^2 + \varepsilon_0^2\right]^{-3/2}$

and $\alpha \delta \hat{r}_1 = \frac{\Gamma_1}{2\pi} \int_0^\infty r \delta \hat{\Phi}_1 \left[\frac{\cos(k_s x_s) + k_s x_s \sin(k_s x_s) - 1}{(x_s^2 + \varepsilon^2)^{3/2}} \right] d x_s.$

Similarly, mutual-inductance terms can be written as

$$\alpha \delta \hat{r}_1 = \frac{\Gamma_2}{2\pi} \int_0^\infty J_{12}^{-3/2} \left[k_T \delta \hat{r}_2 \left\{ -\frac{\omega_1 x_s}{k_T} \sin\left(\frac{x_s}{k_T} + \pi\right) \cos\left(\frac{\omega x_s}{k_T}\right) \right.\right.$$

$$\left.\left. + i \sin\left(\frac{x_s}{k_T} + \pi\right) \sin\left(\frac{\omega x_s}{k_T}\right) - \frac{i x_s}{k_T} \cos\left(\frac{x_s}{k_T} + \pi\right) \sin\left(\frac{\omega x_s}{k_T}\right) \right\} \right] d\frac{x_s}{k_T}$$

$$+\frac{\Gamma_2}{2\pi}\int_0^\infty J_{12}^{-3/2}\, kr^2\,\delta\hat{\phi}_2\left[\cos\left(\frac{x_s}{kr}+\pi\right)\cos(k_s x_s)+\frac{x_s}{kr}\sin\left(\frac{x_s}{kr}+\pi\right)\cos(k_s x_s)\right.$$

$$\left.+\,k_s x_s\cos\left(\frac{x_s}{kr}+\pi\right)\sin k_s x_s\right]\frac{dx_s}{kr}$$

$$+\frac{\Gamma_2}{2\pi}\int_0^\infty J_{12}^{-3/2}\, kr^2\,\delta\hat{\phi}_1\left[-\cos\left(\frac{x_s}{kr}+\pi\right)-\frac{x_s}{kr}\sin\left(\frac{x_s}{kr}+\pi\right)\right]\frac{dx_s}{kr}$$

$$J_{12}^{-3/2}=\left[2r^2-2r^2\cos\left(\frac{x_s}{kr}+\pi\right)+\frac{k^2r^2x_s^2}{k^2r^2}\right]^{-3/2}$$

Taking the limits again yields $J_{12}^{-3/2}=\left[x_s^2+4r^2\right]^{-3/2}=\left[x_s^2+b^2\right]^{-3/2}$

and $\propto\delta\hat{r}_1=-\frac{\Gamma_2}{2\pi}\int_0^\infty r\delta\hat{\phi}_2\left[\frac{\cos k_s x_s+k_s x_s\sin k_s x_s}{(x_s^2+b^2)^{3/2}}\right]dx_s+\frac{\Gamma_2}{2\pi}\int_0^\infty\frac{r\delta\hat{\phi}_2\,dx_s}{(x_s^2+b^2)^{3/}}$

Writing $\delta\hat{r}_1=\hat{y}_{1s}$, $r\delta\hat{\phi}_1=\hat{z}_{1s}$, $\delta\hat{r}_2=\hat{y}_{2s}$ and $r\delta\hat{\phi}_2=\hat{z}_{2s}$, and remembering that $\delta\hat{r}$ is positive outward, while $\hat{y}_1$ and $\hat{y}_2$ are parallel (thereby changing sign of either the self- or mutual-inductance terms),

$$\propto\hat{y}_{1s}=\frac{\Gamma_1}{2\pi}\int_0^\infty\hat{z}_{1s}\frac{\cos k_s x_s+k_s x_s\sin k_s x_s-1}{(x_s^2+\varepsilon_0^2)^{3/2}}\,dx_s$$

$$-\frac{\Gamma_2}{2\pi}\int_0^\infty\hat{z}_{1s}\frac{1}{(x_s^2+b^2)^{3/2}}\,dx_s+\frac{\Gamma_2}{2\pi}\int_0^\infty\hat{z}_{2s}\frac{\cos(k_s x_s)+k_s x_s\sin(k_s x_s)}{(x_s^2+b^2)^{3/2}}\,dx_s$$

This is the same equation that results when Parks' modification is applied to Crow's theory. The one remaining equation relating $\hat{z}_{1s}$ with $\hat{y}_{1s}$ and $\hat{y}_{2s}$ can be obtained by following the same process for $r\delta\hat{\phi}_1$ perturbation equation.

APPENDIX II
FORTRAN IV SOURCE LISTING

	Page
Main Program	101
Subroutine ALLMAT	112
Subroutine QG9	121
Subroutine INTG	123
Function Subprogram DSIMP.	130

```
C                    * * * * * * * * * * * * * * * * *                  MAINC001
C                    *          MAIN PROGRAM          *                  MAIN0002
C                    * * * * * * * * * * * * * * * * *                  MAIN0003
      IMPLICIT REAL*8 (A-H,O-Z)                                         MAINC004
       REAL*4 PK                                                        MAIN0005
      REAL*4 CP(27) .                                                   MAINC006
      REAL*4 P1,P2,P3,P1,P2,B3,DELTA                                    MAINC007
      COMPLEX*8 A(18,18),CMPLX                                          MAINC008
       COMPLEX*8 COMPA(3,3),COMPB(3,3)                                  MAINC009
      COMPLEX*8  LAMBDA(3),LAMBDB(3)                                    MAIN0010
      COMPLEX*8 ADD(3,3)                                                MAIN0011
       COMPLEX*8  LAMBD(18)                                             MAIN0012
      DIMENSION Y(61),YA(61),B(27)                                      MAIN0013
      DIMENSION BD(61,51),CC(8),Z(61),C(51)                             MAIN0014
       COMMON A,AK,EPS                                                  MAIN0015
      COMMON P,L1,THETA,LL1                                             MAIN0016
C     INPUT NUMBER OF BLADES                                            MAIN0017
  100 READ(5,110) N,P                                                   MAIN0018
  110 FORMAT(I3,I3)                                                     MAIN0019
      IF(N.EQ.0) GO TO 600                                              MAIN0020
C     INPUT PITCH,WAVE NUMBER  AND CORE SIZE                            MAIN0021
  120 READ(5,130)AK,A,EPS                                               MAIN0022
  130 FORMAT(F8.3,2X,D10.3,10X,D10.3)                                   MAIN0023
      IF(AK.EQ.0.0)GO TO 100                                            MAIN0024
      AK=AK*1.000                                                       MAIN0025
      N2=3*N                                                            MAIN0026
      J1=61                                                             MAIN0027
      DO 140 I=1,N2                                                     MAIN0028
      DO 140 J=1,N2                                                     MAIN0029
  140 A(I,J)=CMPLX(0.0,0.0)                                             MAIN0030
      PI=3.14159265358979320D0                                          MAIN0031
      XU=2.D0*PI                                                        MAIN0032
      AAV=(1.D0+AK*AK)                                                  MAIN0033
```

```
      AA=EPS/DSQRT(AAK)                                                 MAIN0034
      ZZ=XU/AA                                                          MAIN0035
      ZI=DLOG(ZZ+(ZZ*ZZ+1.DO)**(.5DO))                                  MAIN0036
      TANHZI=DTANH(ZI)                                                  MAIN0037
      DEN=AAK*XU*XU+EPS*EPS                                             MAIN0038
C     CALCULATION OF ANALYTICALLY KNOWN  INTEGRALS FOR MODIFICATION OF  MAIN0039
C     SINGULAR SELF INDUCTION PERTURBATION INTEGRALS                    MAIN0040
      CC(1)=TANHZI/(EPS*EPS*DSQRT(AAK))                                 MAIN0041
      CC(2)=((1.DO/EPS)-(1.DO/DSQRT(DEN)))/AAK                          MAIN0042
      CC(3)=(ZI-TANHZI)/(AAK*DSQRT(AAK))                                MAIN0043
      CC(4)=(TANHZI-(TANHZI*TANHZI*TANHZI)/3.DO)/(AA**(4.DO))           MAIN0044
       CC(5)=(((1.DO/(EPS*EPS*EPS))-(1.DO/(DEN*DSQRT(DEN))))/(3.DO*AAK) MAIN0045
      CC(6)=(TANHZI*TANHZI*TANHZI)/(3.DO*EPS*EPS*AAK*DSQRT(AAK))        MAIN0046
      CC(7)=((2.DO/(3.DO*EPS))-1.DO/DSQRT(DEN)+(EPS*EPS)/(3.DO*(DEN*    MAIN0047
     1  DSQRT(DEN))))/(AAK*AAK)                                         MAIN0048
       CC(8)=(ZI-TANHZI-(TANHZI*TANHZI*TANHZI)/3.DO)/(AAK*AAK*DSQRT(AAK)MAIN0049
     1  )                                                              MAIN0050
      IF(N.NE.2) GO TO 150                                              MAIN0051
      CC(2)=0.0D0                                                       MAIN0052
      CC(5)=0.0D0                                                       MAIN0053
      CC(7)=0.0D0                                                       MAIN0054
  150 WRITE(6,160)(CC(I),I=1,8)                                         MAIN0055
  160 FORMAT(5X,8(D12.5,2X))                                            MAIN0056
      KL=2*N-1                                                          MAIN0057
      IF(N.EQ.2) KL=N                                                   MAIN0058
      DO 460 K=1,KU                                                     MAIN0059
      DO 170 I=1,J1                                                     MAIN0060
      Y(I)=0.0D0                                                        MAIN0061
      Z(I)=0.0D0                                                        MAIN0062
  170 YA(I)=0.0D0                                                       MAIN0063
      DO 180 I=1,27                                                     MAIN0064
  180 B(I)=0.0D0                                                        MAIN0065
      LL1=1                                                             MAIN0066
```

```
C       SET LL1=2 FOR SELF INDUCTION INTEGRALS                          MAIN0067
        IF(K.EQ.N)LL1=2                                                 MAIN0068
C       CORE SIZE FACTOR EPS IS SET ZERO IN MUTUAL INDUCTION INTEGRALS  MAIN0069
        EPS1=EPS                                                        MAIN0070
        IF(K.NE.N)EPS=0.000                                             MAIN0071
        IF(N.EQ.1)EPS=EPS1                                              MAIN0072
        DK=K                                                            MAIN0073
        DN=N                                                            MAIN0074
        THETA=2.000*PI*(1.00-DK/DN)                                     MAIN0075
C       SET UPPER CUT OFF LIMIT ON INFINITE INTEGRALS DEPENDING UPON PITCHMAIN0076
         IF(DK.LE.0.1)GO TO 220                                         MAIN0077
        IF(DK.LE.0.2) GO TO 210                                         MAIN0078
        IF(DK.LT.0.4) GO TO 200                                         MAIN0079
        IF(DK.LT.1.0) GO TO 190                                         MAIN0080
        J2=40                                                           MAIN0081
        GO TO 230                                                       MAIN0082
  190   J2=50                                                           MAIN0083
        GO TO 230                                                       MAIN0084
  200   J2=70                                                           MAIN0085
        GO TO 230                                                       MAIN0086
  210   J2=100                                                          MAIN0087
        GO TO 230                                                       MAIN0088
  220   J2=200                                                          MAIN0089
C       INTEGRATE USING QSIMP UP TO AN UPPER LIMIT OF 14*PI             MAIN0090
  230   DO 320 J=1,J2                                                   MAIN0091
        XL=(J-1)*(PI/3.00)                                              MAIN0092
        IF(J.LE.42)GO TO 250                                            MAIN0093
        L1=2                                                            MAIN0094
C       INTEGRATE USING QUADRATURE BEYOND 14*PI UP TO UPPER CUT OFF LIMIT MAIN0095
C       AT AN INTERVAL OF PI                                            MAIN0096
        XL=(J-2)*PI                                                     MAIN0097
        XU=(J-1)*PI                                                     MAIN0098
        CALL GQS(XL,XU,YA)                                              MAIN0099
```

```
      DO 240 KT=1,J1                                                    MAIN0100
  240 Z(KT)=Z(KT)+YA(KT)                                                MAIN0101
      GO TO 320                                                         MAIN0102
  250 L1=1                                                              MAIN0103
      IF(J.GT.6)L1=2                                                    MAIN0104
       H=PI/150.00                                                      MAIN0105
  260 DO 280 I=1,51                                                     MAIN0106
      X=XL+(I-1)*H                                                      MAIN0107
      CALL INTG(X,YA)                                                   MAIN0108
      DO 270 KR=1,J1                                                    MAIN0109
  270 BD(KR,I)=YA(KR)                                                   MAIN0110
  280 CONTINUE                                                          MAIN0111
       DO  300 KS=1,J1                                                  MAIN0112
      DO 290 I=1,51                                                     MAIN0113
  290 C(I)=BD(KS,I)                                                     MAIN0114
      Y(KS)=DSIMP(H,1,51,C)                                             MAIN0115
  300 CONTINUE                                                          MAIN0116
      DO 310 I=1,J1                                                     MAIN0117
  310 Z(I)=Z(I)+Y(I)                                                    MAIN0118
  320 CONTINUE                                                          MAIN0119
      IF(LL1.NE.2)GO TO 330                                             MAIN0120
C     ADD ANALYTICALLY EVALUATED INTEGRAL VALUES TO THE MODIFIED        MAIN0121
C     SELF INDUCTION INTEGRALS                                          MAIN0122
      Z(1)=Z(1)+CC(1)                                                   MAIN0123
      Z(2)=Z(2)+CC(1)                                                   MAIN0124
       Z(3)=Z(3)+CC(2)                                                  MAIN0125
      Z(4)=Z(4)+CC(2)                                                   MAIN0126
      Z(5)=Z(5)+CC(3)                                                   MAIN0127
      Z(6)=Z(6)+CC(1)                                                   MAIN0128
      Z(7)=Z(7)+CC(2)                                                   MAIN0129
      Z(8)=Z(8)+CC(1)                                                   MAIN0130
       Z(9)=Z(9)+CC(2)                                                  MAIN0131
      Z(10)=Z(10)+CC(2)                                                 MAIN0132
```

```
C       SET LL1=2 FOR SELF INDUCTION INTEGRALS                          MAIN0067
        IF(K.EQ.N)LL1=2                                                 MAIN0068
C       CORE SIZE FACTOR EPS IS SET ZERO IN MUTUAL INDUCTION INTEGRALS  MAIN0069
        EPS1=EPS                                                        MAIN0070
        IF(K.NE.N)EPS=0.000                                             MAIN0071
        IF(N.EQ.1)EPS=EPS1                                              MAIN0072
        DK=K                                                            MAIN0073
        DN=N                                                            MAIN0074
        THETA=2.00*PI*(1.00-DK/DN)                                      MAIN0075
C       SET UPPER CUT OFF LIMIT ON INFINITE INTEGRALS DEPENDING UPON PITCHMAIN0076
         IF(DK.LE.0.1)GO TO 220                                         MAIN0077
        IF(DK.LE.0.2) GO TO 210                                         MAIN0078
        IF(DK.LT.0.4) GO TO 200                                         MAIN0079
        IF(DK.LT.1.0) GO TO 190                                         MAIN0080
        J2=40                                                           MAIN0081
        GO TO 230                                                       MAIN0082
  190   J2=50                                                           MAIN0083
        GO TO 230                                                       MAIN0084
  200   J2=70                                                           MAIN0085
        GO TO 230                                                       MAIN0086
  210   J2=100                                                          MAIN0087
        GO TO 230                                                       MAIN0088
  220   J2=200                                                          MAIN0089
C       INTEGRATE USING DSIMP UP TO AN UPPER LIMIT OF 14*PI             MAIN0090
  230   DO 320 J=1,J2                                                   MAIN0091
        XL=(J-1)*(PI/3.00)                                              MAIN0092
        IF(J.LE.42)GO TO 250                                            MAIN0093
        LL=2                                                            MAIN0094
C       INTEGRATE USING QUADRATURE BEYOND 14*PI UP TO UPPER CUT OFF LIMIT MAIN0095
C       AT AN INTERVAL OF PI                                            MAIN0096
        XL=(J-25)*PI                                                    MAIN0097
        XU=(J-24)*PI                                                    MAIN0098
        CALL COS(XL,XU,YA)                                              MAIN0099
```

```
MAIN0133
MAIN0134
MAIN0135
MAIN0136
MAIN0137
MAIN0138
MAIN0139
MAIN0140
MAIN0141
MAIN0142
MAIN0143
MAIN0144
MAIN0145
MAIN0146
MAIN0147
MAIN0148
MAIN0149
MAIN0150
MAIN0151
MAIN0152
MAIN0153
MAIN0154
MAIN0155
MAIN0156
MAIN0157
MAIN0158
MAIN0159
MAIN0160
MAIN0161
MAIN0162
MAIN0163
MAIN0164
MAIN0165
```

```
Z(111)=Z(111)*CO(3)
Z(112)=Z(112)*CC(2)
Z(113)=Z(113)*CC(3)
Z(114)=Z(114)*CC(3)
Z(11E)=Z(116)*CC(4)
Z(117)=Z(117)*CC(5)
Z(11E)=Z(11E)*CC(4)
Z(119)=Z(119)*CO(5)
Z(12C)=Z(12C)*CC(5)
Z(121)=Z(121)*CC(6)
Z(122)=Z(122)*CC(4)
Z(123)=Z(123)*CO(5)
Z(124)=Z(124)*CC(6)
Z(125)=Z(125)*CC(5)
Z(126)=Z(126)*CO(6)
Z(127)=Z(127)*CC(7)
Z(12E)=Z(12E)*CC(6)
Z(129)=Z(129)*CC(7)
Z(13C)=Z(13C)*CC(4)
Z(131)=Z(131)*CO(5)
Z(132)=Z(132)*CO(6)
Z(133)=Z(133)*CC(5)
Z(134)=Z(134)*CC(6)
Z(135)=Z(135)*CC(7)
Z(13E)=Z(136)*CC(5)
Z(137)=Z(137)*CC(6)
Z(138)=Z(138)*CC(7)
Z(139)=Z(139)*CO(6)
Z(14C)=Z(14C)*CC(7)
Z(141)=Z(141)*CC(E)
Z(142)=Z(142)*CC(6)
Z(143)=Z(143)*CC(7)
Z(144)=Z(144)*CC(7)
```

```
      Z(45)=Z(45)+CC(8)                                                 MAIN0166
       Z(46)=Z(46)+CC(4)                                                MAIN0167
      Z(47)=Z(47)+CC(5)                                                 MAIN0168
      Z(48)=Z(48)+CC(4)                                                 MAIN0169
      Z(49)=Z(49)+CC(5)                                                 MAIN0170
       Z(50)=Z(50)+CC(5)                                                MAIN0171
      Z(51)=Z(51)+CC(6)                                                 MAIN0172
      Z(52)=Z(52)+CC(5)                                                 MAIN0173
      Z(53)=Z(53)+CC(6)                                                 MAIN0174
      Z(54)=Z(54)+CC(6)                                                 MAIN0175
      Z(55)=Z(55)+CC(7)                                                 MAIN0176
      Z(56)=Z(56)+CC(6)                                                 MAIN0177
      Z(57)=Z(57)+CC(7)                                                 MAIN0178
      Z(58)=Z(58)+CC(7)                                                 MAIN0179
      Z(59)=Z(59)+CC(8)                                                 MAIN0180
      Z(60)=Z(60)+CC(5)                                                 MAIN0181
      Z(61)=Z(61)+CC(6)                                                 MAIN0182
  330 DO 340 J=1,J1                                                     MAIN0183
  340 Y(J)=Z(J)                                                         MAIN0184
      EPS=EPS1                                                          MAIN0185
       CC=3.000                                                         MAIN0186
      CE=2.000                                                          MAIN0187
C     FORM THE 3*3 COMPLEX SELF OR MUTUAL INDUCTION MATRIX              MAIN0188
      P(1)=AK*(W*Y(15)+Y(10)-Y(12))-CC*AK*(Y(49)-Y(52)-Y(31)+Y(36))     MAIN0189
      P(2)=AK*(-W*Y(14)+Y(11)-Y(13))-CC*AK*(Y(51)-Y(34)-Y(54)+Y(39))    MAIN0190
      P(3)=AK*(W*Y(13)+Y(8)+Y(14))-CC*AK*(Y(32)-Y(37))                  MAIN0191
      P(4)=AK*(-W*Y(12)+Y(9)+Y(15))-CC*AK*(Y(35)-Y(40))                 MAIN0192
       P(5)=-W*Y(11)-Y(8)-CC*AK*AK*(Y(53)-Y(56))                        MAIN0193
      P(6)=W*Y(10)-Y(9)-CC*AK*AK*(Y(55)-Y(58))                          MAIN0194
      P(7)=AK*(-W*Y(13)-Y(8)-Y(14))-CC*AK*(Y(46)-CE*Y(48)-Y(53)+        MAIN0195
     1 Y(30)+Y(37))                                                     MAIN0196
      P(8)=AK*(W*Y(12)-Y(9)-Y(15))-CC*AK*(Y(47)-CE*Y(50)-Y(55)+Y(33)    MAIN0197
     1  +Y(40))                                                         MAIN0198
```

```
      B(5)=AK*(H*Y(15)+Y(10)-Y(12))-CD*AK*(Y(45)-Y(31)-Y(38))                    MAIN0199
       B(10)=AK*(-H*Y(14)+Y(11)-Y(13))-CD*AK*(Y(51)-Y(34)-Y(41))                MAIN0200
       B(11)=-Y(10)-CD*AK*AK*( Y(40)-Y(52)-Y(57))-H*Y(7)+H*Y(9)                 MAIN0201
      B(12)=-Y(11)-CD*AK*AK*(Y(61)-Y(54)-Y(55))+H*Y(6)-H*Y(8)                   MAIN0202
       B(13)=CE*Y(6)-Y(8)+H*Y(11)-CD*(Y(46)-CE*Y(46)+Y(30))                     MAIN0203
      B(14)=CE*Y(7)-Y(9)-H*Y(12)-CD*(Y(47)-CE*Y(50)+Y(33))                     MAIN0204
       B(15)=Y(10)-H*Y(7)+H*Y(9)-CD*(Y(45)-Y(31))                              MAIN0205
      B(16)=Y(11)+H*Y(6)-H*Y(8)-CD*(Y(51)-Y(34))                               MAIN0206
      B(17)=-CD*AK*(Y(40)-Y(52))                                               MAIN0207
      B(18)=-CD*AK*(Y(61)-Y(54))                                               MAIN0208
       B(19)=-CD*AK*(Y(19)+Y(25)-Y(23)-Y(20))                                  MAIN0209
      B(21)=CD*AK*AK*(Y(21)-Y(28))+Y(2)                                        MAIN0210
       B(24)=CD*AK*AK*(Y(17)-Y(20)-Y(29))+Y(3)                                 MAIN0211
      B(25)=-CD*(Y(16)-CE*Y(18)+Y(22))-Y(2)                                    MAIN0212
      B(26)=CD*(Y(19)-Y(23))-Y(3)                                              MAIN0213
      B(27)=CD*AK*(Y(17)-Y(20))                                                MAIN0214
  350  B(20)=CD*AK*(Y(24)-Y(26))-AK*(Y(2)+Y(5))                                 MAIN0215
      B(22)=-CD*AK*(Y(16)-CE*Y(18)-Y(21)+Y(22)+Y(26))+AK*(Y(2)+Y(5))           MAIN0216
      B(23)=CD*AK*(Y(19)-Y(23)-Y(27))+AK*(Y(4)-Y(3))                           MAIN0217
  360 WRITE(6,370) J2,AK                                                       MAIN0218
  370 FORMAT(5X,////,5X,I3,5H,*K=*,F5.2)                                       MAIN0219
       WRITE(6,380) (B(I),I=1,9)                                               MAIN0220
      WRITE(6,380) (B(I),I=10,18)                                              MAIN0221
      WRITE(6,380) (B(I),I=19,27)                                              MAIN0222
  380 FORMAT(2X,9(1PE12.5))                                                    MAIN0223
      CALL NOUNFL                                                              MAIN0224
C     FORM THE COMPLETE EIGENMATRIX AFTER CALCULATING ALL THE SELF AND         MAIN0225
C     MUTUAL INDUCTION MATRICES AND BY USING THE SYMMETRY CONSIDERATIONSMAIN0226
      IF(K.GT.A)GO TO 390                                                      MAIN0227
      IJ1=1                                                                    MAIN0228
      IJ2=K                                                                    MAIN0229
      MJ1=N+1-K                                                                MAIN0230
      MJ2=N                                                                    MAIN0231
```

```
      GO TO 400                                                          MAIN0232
  390 IJ1=K-N+1                                                          MAIN0233
       IJ2=N                                                             MAIN0234
      PJ1=1                                                              MAIN0235
      PJ2=2*N-K                                                          MAIN0236
  400 IJU=IJ2-IJ1+1                                                      MAIN0237
      IF(IJ1.NE.PJ1) GO TO 420                                           MAIN0238
      DO 410 L=1,18,2                                                    MAIN0239
      L2=(L+1)/2+18                                                      MAIN0240
  410 B(L)=B(L)+B(L2)                                                    MAIN0241
  420 DO 430 I=1,27                                                      MAIN0242
  430 CB(I)=B(I)                                                         MAIN0243
      DO 480 IJ=1,IJU                                                    MAIN0244
  440 IF(N.GT.1)GO TO 460                                                MAIN0245
      P1=CB(2)+CB(10)+CB(18)                                             MAIN0246
      P2=CB(12)*CB(16)-CB(10)*CB(18)-CB(2)*CB(10)-CB(2)*CB(18)           MAIN0247
     1  -CB(3)*CB(7)-CB(5)*CB(13)                                        MAIN0248
      P3=CB(2)*CB(12)*CB(16)+CB(3)*CB(13)*CB(12)+CB(5)*CB(7)*CB(16)-     MAIN0249
     1 CB(2)*CB(10)*CB(18)-CB(3)*CB(7)*CB(18)-CB(5)*CB(10)*CB(13)        MAIN0250
      P1=P1/3                                                            MAIN0251
      B2=-P2/3                                                           MAIN0252
      B3=-P3                                                             MAIN0253
      DELTA=3.*B1*B2*P1*B2+6.*(B1*B2*B3)-B3*B3*B3-4.*B2*B2*B2            MAIN0254
     1  -4.*B3*B1*B1*B1                                                  MAIN0255
      WRITE(6,450) P1,P2,P3,DELTA                                        MAIN0256
  450 FORMAT(5X,E12.5,5X,F12.5,5X,E12.5,5X,'DELTA=',E12.5)               MAIN0257
  460 I2=3*(IJ+IJ1-1)                                                    MAIN0258
       P2=3*(IJ+PJ1-1)                                                   MAIN0259
      A(I2-2,P2-2)=CMPLX(CB(1),CB(2))+A(I2-2,P2-2)                       MAIN0260
       A(I2-2,P2-1)=CMPLX(CB(3),CB(4)) +A(I2-2,P2-1)                     MAIN0261
      A(I2-2,P2)=CMPLX(CB(5),CB(6)) +A(I2-2,P2)                          MAIN0262
      A(I2-1,P2-2)=CMPLX(CB(7),CB(8))+A(I2-1,P2-2)                       MAIN0263
      A(I2-1,P2-1)=CMPLX(CB(9),CB(10)) +A(I2-1,P2-1)                     MAIN0264
```

```
      A(I2-1,M2)=CMPLX(CR(11),CR(12))+A(I2-1,M2)                        MAIN0265
      A(I2,M2-2)=CMPLX(CR(13),CR(14))+A(I2,M2-2)                        MAIN0266
      A(I2,M2-1)=CMPLX(CR(15),CR(16)) +A(I2,M2-1)                       MAIN0267
      A(I2,M2)=CMPLX(CR(17),CR(18)) +A(I2,M2)                           MAIN0268
      IF(I2.EQ.M2) GO TO 480                                            MAIN0269
      ACC(1,1)=CMPLX(CR(19),C.C)                                        MAIN0270
      ACC(1,2)=CMPLX(CR(20),C.C)                                        MAIN0271
      ACC(1,3)=CMPLX(CR(21),C.C)                                        MAIN0272
      ACC(2,1)=CMPLX(CR(22),C.C)                                        MAIN0273
      ACC(2,2)=CMPLX(CR(23),C.C)                                        MAIN0274
      ACC(2,3)=CMPLX(CR(24),C.C)                                        MAIN0275
      ACC(3,1)=CMPLX(CR(25),C.C)                                        MAIN0276
      ACC(3,2)=CMPLX(CR(26),C.C)                                        MAIN0277
      ACC(3,3)=CMPLX(CR(27),C.C)                                        MAIN0278
      DO 470 I=1,3                                                      MAIN0279
      DO 470 J=1,3                                                      MAIN0280
      A(I2-3+I,I2-3+J)=A(I2-3+I,I2-3+J)+ACC(I,J)                        MAIN0281
      IF(M.NE.2)GO TO 470                                               MAIN0282
       A(M2-3+I,M2-3+J)=A(M2-3+I,M2-3+J)+ACC(I,J)                       MAIN0283
  470 CONTINUE                                                          MAIN0284
  480 CONTINUE                                                          MAIN0285
       IF(N.EQ.1)GO TO 530                                              MAIN0286
      IF(M.NE.2)GO TO 530                                               MAIN0287
      IMO=N-1                                                           MAIN0288
      DO 500 IMI=1,IMO                                                  MAIN0289
      IM2=IMI+1                                                         MAIN0290
      DO 500 IMJ=IM2,N                                                  MAIN0291
        DO 490 I=1,3                                                    MAIN0292
      DO 490 J=1,3                                                      MAIN0293
       A(3*IMJ-3+I,3*IMI-3+J)=A(3*IMI-3+I,3*IMJ-3+J)                    MAIN0294
  490 CONTINUE                                                          MAIN0295
  500 CONTINUE                                                          MAIN0296
C     EXAMINE SPECIAL POSSIBLE SYMMETRY COMBINATIONS OF SYMMETRIC AND   MAIN0297
```

```
C     ANTI-SYMMETRIC MODES GIVING RISE TO MAX. AND MIN. DIVERGENCE      MAIN0298
C     RATES FOR THE CASE OF A TWO BLADED ROTOR                          MAIN0299
      IF(N.NE.2)GO TO 530                                               MAIN0300
      DO 510 I=1,3                                                      MAIN0301
      DO 510 J=1,3                                                      MAIN0302
      COMPA(I,J)=A(I,J)+A(I,J+3)                                        MAIN0303
      COMPM(I,J)=A(I,J)-A(I,J+3)                                        MAIN0304
  510 CONTINUE                                                          MAIN0305
      WRITE(6,520)                                                      MAIN0306
  520 FORMAT(////)                                                      MAIN0307
  530 WRITE(6,540)AK,L,EPS,N,M                                          MAIN0308
  540 FORMAT(5X,'PITCH=',F8.3,5X,'WAVE NUMBER=',D10.3,5X,'CORE SIZE=',  MAIN0309
     1  E10.3,5X,//,5X,'NUMBER OF BLADES=',I3,5X,'M=',I3,//)            MAIN0310
      WRITE(6,520)                                                      MAIN0311
  550 WRITE(6,560)                                                      MAIN0312
  560 FORMAT(5X,'MATRIX BEFORE  DIAGONALISATION',///)                   MAIN0313
      DO 570 I=1,N2                                                     MAIN0314
      DO 570 J=1,N2                                                     MAIN0315
  570 WRITE(6,580) A(I,J),I,J                                           MAIN0316
  580 FORMAT(5X,E12.5,5X,E12.5,5X,I3,5X,I3)                             MAIN0317
      KVEC=1                                                            MAIN0318
C     EIGENVALUE ANALYSIS PERFORMED BY CALLING ALLMAT                   MAIN0319
      CALL ALLMAT(A,LAMBD,N2,IR,NCAL,KVEC)                              MAIN0320
      WRITE(6,520)                                                      MAIN0321
      WRITE(6,590)                                                      MAIN0322
  590 FORMAT(5X,'EIGENFUNCTIONS',///)                                   MAIN0323
      DO 600 I=1,N2                                                     MAIN0324
      DO 600 J=1,N2                                                     MAIN0325
  600 WRITE(6,580) A(I,J),I,J                                           MAIN0326
      WRITE(6,610)                                                      MAIN0327
C     PRINT OUT REAL AND IMAGINARY PARTS OF EIGENVALUES                 MAIN0328
  610 FORMAT(5X,//,5X,'EIGENVALUES',//,19X,'REAL',11X,'IMAGINARY')      MAIN0329
      DO 620 I=1,N2                                                     MAIN0330
```

```
      620 WRITE(6,630) I,LAMBR(I)                                          MAIN0331
      630 FORMAT(5X,I3,5X,E12.5,5X,E12.5)                                  MAIN0332
          IF(N.NE.2) GO TO 670                                             MAIN0333
C         PRINT OUT SYMMETRIC AND ANTI-SYMMETRIC EIGENVALUES FOR THE CASE OFMAIN0334
C         TWO BLADED ROTOR                                                 MAIN0335
          CALL ALLMAT (COMMA,LAMMDA,3,3,NCAL,KVEC)                         MAIN0336
          CALL ALLMAT(COMMB,LAMMDB,3,3,NCAL,KVEC)                          MAIN0337
          WRITE(6,640)                                                     MAIN0338
      640 FORMAT(5X,//,9X,'SPECIAL POSSIBLE SYMMETRY COMBINATIONS GIVING   MAIN0339
         1  RISE TO MAX. DIVERGENCE RATE',//,9X,'EIGENVALUES',//,17X,'REAL' MAIN0340
         2 ,11X,'IMAGINARY',14X,'REAL',11X,'IMAGINARY',//)                 MAIN0341
          DO 650 I=1,3                                                     MAIN0342
      650 WRITE(6,660)LAMMDA(I),LAMMDB(I),I                                MAIN0343
      660 FORMAT(13X,E12.5,5X,E12.5,10X,E12.5,5X,E12.5,5X,I3)              MAIN0344
      670 GO TO 120                                                        MAIN0345
      680 STOP                                                             MAIN0346
          END                                                              MAIN0347
```

```
C                    * * * * * * * * * * * * * * * * *                  ALMT0001
C                    *    SUBROUTINE ALLPAT          *                  ALMT0002
C                    * * * * * * * * * * * * * * * * *                  ALMT0003
      SUBROUTINE ALLPAT(A,LAMBDA,M,IA,NCAL,KVEC)                        ALMT0004
C                                                                       ALMT0005
C     UNIVERSITY OF ROCHESTER FILE NO. 310.2.5C8.                       ALMT0006
C     A FORTRAN IV SUBROUTINE TO CALCULATE THE RIGHT EIGENVALUES AND/OR ALMT0007
C     EIGENVECTORS OF ARBITRARY COMPLEX MATRICES BY USE OF THE          ALMT0008
C     QR ALGORITHM AND WIELANDT INVERSE POWER METHOD FOR VECTORS.       ALMT0009
C     ALLPAT WAS WRITTEN BY R.E. FUNDERLIC AND J. RENZEL FOR THE        ALMT0010
C     IBM 7C9C COMPUTER AT OAK RIDGE AND SUBMITTED TO THE SHARE         ALMT0011
C     PROGRAM LIBRARY (OR AMAT).                                        ALMT0012
C                                                                       ALMT0013
C     ALLPAT IS ADOPTED FROM THE 7C9C FORTRAN IV PROGRAM OR AMAT FROM   ALMT0014
C     THE SHARE PROGRAM LIBRARY                                         ALMT0015
C                                                                       ALMT0016
C     THE MAXIMUM ORDER OF MATRIX A IS 60*6C                            ALMT0017
C                                                                       ALMT0018
C     THE SUBPROGRAM IS CALLED BY THE STATEMENT .                       ALMT0019
C                                                                       ALMT0020
C           CALL ALLPAT(A,LAMBDA,M,IA,NCAL,KVEC)                        ALMT0021
C                                                                       ALMT0022
C                        DESCRIPTION OF ARGUMENTS                       ALMT0023
C                                                                       ALMT0024
C     A      = COMPLEX*8,INPUT MATRIX. ON RETURN CONTAINS THE COMPLEX   ALMT0025
C              EIGENVECTORS OF THE ORIGINAL MATRIX AS COLUMNS, IF       ALMT0026
C              REQUESTED                                                ALMT0027
C     LAMBDA = COMPLEX*8,ARRAY OF EIGENVALUES OF MATRIX A UPON RETURN   ALMT0028
C     M      = INTEGER*4,ORDER OF MATRIX A                              ALMT0029
C     IA     = INTEGER*4, THE ROW DIMENSION OF MATRIX A                 ALMT0030
C     NCAL   = INTEGER*4, NUMBER OF EIGENVALUES CALCULATED UPON RETURN. ALMT0031
C     KVEC   = INTEGER*4, KVEC = C NO EIGENVECTORS CALCULATED, OTHERWISEALMT0032
C              EIGENVECTORS RETURNED AS COLUMNS OF A                    ALMT0033
```

```
C                                                                                ALMTC034
      CCMPLEX A(IA,IA),H(6C,6C),HL(6C,6C),LAMCLA(IA),VECT(6C),                   ALMT0035
     1HLLT(6C),SHIFT(3),TEMP,SUM,CIS,TEMP1,TEMP2                                 ALMT0036
      CCMPLEX*16 SUMT                                                            ALMTC037
      CCMPLEX*16 CP1,CP2                                                         ALMT0038
      CCMPLEX CSCRT,CCNJG                                                        ALMT0039
      LCGICAL INTR(6C),TWICE                                                     ALMT0040
      INTEGER INT(6C),R,RP1,RP2                                                  ALMTC041
      N=M                                                                        ALMT0042
      NCAL=N                                                                     ALMT0043
      IF(N.NE.1)GC TO 1CC                                                        ALMT0044
      LAMBDA(1)=A(1,1)                                                           ALMT0045
      A(1,1)=1.                                                                  ALMT0046
      GC TC 67C                                                                  ALMTC047
  1CC ICCUNT=C                                                                   ALMT0048
      SHIFT(1)=(C.,0.)                                                           ALMTC049
      SHIFT(2)=(C.,C.)                                                           ALMT0050
      SHIFT(3)=(C.,0.)                                                           ALMT0051
      IF(N.NE.2)GO TO 13C                                                        ALMT0052
  11C TEMP=(A(1,1)+A(2,2)+CSCRT((A(1,1)+A(2,2))**2-                              ALMT0053
     14.*(A(2,2)*A(1,1)-A(2,1)*A(1,2))))/2.                                      ALMT0054
      IF(REAL(TEMP).NE.C..CR.AIMAG(TEMP).NE.C.)GO TC 120                         ALMT0055
      LAMBDA(M)=SHIFT(1)                                                         ALMT0056
      LAMBDA(M-1)=A(1,1)+A(2,2)+SHIFT(1)                                         ALMT0057
      GC TC 470                                                                  ALMT0058
  12C LAMBDA(M)=TEMP+SHIFT(1)                                                    ALMT0059
      LAMBDA(M-1)=(A(2,2)*A(1,1)-A(2,1)*A(1,2))/(LAMBDA(M)-SHIFT(1))+SHIALMT0060
     1FT(1)                                                                      ALMT0061
      GC TC 470                                                                  ALMTC062
C                                                                                ALMTC063
C     REDUCE MATRIX A TO HESSENBERG FORM                                         ALMTC064
C                                                                                ALMTC065
  13C NM2=N-2                                                                    ALMTCC66
```

```
      DO 240 R=1,NP2                                                    ALMT0067
      RP1=R+1                                                           ALMT0068
      RP2=R+2                                                           ALMT0069
      ABIG=C.                                                           ALMT0070
      INT(R)=RP1                                                        ALMT0071
      DO 140 I=RP1,N                                                    ALMT0072
      ABSSC=REAL(A(I,R))**2+AIMAG(A(I,R))**2                            ALMT0073
      IF(ABSSC.LE.ABIG)GO TO 140                                        ALMT0074
      INT(R)=I                                                          ALMT0075
      ABIG=ABSSC                                                        ALMT0076
  140 CONTINUE                                                          ALMT0077
      INTER=INT(R)                                                      ALMT0078
      IF(ABS(ABIG).LT.1.E-50) GO TO 240                                 ALMT0079
      IF(INTER.EQ.RP1)GO TO 170                                         ALMT0080
      DO 150 I=R,N                                                      ALMT0081
      TEMP=A(RP1,I)                                                     ALMT0082
      A(RP1,I)=A(INTER,I)                                               ALMT0083
  150 A(INTER,I)=TEMP                                                   ALMT0084
      DO 160 I=1,N                                                      ALMT0085
      TEMP=A(I,RP1)                                                     ALMT0086
      A(I,RP1)=A(I,INTER)                                               ALMT0087
  160 A(I,INTER)=TEMP                                                   ALMT0088
  170 DO 180 I=RP2,N                                                    ALMT0089
      MULT(I) = A(I,R)/A(RP1,R)                                         ALMT0090
  180 A(I,R)=MULT(I)                                                    ALMT0091
      DO 200 I=1,RP1                                                    ALMT0092
      SUMT=C.C                                                          ALMT0093
      DO 190 J=RP2,N                                                    ALMT0094
      TP1=A(I,J)                                                        ALMT0095
      TP2=MULT(J)                                                       ALMT0096
  190 SUMT=SUMT+TP1*TP2                                                 ALMT0097
  200 A(I,RP1)=A(I,RP1)+SUMT                                            ALMT0098
      DO 220 I=RP2,N                                                    ALMT0099
```

```
      SUMT=0.0                                                          ALMT0100
      DO 210 J=RP2,N                                                    ALMT0101
      TP1=A(I,J)                                                        ALMT0102
      TP2=MULT(J)                                                       ALMT0103
  210 SUMT=SUMT+TP1*TP2                                                 ALMT0104
  220 A(I,RP1)=A(I,RP1)+SUMT-MULT(I)*A(RP1,RP1)                         ALMT0105
      DO 230 I=RP2,N                                                    ALMT0106
      DO 230 J=RP2,N                                                    ALMT0107
  230 A(I,J)=A(I,J)-MULT(I)*A(RP1,J)                                    ALMT0108
  240 CONTINUE                                                          ALMT0109
C                                                                       ALMT0110
C     CALCULATE EPSILON                                                 ALMT0111
C                                                                       ALMT0112
      EPS=0.                                                            ALMT0113
      DO 250 I=1,N                                                      ALMT0114
  250 EPS=EPS+CABS(A(1,I))                                              ALMT0115
      DO 270 I=2,N                                                      ALMT0116
      SUM=0.                                                            ALMT0117
      IM1=I-1                                                           ALMT0118
      DO 260 J=IM1,N                                                    ALMT0119
  260 SUM=SUM+CABS(A(I,J))                                              ALMT0120
  270 IF(SUM.GT.EPS)EPS=SUM                                             ALMT0121
      EPS=SQRT(FLOAT(N))*EPS*1.E-12                                     ALMT0122
      IF(EPS.EQ.0.)EPS=1.E-12                                           ALMT0123
      DO 280 I=1,N                                                      ALMT0124
      DO 280 J=1,N                                                      ALMT0125
  280 B(I,J)=A(I,J)                                                     ALMT0126
  290 IF(N.NE.1)GO TO 300                                               ALMT0127
      EIGEN(M)=A(1,1)+SHIFT(1)                                          ALMT0128
      GO TO 470                                                         ALMT0129
  300 IF(N.EQ.2)GO TO 110                                               ALMT0130
  310 NM1=N-1                                                           ALMT0131
      IF(REAL(A(N,N)).NE.0..OR.AIMAG(A(N,N)).NE.0.)                     ALMT0132
```

```
     1 IF(ABS(REAL(A(N,N-1)/A(N,N)))+ABS(AIMAG(A(N,N-1)/A(N,N)))-1.E-7) ALMT0133
     2 33C,33C,320                                                     ALMT0134
  320 IF(ABS(REAL(A(N,N-1)))+ABS(AIMAG(A(N,N-1))).GE.EPS)GO TO 34C     ALMT0135
  330 LAMBDA(PN1)=A(N,N)+SHIFT(1)                                      ALMT0136
      ICOUNT=0                                                         ALMT0137
      N=N-1                                                            ALMT0138
      GO TO 3CC                                                        ALMT0139
C                                                                      ALMT0140
C     DETERMINE SHIFT                                                  ALMT0141
C                                                                      ALMT0142
  34C SHIFT(2)=(A(N-1,N-1)+A(N,N)+CSQRT((A(N-1,N-1)+A(N,N))**2        ALMT0143
     1 -4.*(A(N,N)*A(N-1,N-1)-A(N,N-1)*A(N-1,N))))/2.                  ALMT0144
      IF(REAL(SHIFT(2)).NE.C..OR.AIMAG(SHIFT(2)).NE.C.)GO TO 350       ALMT0145
      SHIFT(3)=A(N-1,N-1)+A(N,N)                                       ALMT0146
      GO TO 36C                                                        ALMT0147
  35C SHIFT(3)=(A(N,N)*A(N-1,N-1)-A(N,N-1)*A(N-1,N))/SHIFT(2)          ALMT0148
  36C IF(CABS(SHIFT(2)-A(N,N)).LT.CABS(SHIFT(3)-A(N,N)))GO TO 370      ALMT0149
      INDEX=3                                                          ALMT0150
      GO TO 38C                                                        ALMT0151
  37C INDEX=2                                                          ALMT0152
  38C IF(CABS(A(N-1,N-2)).GE.EPS)GO TO 39C                             ALMT0153
      LAMBDA(PN1)=SHIFT(2)+SHIFT(1)                                    ALMT0154
      LAMBDA(PN1+1)=SHIFT(3)+SHIFT(1)                                  ALMT0155
      ICOUNT=0                                                         ALMT0156
      N=N-2                                                            ALMT0157
      GO TO 29C                                                        ALMT0158
  39C SHIFT(1)=SHIFT(1)+SHIFT(INDEX)                                   ALMT0159
      DO 4CC I=1,N                                                     ALMT0160
  4CC A(I,I)=A(I,I)-SHIFT(INDEX)                                       ALMT0161
C                                                                      ALMT0162
C     PERFORM GIVENS ROTATIONS, OR ITERATES                            ALMT0163
C                                                                      ALMT0164
      IF(ICOUNT.LE.1C)GO TO 41C                                        ALMT0165
```

```
      NCAL=P-K                                                          ALMT0166
      GO TO 470                                                         ALMT0167
  410 NP1=K-1                                                           ALMT0168
      TEMP1=A(1,1)                                                      ALMT0169
      TEMP2=A(2,1)                                                      ALMT0170
      DO 460 R=1,NP1                                                    ALMT0171
      RP1=R+1                                                           ALMT0172
      RHO=SQRT(REAL(TEMP1)**2+AIMAG(TEMP1)**2+                          ALMT0173
     1 REAL(TEMP2)**2+AIMAG(TEMP2)**2)                                  ALMT0174
      IF(RHO.EQ.0.)GO TO 460                                            ALMT0175
      CIS=TEMP1/RHO                                                     ALMT0176
      SCN=TEMP2/RHO                                                     ALMT0177
      INDEX=MAXO(R-1,1)                                                 ALMT0178
      DO 420 I=INDEX,N                                                  ALMT0179
      TEMP=CONJG(CIS)*A(R,I)+CONJG(SCN)*A(RP1,I)                        ALMT0180
      A(RP1,I)=-SCN*A(R,I)+CIS*A(RP1,I)                                 ALMT0181
  420 A(R,I)=TEMP                                                       ALMT0182
      TEMP1=A(RP1,RP1)                                                  ALMT0183
      IF(R+2.GT.N)GO TO 430                                             ALMT0184
      TEMP2=A(R+2,R+1)                                                  ALMT0185
  430 DO 440 I=1,R                                                      ALMT0186
      TEMP=CIS*A(I,R)+SCN*A(I,RP1)                                      ALMT0187
      A(I,RP1)=-CONJG(SCN)*A(I,R)+CONJG(CIS)*A(I,RP1)                   ALMT0188
  440 A(I,R)=TEMP                                                       ALMT0189
      INDEX=MINO(R+2,N)                                                 ALMT0190
      DO 450 I=RP1,INDEX                                                ALMT0191
      A(I,R)=SCN*A(I,RP1)                                               ALMT0192
  450 A(I,RP1)=CONJG(CIS)*A(I,RP1)                                      ALMT0193
  460 CONTINUE                                                          ALMT0194
      ICOUNT=ICOUNT+1                                                   ALMT0195
      GO TO 310                                                         ALMT0196
C                                                                       ALMT0197
C     CALCULATE VECTORS                                                 ALMT0198
```

```
C                                                                       ALMT0199
  470 IF(NCAL.EQ.0)GO TO 670                                            ALMT0200
      IF(NVEC.EQ.0)GO TO 670                                            ALMT0201
      N=M                                                               ALMT0202
      NM1=N-1                                                           ALMT0203
      IF(N.NE.2)GO TO 480                                               ALMT0204
      EPS=AMAX1(CABS(LAMBDA(1)),CABS(LAMBDA(2)))*1.E-8                  ALMT0205
      IF(EPS.EQ.0.)EPS=1.E-12                                           ALMT0206
      H(1,1)=A(1,1)                                                     ALMT0207
      H(1,2)=A(1,2)                                                     ALMT0208
      H(2,1)=A(2,1)                                                     ALMT0209
      H(2,2)=A(2,2)                                                     ALMT0210
  480 DO 660 L=1,NCAL                                                   ALMT0211
      DO 500 I=1,N                                                      ALMT0212
      DO 490 J=1,N                                                      ALMT0213
  490 HL(I,J)=H(I,J)                                                    ALMT0214
  500 HL(I,I)=HL(I,I)-LAMBDA(L)                                         ALMT0215
      DO 540 I=1,NM1                                                    ALMT0216
      MULT(I)=0.                                                        ALMT0217
      INTH(I)=.FALSE.                                                   ALMT0218
      IP1=I+1                                                           ALMT0219
      IF(CABS(HL(I+1,I)).LE.CABS(HL(I,I)))GO TO 520                     ALMT0220
      INTH(I)=.TRUE.                                                    ALMT0221
      DO 510 J=I,N                                                      ALMT0222
      TEMP=HL(I+1,J)                                                    ALMT0223
      HL(I+1,J)=HL(I,J)                                                 ALMT0224
  510 HL(I,J)=TEMP                                                      ALMT0225
  520 IF(REAL(HL(I,I)).EQ.0..AND.AIMAG(HL(I,I)).EQ.0.)GO TO 540         ALMT0226
      MULT(I)=-HL(I+1,I)/HL(I,I)                                        ALMT0227
      DO 530 J=IP1,N                                                    ALMT0228
  530 HL(I+1,J)=HL(I+1,J)+MULT(I)*HL(I,J)                               ALMT0229
  540 CONTINUE                                                          ALMT0230
      DO 550 I=1,N                                                      ALMT0231
```

```
      550 VECT(II)=1.                                                          ALMT0232
          TWICE=.FALSE.                                                        ALMT0233
      560 IF(REAL(HL(N,N)).EQ.0..AND.AIMAG(HL(N,N)).EQ.0.)HL(N,N)=EPS          ALMT0234
          VECT(N)=VECT(N)/HL(N,N)                                              ALMT0235
          DO 580 I=1,NM1                                                       ALMT0236
          K=N-I                                                                ALMT0237
          DO 570 J=K,NM1                                                       ALMT0238
      570 VECT(K)=VECT(K)-HL(K,J+1)*VECT(J+1)                                  ALMT0239
          IF(REAL(HL(K,K)).EQ.0..AND.AIMAG(HL(K,K)).EQ.0.)HL(K,K)=EPS          ALMT0240
      580 VECT(K)=VECT(K)/HL(K,K)                                              ALMT0241
          BIG=0.                                                               ALMT0242
          DO 590 I=1,N                                                         ALMT0243
          SUM=ABS(REAL(VECT(I)))+ABS(AIMAG(VECT(I)))                           ALMT0244
      590 IF(SUM.GT.BIG)BIG=SUM                                                ALMT0245
          DO 600 I=1,N                                                         ALMT0246
      600 VECT(I)=VECT(I)/BIG                                                  ALMT0247
          IF(TWICE)GO TO 620                                                   ALMT0248
          DO 610 I=1,NM1                                                       ALMT0249
          IF(.NOT.INTR(I))GO TO 610                                            ALMT0250
          TEMP=VECT(I)                                                         ALMT0251
          VECT(I)=VECT(I+1)                                                    ALMT0252
          VECT(I+1)=TEMP                                                       ALMT0253
      610 VECT(I+1)=VECT(I+1)+MULT(I)*VECT(I)                                  ALMT0254
          TWICE=.TRUE.                                                         ALMT0255
          GO TO 560                                                            ALMT0256
      620 IF(N.EQ.2)GO TO 650                                                  ALMT0257
          NM2=N-2                                                              ALMT0258
          DO 640 I=1,NM2                                                       ALMT0259
          NII=N-1-I                                                            ALMT0260
          NII1=N-I+1                                                           ALMT0261
          DO 630 J=NII,N                                                       ALMT0262
      630 VECT(J)=HL(J,NII)*VECT(NII+1)+VECT(J)                                ALMT0263
          INDEX=INT(NII)                                                       ALMT0264
```

```
      TEMP=VECT(N11+1)                                          ALMT0265
      VECT(N11+1)=VECT(INDEX)                                   ALMT0266
  640 VECT(INDEX)=TEMP                                          ALMT0267
  650 DO 660 I=1,N                                              ALMT0268
  660 A(I,L)=VECT(I)                                            ALMT0269
  670 RETURN                                                    ALMT0270
      END                                                       ALMT0271
```

```
C                    * * * * * * * * * * * * * * * * *                  CG90001
C                    *      SUBROUTINE CGS           *                  CG90002
C                    * * * * * * * * * * * * * * * * *                  CG90003
C                                                                       CG90004
C     SUBROUTINE CGS EVALUATES THE INTEGRALS BY MEANS OF A 12-POINT     CG90005
C     GAUSS QUADRATURE FORMULA.THE NODES AND COEFFICIENTS ARE TAKEN FROM CG90006
C     KRYLOV(1962,10)AND IBM PUBLICATION SYSTEM/360 SCIENTIFIC SUBROUTINE CG90007
C     PACKAGE .SUBROUTINE INTG SUPPLIES THE INTEGRAND FUNCTIONS TO BE   CG90008
C     INTEGRATED                                                        CG90009
C                                                                       CG90010
C     THE SUBROUTINE IS CALLED BY THE STATEMENT.                        CG90011
C                                                                       CG90012
C              CALL CG9(XL,XU,Y)                                        CG90013
C     WHERE                                                             CG90014
C     XL=REAL*8,LOWER LIMIT ON THE INTEGRAL                             CG90015
C     XU=REAL*8,UPPER LIMIT ON THE INTEGRAL                             CG90016
C      Y=REAL*8,ARRAY OF INTEGRATED VALUES BETWEEN THE LIMITS XL AND XU CG90017
      SUBROUTINE CGS(XL,XU,Y)                                           CG90018
       IMPLICIT REAL*8 (A-H,O-Z)                                        CG90019
      DIMENSION Y(61),ZA(61),ZB(61)                                     CG90020
      J1=61                                                             CG90021
      A=.5D0*(XU+XL)                                                    CG90022
       B=XU-XL                                                          CG90023
      C=.49078031712335960D0*B                                          CG90024
      CALL INTG(A+C,ZA)                                                 CG90025
      CALL INTG(A-C,ZB)                                                 CG90026
      DO 10C I=1,J1                                                     CG90027
   10C Y(I)=.2358766819325591D-1*(ZA(I)+ZB(I))                          CG90028
      C=.45205962818523746D0*B                                          CG90029
      CALL INTG(A+C,ZA)                                                 CG90030
      CALL INTG(A-C,ZB)                                                 CG90031
      DO 11C I=1,J1                                                     CG90032
   11C Y(I)=Y(I)+.5346966295765922D-1*(ZA(I)+ZB(I))                     CG90033
```

```
      C=.3E4551337057152300*B                                          GG90034
      CALL INTG(A+C,ZA)                                                GG90035
      CALL INTG(A-C,ZB)                                                GG90036
      DO 120 I=1,J1                                                    GG90037
  120 Y(I)=Y(I)+.ACC3516427167310-1*(ZA(I)+ZB(I))                      GG90038
      C=.2936595771433C87DC*B                                          GG90039
      CALL INTG(A+C,ZA)                                                GG90040
      CALL INTG(A-C,ZB)                                                GG90041
      DO 130 I=1,J1                                                    GG90042
  130 Y(I)=Y(I)+.1015837133615330DC*(ZA(I)+ZB(I))                      GG90043
      C=.1E3915749455C901DC*B                                          GG90044
      CALL INTG(A+C,ZA)                                                GG90045
      CALL INTG(A-C,ZB)                                                GG90046
      DO 140 I=1,J1                                                    GG90047
  140 Y(I)=Y(I)+.11674626F2651770C*(ZA(I)+ZB(I))                       GG90048
      C=.E2C167C425573446D-1*B                                         GG90049
      CALL INTG(A+C,ZA)                                                GG90050
      CALL INTG(A-C,ZB)                                                GG90051
      DO 150 I=1,J1                                                    GG90052
  150 Y(I)=B*(Y(I)+.1245735229067C14DC*(ZA(I)+ZB(I)))                  GG90053
      RETURN                                                           GG90054
      END                                                              GG90055
```

```
C                    * * * * * * * * * * * * * * * * * *                    INTGC001
C                    *      SUBROUTINE INTG              *                  INTGC002
C                    * * * * * * * * * * * * * * * * * *                    INTG0003
C                                                                           INTGC004
C     THIS SUBPROGRAM SUPPLIES THE INTEGRAND FUNCTIONS FOR A GIVEN VALUE    INTG0005
C     OF THE ARGUEMENT EITHER TO THE MAIN PROGRAM OR TO SUBROUTINE GG       INTG0006
C                                                                           INTG0007
C     THE CALLING STATEMENT IS .                                            INTGC008
C          CALL INTG(X,Z)                                                   INTGC009
C     WHERE                                                                 INTG0010
C     X=REAL*8 VARIABLE OF INTEGRATION                                      INTG0011
C     Z=REAL*8 ARRAY OF INTEGRAND FUNCTIONS FOR GIVEN VALUE OF X            INTG0012
C     UPON RETURN                                                           INTGC013
      SUBROUTINE INTG(X,Z)                                                  INTG0014
      IMPLICIT REAL*8 (A-H,O-Z)                                             INTGC015
       DIMENSION Z(61)                                                      INTGC016
      DIMENSION CC(8)                                                       INTGC017
       COMMON B,AK,EPS                                                      INTG0018
      COMMON P,L1,THETA,LL1                                                 INTGC019
      I=L1                                                                  INTGC020
      DO 100 J=1,61                                                         INTG0021
  100 Z(J)=0.000                                                            INTG0022
      A1=DCOS(X+THETA)                                                      INTG0023
      A2=DSIN(X+THETA)                                                      INTG0024
      A3=DCOS(W*X)                                                          INTG0025
      A4=DSIN(W*X)                                                          INTG0026
      AJ=2.000-2.000*A1*AK*AK*X*X+EPS*EPS                                   INTG0027
      AP=AJ**(-1.500)                                                       INTG0028
      AP=AJ**(-2.500)                                                       INTG0029
      Z(1)=AP                                                               INTG0030
      Z(2)=A1*AP                                                            INTG0031
      Z(3)=A2*AP                                                            INTGC032
      Z(4)=X*A1*AP                                                          INTG0033
```

```
INTG0034
INTG0035
INTG0036
INTG0037
INTG0038
INTG0039
INTG0040
INTG0041
INTG0042
INTG0043
INTG0044
INTG0045
INTG0046
INTG0047
INTG0048
INTG0049
INTG0050
INTG0051
INTG0052
INTG0053
INTG0054
INTG0055
INTG0056
INTG0057
INTG0058
INTG0059
INTG0060
INTG0061
INTG0062
INTG0063
INTG0064
INTG0065
INTG0066
```

```
2151=X*A20AP
2161=A30AP
2171=A40AP
2181=A1*A20AP
2151=A1*7(7)
2101=A2*2(6)
2111=A2*2(7)
2121=X*7(8)
2131=X*7(9)
2141=X*7(10)
2151=X*7(11)
2161=AP
2171=X*AP
2181=A1*AP
2191=A2*AP
2201=X*7(18)
2211=X*7(19)
2221=A1*7(18)
2231=A2*7(18)
2241=A*2(19)
2251=X*7(22)
2261=X*7(23)
2271=X*7(24)
2281=X*2(2C)
2291=X*2(21)
2301=A3*2(22)
2311=A4*2(23)
2321=A3*2(24)
2331=A4*7(22)
2341=A4*2(23)
2351=A4*7(24)
2361=X*2(3C)
2371=X*7(31)
```

```
      Z(38)=X*Z(32)                                                     INTG0067
      Z(39)=X*Z(33)                                                     INTG0068
      Z(40)=X*Z(34)                                                     INTG0069
       Z(41)=X*Z(35)                                                    INTG0070
      Z(42)=A3*Z(28)                                                    INTG0071
      Z(43)=A3*Z(29)                                                    INTG0072
      Z(44)=A4*Z(28)                                                    INTG0073
      Z(45)=A4*Z(29)                                                    INTG0074
      Z(46)=A3*AP                                                       INTG0075
      Z(47)=A4*AP                                                       INTG0076
      Z(48)=A1*Z(46)                                                    INTG0077
      Z(49)=A2*Z(46)                                                    INTG0078
      Z(50)=A1*Z(47)                                                    INTG0079
      Z(51)=A2*Z(47)                                                    INTG0080
      Z(52)=X*Z(48)                                                     INTG0081
      Z(53)=X*Z(49)                                                     INTG0082
      Z(54)=X*Z(50)                                                     INTG0083
      Z(55)=X*Z(51)                                                     INTG0084
      Z(56)=X*Z(52)                                                     INTG0085
      Z(57)=X*Z(53)                                                     INTG0086
      Z(58)=X*Z(54)                                                     INTG0087
       Z(59)=X*Z(55)                                                    INTG0088
      Z(60)=X*Z(46)                                                     INTG0089
      Z(61)=X*Z(47)                                                     INTG0090
C     LL1 IS SET EQUAL TO 2 FOR CALCULATION OF SELF INDUCED INTEGRAL ,  INTG0091
C     IN THIS SITUATION  THE PERTURBATION INTEGRAL BECOMES SINGULAR     INTG0092
C     AND INTEGRALS ARE TO BE MODIFIED FOR NUMERICAL INTEGRATION        INTG0093
      IF(LL1.NE.2)GO TO 110                                             INTG0094
C     L1 IS SET EQUAL TO 2 FOR INTEGRATION LIMIT BEYOND 2*PI AFTER WHICHINTG0095
C     THE SELF INDUCTION INTEGRALS ARE NO MORE MODIFIED                 INTG0096
      IF(I.EQ.2)GO TO 110                                               INTG0097
      AI=(AK*AK+1)*X*X+EPS*EPS                                          INTG0098
      AA=AI**(-1.5D0)                                                   INTG0099
```

```
AC=A100*(-2.5CC)                                                INTG0100
CC(1)=AC                                                        INTG0101
CC(2)=XCC(1)                                                    INTG0102
CC(3)=XCC(2)                                                    INTG0103
CC(4)=AC                                                        INTG0104
CC(5)=XCC(4)                                                    INTG0105
CC(6)=XCC(5)                                                    INTG0106
CC(7)=XCC(6)                                                    INTG0107
CC(8)=XCC(7)                                                    INTG0108
Z(1)=Z(1)-CC(1)                                                 INTG0109
Z(2)=Z(2)-CC(1)                                                 INTG0110
  Z(3)=Z(3)-CC(2)                                               INTG0111
Z(4)=Z(4)-CC(2)                                                 INTG0112
Z(5)=Z(5)-CC(3)                                                 INTG0113
Z(6)=Z(6)-CC(1)                                                 INTG0114
Z(7)=Z(7)-CC(2)                                                 INTG0115
Z(8)=Z(8)-CC(1)                                                 INTG0116
  Z(9)=Z(9)-CC(2)                                               INTG0117
Z(10)=Z(10)-CC(3)                                               INTG0118
  Z(11)=Z(11)-CC(3)                                             INTG0119
Z(12)=Z(12)-CC(2)                                               INTG0120
Z(13)=Z(13)-CC(3)                                               INTG0121
Z(14)=Z(14)-CC(3)                                               INTG0122
Z(16)=Z(16)-CC(4)                                               INTG0123
Z(17)=Z(17)-CC(5)                                               INTG0124
  Z(18)=Z(18)-CC(4)                                             INTG0125
  Z(19)=Z(19)-CC(5)                                             INTG0126
Z(20)=Z(20)-CC(5)                                               INTG0127
Z(21)=Z(21)-CC(6)                                               INTG0128
Z(22)=Z(22)-CC(4)                                               INTG0129
Z(23)=Z(23)-CC(5)                                               INTG0130
Z(24)=Z(24)-CC(6)                                               INTG0131
Z(25)=Z(25)-CC(5)                                               INTG0132
```

```
INTG0133
INTG0134
INTG0135
INTG0136
INTG0137
INTG0138
INTG0139
INTG0140
INTG0141
INTG0142
INTG0143
INTG0144
INTG0145
INTG0146
INTG0147
INTG0148
INTG0149
INTG0150
INTG0151
INTG0152
INTG0153
INTG0154
INTG0155
INTG0156
INTG0157
INTG0158
INTG0159
INTG0160
INTG0161
INTG0162
INTG0163
INTG0164
INTG0165
```

```
2126)=Z(126)-CC(6)
2127)=Z(127)-CC(7)
2128)=Z(128)-CC(6)
2129)=Z(129)-CC(7)
2130)=Z(130)-CC(4)
2131)=Z(131)-CC(5)
2132)=Z(132)-CC(6)
2133)=Z(133)-CC(5)
2134)=Z(134)-CC(6)
2135)=Z(135)-CC(7)
2136)=Z(136)-CC(5)
2137)=Z(137)-CC(6)
2138)=Z(138)-CC(7)
2139)=Z(139)-CC(6)
2140)=Z(140)-CC(7)
2141)=Z(141)-CC(8)
2142)=Z(142)-CC(6)
2143)=Z(143)-CC(7)
2144)=Z(144)-CC(7)
2145)=Z(145)-CC(8)
2146)=Z(146)-CC(4)
2147)=Z(147)-CC(5)
2148)=Z(148)-CC(4)
2149)=Z(149)-CC(5)
2150)=Z(150)-CC(5)
2151)=Z(151)-CC(6)
2152)=Z(152)-CC(5)
2153)=Z(153)-CC(6)
2154)=Z(154)-CC(6)
2155)=Z(155)-CC(7)
2156)=Z(156)-CC(6)
2157)=Z(157)-CC(7)
2158)=Z(158)-CC(7)
```

```
      Z(59)=Z(59)-CC(8)                                                 INTG0166
      Z(60)=Z(60)-CC(5)                                                 INTG0167
      Z(61)=Z(61)-CC(6)                                                 INTG0168
C     M IS READ AS EQUAL TO 2 FOR FAR WAKE STABILITY                    INTG0169
  110 IF(M.EQ.2) GO TO 120                                              INTG0170
      RETURN                                                            INTG0171
  120 Z(3)=0.000                                                        INTG0172
      Z(4)=0.000                                                        INTG0173
      Z(7)=0.000                                                        INTG0174
      Z(9)=0.000                                                        INTG0175
       Z(10)=0.000                                                      INTG0176
      Z(12)=0.000                                                       INTG0177
      Z(15)=0.000                                                       INTG0178
      Z(17)=0.000                                                       INTG0179
      Z(19)=0.000                                                       INTG0180
      Z(20)=0.000                                                       INTG0181
      Z(23)=0.000                                                       INTG0182
      Z(25)=0.000                                                       INTG0183
      Z(27)=0.000                                                       INTG0184
      Z(29)=0.000                                                       INTG0185
      Z(31)=0.000                                                       INTG0186
      Z(33)=0.000                                                       INTG0187
      Z(35)=0.000                                                       INTG0188
      Z(36)=0.000                                                       INTG0189
      Z(38)=0.000                                                       INTG0190
      Z(40)=0.000                                                       INTG0191
      Z(43)=0.000                                                       INTG0192
      Z(44)=0.000                                                       INTG0193
      Z(47)=0.000                                                       INTG0194
      Z(49)=0.000                                                       INTG0195
      Z(50)=0.000                                                       INTG0196
      Z(52)=0.000                                                       INTG0197
      Z(55)=0.000                                                       INTG0198
```

```
INTG0199
INTG0200
INTGC201
INTGC202
INTGC203
```

```
/1571=C.CDC
/1581=G.CDC
/1601=C.CDC
RETURN
END
```

```
C                    * * * * * * * * * * * * * * * * *                  DSIM0001
C                    *      FUNCTION DSIMP             *                DSIM0002
C                    * * * * * * * * * * * * * * * * *                  DSIM0003
C                                                                       DSIM0004
C     FUNCTION SUBPROGRAM DSIMP EVALUATES THE INTEGRAL OF  F(X) OVER AN DSIM0005
C     INTERVAL FROM THE POINT A TO THE POINT B USING SIMPSONS'S RULE AND DSIM0006
C     THE THREE-EIGHTS RULE.THE TOTAL NUMBER OF POINTS OVER THE RANGE   DSIM0007
C     OF INTEGRATION MAY BE EVEN OR ODD .THE ABSCISSAE OF THE POINTS    DSIM0008
C     MUST BE EVENLY SPACED                                             DSIM0009
C                                                                       DSIM0010
C     THE FUNCTION IS CALLED BY THE FOLLOWING STATEMENT,                DSIM0011
C         Z=DSIMP(H,IS,IE,FUNC)                                         DSIM0012
C     WHERE                                                             DSIM0013
C                                                                       DSIM0014
C     H    =REAL*8,VARIABLE OR CONSTANT NAMING THE INTERVAL BETWEEN     DSIM0015
C           POINTS OF INTEGRATION                                       DSIM0016
C     IS   =INTEGER*4,CONSTANT OR VARIABLE , SPECIFYING THE SUBSCRIPT OF DSIM0017
C           THE FIRST VALUE OF THE ARRAY,FUNC.                          DSIM0018
C     IE    =INTEGER*4, CONSTANT OR VARIABLE,SPECIFYING THE SUBSCRIPT OF DSIM0019
C           THE LAST VALUE OF THE ARRAY,FUNC.                           DSIM0020
C     FUNC=REAL*8, ONE-DIMENSIONAL ARRAY CONTAINING THE VALUES OF THE   DSIM0021
C           FUNCTION TO BE INTEGRATED, EVALUATED AT INTERVALS OF H OVER DSIM0022
C           THE RANGE OF THE DESIRED INTEGRATION.                       DSIM0023
      FUNCTION DSIMP(H,IS,IE,FUNC)                                      DSIM0024
      IMPLICIT REAL*8(A-H,O-Z)                                          DSIM0025
       DIMENSION FUNC(101)                                              DSIM0026
      TOT=0.000                                                         DSIM0027
      IT=IE-IS+1                                                        DSIM0028
      IF(IT-2)100,110,120                                               DSIM0029
C               ONLY  ONE POINT -NO INTERVAL                            DSIM0030
  100 DSIMP=0.000                                                       DSIM0031
      RETURN                                                            DSIM0032
C             ONE INTERVAL                                              DSIM0033
```

```
  110 DSIMP=(FUNC(IS)+FUNC(IE))*H*.5DC                                  DSIM0034
      RETURN                                                            DSIM0035
  120 IF(IT-4)130,140,150                                               DSIM0036
C           TWO INTERVAL                                                DSIM0037
  130 DSIMP=H/3.CDC*(FUNC(IS)+4.CDC*FUNC(IS+1)+FUNC(IE))                DSIM0038
      RETURN                                                            DSIM0039
C           ONLY THREE INTERVALSOR LAST THREE INTERVALS                 DSIM0040
  140 DSIMP=TCT+(3.CDC/8.CDC)*H*(FUNC(IE-3)+3.CDC*FUNC(IE-2)+3.CDC*     DSIM0041
     1  FUNC(IE-1)+FUNC(IE))                                            DSIM0042
      RETURN                                                            DSIM0043
C       CLC NUMBER OF INTERVALS                                         DSIM0044
  150 IREM=IT-(IT/2)*2                                                  DSIM0045
      IF(IREM.GT.0) GO TO 170                                           DSIM0046
  160 IL=IE-3                                                           DSIM0047
      GO TO 180                                                         DSIM0048
C         EVEN NO. OF INTERVALS                                         DSIM0049
  170 IL=IE                                                             DSIM0050
  180 TCT=FUNC(IS)+FUNC(IL)                                             DSIM0051
      LA=IS+1                                                           DSIM0052
      LB=IL-1                                                           DSIM0053
      KA=LA+1                                                           DSIM0054
      KB=LB-1                                                           DSIM0055
      SUM=C.CDC                                                         DSIM0056
      DO 190 I=LA,LB,2                                                  DSIM0057
  190 SUM=SUM+FUNC(I)                                                   DSIM0058
       TCT=TCT+4.CDC*SUM                                                DSIM0059
      SUM=C.CDC                                                         DSIM0060
       DO 200 I=KA,KB,2                                                 DSIM0061
  200 SUM=SUM+FUNC(I)                                                   DSIM0062
      TCT=TCT+2.CDC*SUM                                                 DSIM0063
      TCT=TCT*(1.CDC/3.CDC)*H                                           DSIM0064
      IF(IREM.LE.0) GO TO 140                                           DSIM0065
  210 DSIMP=TCT                                                         DSIM0066
```

```
DSIP3067
CSIM0068
```

```
RETURN
END
```